TRANSPORT OF PROTEINS, BIOPHARMACEUTICALS AND SMALL PHARMACEUTICAL COMPOUNDS INTO NORMAL AND INJURED CARTILAGE

by

SANGWON BYUN

M.S., Electrical Engineering and Computer Science, Seoul National University, 2004
B.S., Electrical Engineering and Computer Science, Seoul National University, 2002

Submitted to the Department of Electrical Engineering and Computer Science
in Partial Fulfillment of the Requirements for the Degree of

DOCTOR OF PHILOSOPHY

at the

MASSACHUSETTS INSTITUTE OF TECHNOLOGY

June 2010

Signature of Author: _____
Department of Electrical Engineering and Computer Science
May 21, 2010

Certified by _____
Alan J. Grodzinsky
Professor of Biological, Electrical and Mechanical Engineering
Thesis Supervisor

Accepted by _____
Terry P. Orlando
Professor of Electrical Engineering and Computer Science
Chair, Department Committee on Graduate Students

Thesis Committee

Alan J. Grodzinsky.....Professor of Biological, Electrical, and Mechanical Engineering
Massachusetts Institute of Technology

Eliot H. Frank.....Principal Research Engineer
Massachusetts Institute of Technology

Dennis M. Freeman.....Professor of Electrical Engineering and Computer Science
Massachusetts Institute of Technology

Stephen B. Trippel.....Professor of Orthopedic Surgery
Indiana University School of Medicine

TRANSPORT OF PROTEINS, BIOPHARMACEUTICALS AND SMALL PHARMACEUTICAL COMPOUNDS INTO NORMAL AND INJURED CARTILAGE

by

Sangwon Byun

Submitted to the Department of Electrical Engineering and Computer Science on May 21, 2010 in Partial Fulfillment of the Requirements for the Degree of Doctor of Philosophy in Electrical Engineering and Computer Science at the Massachusetts Institute of Technology

Abstract

Traumatic joint injury can induce acute damage to cartilage and surrounding joint tissues accompanied by an inflammatory response, which can significantly increase the risk of developing osteoarthritis. The mechanism by which joint injury results in disease development is not fully understood. However, chondrocyte metabolism is greatly affected by the transport properties of cartilage extracellular matrix, which determine the accessibility and the concentrations of various proteins and therapeutic agents to cells and cell receptors. Using in vitro models of mechanical injury to cartilage, we have characterized the uptake and binding of proteins and biopharmaceuticals in normal articular cartilage and have compared the results to those in cartilage subjected to mechanical injury and pro-inflammatory cytokines.

We studied equilibrium partitioning and non-equilibrium transport into cartilage of Pf-pep, a 760 Da positively charged peptide inhibitor of the proprotein convertase PACE4. Competitive binding measurements revealed negligible binding to sites in the matrix. The uptake of Pf-pep depended on GAG charge density, consistent with predictions of Donnan equilibrium. The diffusivity of Pf-pep was measured to be $\sim 1 \times 10^{-6}$ cm^2/s, close to other similarly-sized non-binding solutes. These results suggest that small positively charged therapeutics will have a higher concentration within cartilage than in the surrounding synovial fluid, a desired property for local delivery; however, such therapeutics may rapidly diffuse out of cartilage unless there is additional specific binding to intratissue substrates that can maintain enhanced intratissue concentration.

We have also examined the effect of mechanical injury and inflammatory cytokines, TNFα, on the uptake of anti-IL-6 antibody Fab fragment (48 kDa). Anti-IL-6 Fab was able to penetrate into cartilage, though final equilibrium uptake would likely occur only after 6-10 days within 1 mm thick explant disks. Uptake of anti-IL-6 Fab was significantly increased following mechanical injury of the cartilage in vitro. A further increase in uptake was caused by TNFα treatment combined with mechanical injury. The increase in uptake was accompanied by GAG loss from the tissue, suggesting that there can be greater accessibility of large solutes into cartilage after direct mechanical injury or inflammatory cytokine treatment to the tissue, where the increase in uptake was related with the severity of matrix damage and loss.

We also studied the binding and uptake of TNFα in articular cartilage and observed

significant binding of TNFα to matrix sites. Binding was stronger for the monomeric form of TNFα compared to trimeric form. Binding of TNFα was not disrupted by pre-treatment of the tissue with trypsin, indicating that the intra-tissue binding sites were not removed by trypsin-induced proteolysis of the matirx. These results suggest that matrix binding as well as monomer-trimer conversion of TNFα both play crucial roles in regulating the accessibility of TNFα to cell receptors.

The results of this thesis are significant in that they suggest that injurious mechanical loading and inflammatory cytokine applied to cartilage can affect transport processes within the tissue. The resulting altered transport, in turn, can influence the accessibility of pro-inflammatory cytokines and anti-catabolic drugs which are designed to treat pathogenesis of OA.

Thesis Supervisor: Alan J. Grodzinsky, Professor of Biological, Electrical, and Mechanical Engineering

Thesis Co-Supervisor: Eliot H. Frank, Principle Research Engineer, Center for Biomedical Engineering

Acknowledgement

I would first like to thank my advisor Professor Alan Grodzinsky, who is not only a great advisor but also a true mentor. His guidance and patience continuously encouraged me through my doctoral degree. It has truly been an honor and great pleasure to work with him. I am also grateful to Dr. Eliot Frank for co-advising my thesis. He provided critical insight and suggestion in numerous aspects of experiment, modeling, and analysis. I also would like to thank my thesis committee members, Prof. Dennis Freeman and Prof. Stephen Trippel. I deeply appreciate their critical advice and encouraging comments.

I would also like extend my gratitude to the whole Grodzinsky group: Han-Hwa, Linda, Yi, Rachel, Hsu-Yi, Emily, Yunna, Yang, Nicole, Fei, Hadi, Shuodan, Bobae, Paul, Eric, Detlef, Lin, Cameron, Diana, and Anna. Han-Hwa has managed our needs in the lab and Linda has taken care of all the administrative issues, allowing us to focus solely on our research. Yi is a trusted friend and a lab-mentor. She was always willing to help me with experiments. She also constantly encouraged me to come through difficult times. Yunna was a dedicated UROP with cheerful spirit and made our experiments more enjoyable. She also introduced me to many great friends and showed me how to enjoy life at MIT. Rachel provided insightful suggestions whenever I asked her. She never hesitated to help me and gave insightful advices on my research. Hsu-Yi always gave me timely consultation and sincere advices. She kept us entertained yet with her poise. It was always fun to talk with Bobae. Thanks to her, I was able to have wonderful memories during the ORS conferences.

I would like to show my appreciation to Dr. Ernst Hunziker at Bern University, who generously performed autoradiography procedures and provided great insights on analysis of images. I would also like to thank collaborators from Pfizer and Centocor. They kindly provided me with reagents and expert advices, which were critical to my research.

I cannot imagine how I would have survived throughout the years without my great friends. Thank you Won Yong, Chiwon, Sang-Il, Jin-Oh, Jaemyung, Taeho, Sang-Jin, Kang Hyeun, Sangmok, Jae Won, Joo-Eun, Youjin, Hyemin, Gyu-Boong, and Jinkuk for looking after me since we all had difficult times getting used to the life at MIT. Thank you Hyung-Suk, Sid, and Daekeun for sharing their wisdom and experience. I would also like to thank Jessie, Sungmin, Yun Seog, Jongsup, Kyunghee, Seung Hyuck, Wonjoon, Jae Hyung, Hansohl, Shin Young, Hyunglae, Yongdae, Kyungchul, Jungmin, and Seeun for embracing me like a true brother. Thank you Jeong Gon, Wonjung, Eunhee, Jae Kyoung, Jeong-Yun, Rhokyun, and Johnny for making my last year at MIT more enjoyable and memorable. I am very grateful to my EECS friends: Jaewook, Sungho, Min, Eun Jong, Daihyun, Jerin, Jungwon, Seongmoo, Junghoon, Hyunil, Soonmin, Byungsub, Sejoon, Jungwoo, Myung Hyun, Kyungbum, Yongwook, Myung Jin, Taeg Sang, Sooho, Kyung-Jae, Ye-Ryoung, Wonyoung, Jiye, and Jinwook for their support. I also appreciate Eun-Suk for showing me true friendship.

Last but not least, I am deeply grateful to my family. No words can express my gratitude for their unconditional trust and love. Without their endless support and sacrifice, I would have never been able to complete my degree.

부모님 감사합니다.

TABLE OF CONTENTS

LIST OF FIGURES

CHAPTER 1

Introduction

1.1 Articular cartilage structure

Articular cartilage is a load-bearing tissue found at the end of long bones within the synovial joints. Main functions of cartilage are to provide a smooth and almost frictionless surface for the joint articulation and also to distribute loads between joint surfaces. Chondrocytes are responsible for maintaining and repairing cartilage to sustain its mechanical properties. However, the ability of the cells to repair tissue post injury is very limited. Since adult articular cartilage is avascular and alymphatic, essential nutrients, signaling molecules, metabolites, and waste products must be delivered to or removed from chondrocytes through the extracellular matrix (ECM) [1], which constitutes ~ 20-40% of the wet weight of cartilage, whereas chondrocytes comprise only few % of the tissue volume in adult articular cartilage [2]. Therefore, transport through the cartilage is mainly regulated by the integrity of structural components of the ECM, primarily type II collagen fibrils and aggrecan molecules.

Chondrocyte is an only cell type that exists in the cartilage tissue. Although chondrocytes account for very small portion of cartilage by volume, the cells are solely responsible for maintaining the tissue homeostasis. To maintain the tissue, chondrocytes synthesize and assemble matrix molecules but also involve in degradation to replace old or

damaged part of the matrix. In healthy tissue, the balance between synthesis and degradation is well maintained. However, in disease, this balance no longer exists, resulting in destruction of cartilage tissue, which suggests critical role of chondrocytes in pathogenesis of OA [3]. Cell size, shape and density vary with depth, accompanying the change in structure and components of matrix [2].

Tissue water comprise up to 80% of the wet weight of articular cartilage, which is most abundant component of the tissue. Osmotic pressure generated from negatively charged GAGs imbibes water, keeping tissue hydrated, and the amount of water in the tissue depends on the structure of GAG and collagen. Collagen fibrils prevent the full swelling of GAG component, which balances with osmotic pressure from GAG, regulating the water content in the tissue. Tissue hydration is highest at the surface and decrease with depth, indicating the heterogeneity of ECM components and interaction at each region. Osteoarthritic cartilage generally shows increased hydration due to damaged collagen, which causes the imbalance between swelling pressure and collagen tension [4].

Type II collagen makes up 70% of dry weight of cartilage tissue. Type II is a most abundant type (~90%) of collagen, and other collagens, such as collagen types IX, XI, VI, and X, are present in small amount. Major mechanical function of collagen network is to resist to tensile strength, which is affected by the degree of cross-linking. Ultrastructure of collagen networks, such as collagen packing density and its orientation, is highly heterogeneous along the depth. Collagen fibers aligned parallel to the surface at the superficial layer, more randomly oriented at the middle zone, and run perpendicular to the surface at the deep zone. Oriented alignment of fibers caused anisotropic diffusion that again varied with in the structure of collagen network [5].

Proteoglycan consists of ~15-25% of the dry weight of cartilage tissue. Large aggregating aggrecan is most abundant form of proteoglycan in cartilage tissue, which is responsible for resisting compressive force. This unique mechanical property is caused by negative charge on sulfated GAG chains, which is attached to core protein backbone. Proteoglycan unit is composed of core protein and GAG-rich region, and this unit, in turn, binds to hyaluronic acid to form a large aggregate. Beyond the mechanical property, proteoglycan content has major impact on the transport property of the cartilage tissue. Proteoglycan is primarily responsible for restricting solute transport [6]. For large solutes, their mobility was significantly affected by GAG content of tissue. Additionally, charge-charge interaction between fixed charges on proteoglycan and charged solutes played a crucial role determining the partitioning of such solutes [7].

1.2 Transport in articular cartilage

1.2.1 Partition coefficient. The partition coefficient is the equilibrium concentration of "unbound" solutes in the cartilage normalized to the concentration of those solutes in the equilibration bath. Partition coefficient represents relative concentration of solutes compared to surrounding fluid. A partition coefficient of 1 suggests that distribution of solutes in the tissue is same as that in the surrounding solution. A partition coefficient greater than 1 indicates enhanced uptake due to charge interaction with negligible effect from steric hindrance, whereas a partition coefficient less than 1 implies exclusion by steric hindrance or charge interaction.

Partition coefficient is significantly affected by the charge and size of solutes, composition of matrix and loading on the tissue [1, 6-10]. Negative charges on GAG chains

interact with charged solutes, resulting in exclusion of negative charged solutes and enhanced uptake of positively charged solutes. Charge-charge interaction between negatively charged matrix and charged solutes was well explained by Donnan partitioning effect. For example, partition coefficients of small charged molecules, such as Na^+ and Cl^-, were consistent with prediction from Donnan theory. The partition coefficient of Na^+ increased with increasing fixed charge density, while the partition coefficient of Cl^- decreased with increasing fixed charge density.

For large solutes, partitioning was significantly affected by steric exclusion by matrix molecules, and thus size of solutes and fixed charge density of the tissue were key factors regulating the partition coefficient. Partition coefficient of solutes decreased with increasing solute size and fixed charge density. Maroudas showed that partitioning of large solutes well followed Ogston's theory, which described the exclusion of globular solutes in rod-like molecules in solution [11]. Partitioning of charged large solutes was also affected charge interaction with negatively charged matrix. For example, cationized bovine serum albumin (BSA), had increased uptake and prolonged retention compared to native BSA [12-14].

1.2.2 Equilibrium binding. Binding of certain solutes (e.g., proteins) to sites within the ECM or, in general, to cell receptors, can change intra-tissue concentration and transport kinetics through cartilage. To study the effect of binding on the concentration of solutes within the tissue, uptake ratio is measured, which is the equilibrium concentration of "unbound" and "bound" solutes in the cartilage normalized to the concentration of those solutes in the equilibration bath. Presence of binding sites can be tested using competitive binding by unlabeled species, which will compete with labeled solutes for the same binding sites. For

example, reversible binding of the anabolic growth factor, insulin-like growth factor-I (IGF-I) to its binding proteins (IGFBP) resulted in the measured uptake ratio above 1 and the uptake ratio significantly decreased by adding increasing amount of unlabeled IGF-I (Fig 1a). By comparing equilibrium uptake to the binding predicted by models such as that of a Langmuir isotherm, i.e., a bimolecular, first order, reversible reaction (Fig. 1a), values of the binding constants can be estimated (e.g., binding site density, dissociation constant, partition coefficient, etc.). Diffusive transport of IGF-I was also affected by binding reaction during the transport process, resulting in increased diffusion lag time of IGF-I through adult bovine cartilage (Fig. 1b) [15].

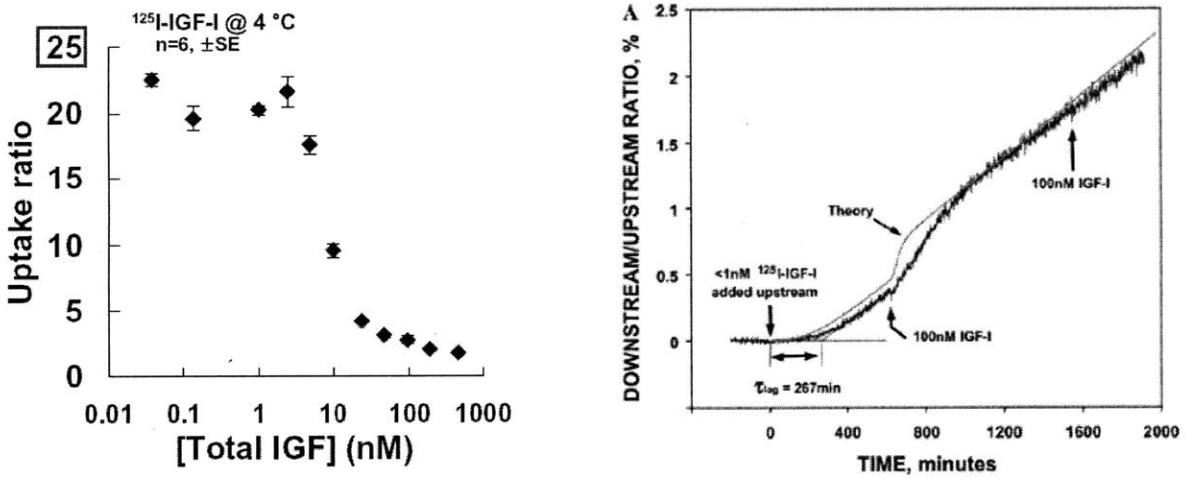

(a) (b)

Figure. 1 (a) Uptake ratio of ^{125}I-IGF-I with graded concentration of unlabeled IGF-I in free swelling explants from bovine calf cartilage (b) Transport kinetics and steady state diffusion flux of ^{125}I-IGF-I through adult bovine cartilage (figure adapted from [15]).

1.2.2 Diffusion in cartilage. Since the adult cartilage is avascular and alymphatic, diffusion is a crucial mechanism that delivers key nutrients and metabolites to chondrocytes. The rate of diffusion in cartilage was significantly affected by several properties of solute and matrix, such as solute size, solute charge, and tissue hydration. Intra-tissue diffusivities of solutes were smaller than diffusivities in free solution due to reduced pore size, increased tortuous path, and friction from diffusing through comparable size of pore. In general, diffusion coefficient in cartilage decreased with increasing size of solute and matrix density. For small solutes, including water molecules and ions, the diffusion coefficient was mainly governed by tissue hydration and well predicted by Mackie-Meares model based on solid volume fraction [1, 7, 16]. For large solutes, the effect of friction between solute and matrix becomes more important, since the spacing between GAG chains is known to be 2-10 nm. Diffusivities of large solutes, indeed, decreased with increasing solute size and GAG density [7, 17].

Due to the crucial role of ECM in solute diffusion, the difference in structure and composition of ECM due to zonal heterogeneity, static compression or enzymatic digestion of matrix can cause significant change in solute diffusivities. For small solutes, there is mixed evidence on the dependence of solute diffusivity on the matrix density. Diffusivities of urea (60 Da) and glucose (180 Da) did not vary significantly with tissue depth [7]; static compression, however, which increases solid volume fraction, reduced the diffusivities of Na^+ and SO_4^{2-} ions [10] and tetramethylrhodamine (TMR, 430 Da) [8, 9]. Removal of proteoglycans using trypsin did not affect the diffusion coefficient of glucose [18], but did change that of gadolinium-DTPA (530 Da) [19]. These differences may be associated with the different methods used in these various studies. For large solutes, including 3kDa, 10 kDa, and 40 kDa dextrans, static compression decreased diffusivities [8, 9, 20]; Proteoglycan removal increased diffusivities of

5 kDa inulin and 70 kDa dextran [18]. Leddy et al. found that diffusivities of 3 kDa and 500 kDa dextrans decreased with tissue depth while diffusivities of 40 kDa and 70 kDa dextrans increased [21].

1.3 Thesis Objectives

The goal of this thesis was to characterize uptake and binding kinetics of proteins, biopharmaceuticals and small pharmaceutical compounds in articular cartilage and to evaluate the effect of joint injury and pro-inflammatory cytokine on transport properties.

The objective of Chapter 2 was to quantify and model the equilibrium uptake and transient transport kinetics in normal cartilage of specific pharmaceutical agents, including small peptides and proteins against OA. The working hypothesis was that transport of peptide or protein therapeutics into and within cartilage tissue is affected by the size and charge of the drugs as well as specific components of the cartilage matrix.

The goal of Chapter 3 was to evaluate the effect of cartilage mechanical injury and inflammatory cytokines on the uptake of anti-catabolic therapeutics, and to relate the alteration in intra-tissue transport of these molecules to the extent of degradation of cartilage. We tested the hypothesis that injurious mechanical loading and inflammatory cytokine applied to cartilage can affect the kinetics of uptake and retention of therapeutic agents within the tissue via degradation and remodeling of the matrix.

In chapter 4, we characterized the uptake and binding of the major pro-inflammatory cytokine, TNF-α, and to discover the key factors determining transport process of TNF into cartilage.

In chapter 5, conclusions from each chapter are summarized and future work is proposed.

1.4 References

[1] Maroudas A. Physicochemical properties of cartilage in light of ion exchange theory. Biophys J 1968;8:575-95.
[2] Buckwalter JA, Mankin HJ, Grodzinsky AJ. Articular cartilage and osteoarthritis. Instr Course Lect 2005;54:465-80.
[3] Goldring MB, Goldring SR. Osteoarthritis. J Cell Physiol 2007;213:626-34.
[4] Maroudas A. Balance between Swelling Pressure and Collagen Tension in Normal and Degenerate Cartilage. Nature 1976;260:808-9.
[5] Leddy HA, Haider MA, Guilak F. Diffusional anisotropy in collagenous tissues: Fluorescence imaging of continuous point photobleaching. Biophysical Journal 2006;91:311-6.
[6] Snowden J, Maroudas A. Distribution and Diffusion of Large Solutes in Articular-Cartilage. Journal of Bone and Joint Surgery-American Volume 1974;A 56:857-.
[7] Maroudas A. Distribution and diffusion of solutes in articular cartilage. Biophys J 1970;10:365-79.
[8] Quinn TM, Kocian P, Meister JJ. Static compression is associated with decreased diffusivity of dextrans in cartilage explants. Arch Biochem Biophys 2000;384:327-34.
[9] Quinn TM, Morel V, Meister JJ. Static compression of articular cartilage can reduce solute diffusivity and partitioning: implications for the chondrocyte biological response. J Biomech 2001;34:1463-9.
[10] Nimer E, Schneiderman R, Maroudas A. Diffusion and partition of solutes in cartilage under static load. Biophys Chem 2003;106:125-46.
[11] Ogston AG. The spaces in a uniform random suspension of fibres. Trans Faraday Soc 1958;54:1754-7.
[12] van den Berg WB, van de Putte LBA, Zwarts WA, Joosten LA. Electrical charge of the antigen determines intraarticular antigen handling and chronicity of arthritis in mice. J Clin Invest 1984;74:1850-9.
[13] van den Berg WB, van de Putte LBA. Electrical charge of the antigen determines its localization in the mouse knee joint deep penetration of cationic bovine serum albumin in hyaline articular cartilage. Am J Pathol 1985;121:224-34.
[14] van den Berg WB, van Lent PLEM, van de Putte LBA, Zwarts WA. Electrical charge of hyaline articular cartilage: its role in the retention of anionic and cationic proteins. Clin Immunol Immunopathol 1986;39:187-97.
[15] Garcia AM, Szasz N, Trippel SB, Morales TI, Grodzinsky AJ, Frank EH. Transport and binding of insulin-like growth factor I through articular cartilage. Arch Biochem Biophys 2003;415:69-79.
[16] Mackie JS, Meares P. The Diffusion of Electrolytes in a Cation-Exchange Resin Membrane .1. Theoretical. Proceedings of the Royal Society of London Series a-Mathematical and Physical Sciences 1955;232:498-509.
[17] Maroudas A. Transport of solutes through cartilage: permeability to large molecules. J Anat 1976;122:335-47.
[18] Torzilli PA, Arduino JM, Gregory JD, Bansal M. Effect of proteoglycan removal on solute mobility in articular cartilage. J Biomech 1997;30:895-902.

[19] Foy BD, Blake J. Diffusion of paramagnetically labeled proteins in cartilage: Enhancement of the 1-D NMR imaging technique. J Magn Reson 2001;148:126-34.
[20] Evans RC, Quinn TM. Solute diffusivity correlates with mechanical properties and matrix density of compressed articular cartilage. Arch Biochem Biophys 2005;442:1-10.
[21] Leddy HA, Guilak F. Site-specific molecular diffusion in articular cartilage measured using fluorescence recovery after photobleaching. Ann Biomed Eng 2003;31:753-60.

CHAPTER 2

Transport and Equilibrium Uptake of a Peptide Inhibitor of PACE4 into Articular Cartilage is Dominated by Electrostatic Interaction*

* This chapter has been accepted to Archives of Biochemistry and Biophysics for publication.

2.1 Introduction

In this study, we focused on the effects of Donnan partitioning and matrix binding interactions on the transport and uptake of a small (760 Da) positively charged peptide inhibitor of paired amino acid converting enzyme-4 (PACE4). PACE4 is a Ca^{2+}-dependent serine endoprotease belonging to the subtilisin-like proprotein convertase family, and is a key proprotein convertase responsible for extracellular activation of aggrecanases from their inactive latent forms within cartilage [1]. ADAMTS-4 (aggrecanase-1) and ADAMTS-5 (aggrecanase-2) are synthesized as latent zymogens [2, 3] by chondrocytes, and their catalytic activity depends on the removal of their prodomains [1, 4, 5]. Both aggrecanases cleave the aggrecan core protein at multiple sites (e.g., Glu^{373}, Glu^{1545}, Glu^{1714}, Glu^{1819}, and Glu^{1919} [6, 7]), resulting in the release of aggrecan fragments from cartilage *in vitro* [8, 9] and into the synovial fluid of osteoarthritic (OA) knees [10, 11] *in vivo*. Since the proteolytic activities of ADAMTS-4 and ADAMTS-5 are believed to play a crucial role in the pathogenesis of OA [12], PACE4 is regarded as a potential therapeutic target for OA. Therefore, studying the physicochemical mechanisms that govern the penetration and transport of such charged peptide inhibitors into cartilage will help to understand their potential therapeutic benefits.

Since adult articular cartilage is avascular and alymphatic, therapeutic agents must be delivered to intratissue targets through the extracellular matrix (ECM) [13], which constitutes ~ 20-40% of the wet weight of the tissue [14]. Transport through cartilage is regulated by the collagen fibrils and proteoglycans of the ECM, primarily, which accounts for ~ 60-70% and ~ 15-25% of the dry weight of the tissue, respectively [15]. The negatively charged glycosaminoglycan (GAG) chains of aggrecan play a unique role in determining the transport

properties of the cartilage. The pioneering studies of Maroudas and co-workers [13, 15, 16] showed that the partitioning of free (unbound) electrolyte ions into cartilage (e.g., Na^+ and Cl^-) is governed by Donnan equilibrium between the tissue and its bathing solution, associated with electrostatic interactions between matrix GAGs and these ionic solutes. Uptake of free cations into cartilage was enhanced by Donnan equilibrium, whereas anions were largely excluded, and partitioning was further affected by the ion valence in a manner predicted by Donnan theory.

In addition, electrostatic interactions between soluble protein factors and GAGs can regulate transport and *binding* of these soluble proteins within cartilage. For example, insulin-like growth factor-1 (IGF-1) is a basic protein (pI ~8.5) that partitions into cartilage on the basis of size (steric interactions) and charge (Donnan equilibrium); in addition, IGF-1 binds to specific IGF binding proteins (IGFBPs) that are contained within the ECM [17, 18]. Recently, an HB-IGF-1 fusion protein consisting of native IGF-1 with the heparin-binding (HB) domain of heparin-binding epidermal growth factor-like growth factor (HB-EGF) was designed, purified [19] and found to bind specifically to chondroitin sulfate (CS) GAGs of aggrecan as well as heparin sulfate (HS) GAGs of HS-proteoglycans [20]. The high concentration of positively charged lysine residues within the heparin-binding domain thereby conferred higher uptake and binding of HB-IGF-1 within cartilage ECM and long-term delivery to chondrocytes compared to wild-type IGF-1 [19], even after the HB-IGF-1 was removed from the medium. Similarly, cationized bovine serum albumin (BSA), had increased uptake and prolonged retention via binding within murine cartilage compared to native BSA [21-23].

Interestingly, however, augmenting the net positive charge of a given small or large solute does not necessarily result in binding interactions to negatively charged ECM molecules. Since binding and Donnan partitioning can independently increase the intratissue uptake of a

basic protein, experimental methods to characterize each separate mechanism are needed. One approach involves the use of competitive binding assays in which radiolabeled and unlabeled ligands compete for the same binding sites within cartilage tissue, such that the uptake of the labeled ligand changes dramatically as the concentration of unlabeled ligand is varied over a wide range. This method was used to characterize binding of IGF-1 to IGFBPs, while Donnan partitioning of IGF-1 was found to play a far less important role [18, 24]. It is important to note that binding to ECM not only increases total solute uptake in cartilage but can slow the initial diffusion kinetics until a final steady concentration profile within the tissue is achieved, giving rise to a diffusion-binding lag time [18, 24]. To understand the transport of charged solutes into cartilage, binding and partitioning must be distinguished from each other, since these two mechanisms affect the uptake and transient diffusion in very different ways.

To achieve this goal, our objectives were (1) to quantify the equilibrium partitioning and non-equilibrium diffusion of the peptide inhibitor Pf-pep in cartilage, and (2) to assess the extent of binding of the peptide to sites within the tissue. The effect of charge-charge interactions and tissue heterogeneity on uptake and transport were examined. Experimental results were compared to theoretical models of Donnan equilibrium partitioning, reversible binding, and non-equilibrium diffusive transport in cartilage.

2.2 Materials and Methods

Tissue harvest. Cartilage explants were harvested from the femoropatellar grooves of three 18-24 months old cows (Bertolino Beef, Boston, MA) and a 1-2 weeks bovine calf (Research 87, Marlborough, MA) [18]. Briefly, 9-mm diameter cartilage-bone cylinders were

cored, mounted on a microtome and sliced sequentially from the top surface to divide explants into level-1 (L1, ~400 μm with superficial zone intact) and level-2 (L2, ~400 μm below L1). To measure time-dependent diffusive transport of the inhibitor into and across cartilage, the 9-mm diameter slices were used as cut. For equilibrium uptake studies, four 3-mm diameter disks were punched from each of the 9-mm slices and distributed evenly into groups from among different harvest sites along joint surfaces. All cartilage specimens were equilibrated overnight at 4°C in 1× phosphate buffered saline (PBS) supplemented with 0.1% bovine serum albumin (BSA), 0.01% sodium azide (NaN_3) and protease inhibitors (Complete, Roche Applied Science, Indianapolis, IN) prior to experiments.

Solute structure and preparation. Pf-pep is a 760 Da, basic (trivalent) peptide inhibitor of PACE4 having the sequence Arg-Tyr-Lys-Arg-Thr, pI = 11, and an IC_{50} = 2 μM measured by screening the peptide against recombinant rat PACE4 and monitoring activity using a peptide substrate as previously described [1]. Radio-iodinated ^{125}I-Pf-pep and unlabeled Pf-pep were provided by Pfizer (St. Louis, MO). For the iodinated species, the tyrosine residue was labeled using lactoperoxidase labeling [25]. Before all experiments using ^{125}I-Pf-pep, Sephadex G10 chromatography was used to separate and remove any small ^{125}I-species that may have resulted from degradation of ^{125}I-Pf-pep, (0.7 × 50 cm columns using an elution buffer of 1×PBS buffer with 0.1% BSA and 0.01% NaN_3, and the void volume collected for the desired ^{125}I-Pf-pep) [18].

Equilibrium uptake of Pf-pep. In order to measure equilibrium partitioning of Pf-pep into cartilage and to determine whether Pf-pep may bind to sites within the tissue [24], disks were equilibrated in a buffer containing a fixed amount of ^{125}I-Pf-pep (0.127 nM, specific activity 2000 Ci/mmol) and graded amounts of unlabeled Pf-pep (0.5, 1, 2, 4, 8, 16, 32, and 64

nM, shown schematically in Fig. 2.1a). The buffer consisted of 1×PBS supplemented with 0.1% BSA, 0.01% NaN_3 and protease inhibitors at 4°C. After 48 hours, disks were removed from the bath and briefly rinsed in fresh PBS buffer (equilibrium was reached by 48 hours; see Results below). The surface of each disk was quickly blotted with Kimwipes and the wet weight was measured. The ^{125}I-radioactivity of each cartilage disk and aliquots of the equilibration baths were quantified individually using a gamma counter. Disks were then lyophilized and the dry weight was measured; the water weight of each disk was calculated from the tissue wet and dry weights. The *inhibitor uptake ratio* was calculated as the concentration of the ^{125}I-Pf-pep in the cartilage disks (per intratissue water weight) normalized to the concentration of ^{125}I-Pf-pep in the equilibration bath. Radio-labeled and unlabeled Pf-pep were assumed to partition into the cartilage in an identical manner.

The disks were then digested with proteinase-K (Roche Applied Science, Indianapolis, IN) and the sulfated glycosaminoglycan (sGAG) content of each disk was measured using the dimethylmethylene blue (DMMB) dye binding assay [26]. Samples from the baths were again analyzed by Sephadex G10 chromatography to determine whether any small labeled species (e.g., ^{125}I) may have accumulated from degradation of ^{125}I-Pf-pep during each experiment. The uptake ratio was corrected to take into account the presence of any such small labeled species, assuming the small species to be ^{125}I [27]. In a separate control experiment, the uptake ratio of ^{125}I alone was measured to calibrate the correction factor, which was ~ 0.6.

To investigate the possibility that Pf-pep may bind to specific sites within the cartilage tissue, we compared the measured uptake ratio to a theoretical model based on a first-order, reversible, bimolecular reaction involving one dominant family of binding sites. The form of this model has been used previously, for example, to characterize the reversible binding of IGF-

1 to a single dominant binding site within cartilage [18], and the reversible binding of H^+ ions to negative carboxyl groups of reconstituted collagen fibrils [28]:

$$R_u = \frac{C_B + C_F}{C_{bath}} = K\left(1 + \frac{N}{K_d + C_F}\right) = K\left(1 + \frac{N}{K_d + KC_{bath}}\right) \quad (1)$$

where, in the present case, R_u is the uptake ratio, C_B is the concentration of Pf-pep bound to sites within cartilage, C_F is the concentration of free (unbound) Pf-pep in cartilage, C_{bath} is the bath concentration of Pf-pep, K is the partition coefficient, N is the density of binding sites, and K_d is the dissociation constant. In general, measurement of the uptake ratio (R_u) over a range of bath concentrations of unlabeled Pf-pep (C_{bath}) would enable a fit of the model to the experimental data and thereby provide best-fit estimates of K and the binding parameters N and K_d using Eq. (1) [18]. However, if there is no significant change in the measured uptake ratio over a wide range of bath concentrations of unlabeled Pf-pep, it is most likely that intratissue binding of Pf-pep to specific sites is negligible (i.e., $N = 0$ in Eq. (1)) and the measured uptake ratio is then identical to the partition coefficient of the solute into the tissue ($R_u = K$).

To further test the relation between uptake of the positively charged peptide Pf-pep and matrix fixed charge density, cartilage disks were treated with trypsin to mimic aspects of matrix degradation. Plugs were incubated for 24 hours with 0.1 mg/ml trypsin at 4°C and then washed at least three times in fresh buffer (total wash time was ~ 48 hours). To determine the decrease in cartilage sGAG content caused by trypsin treatment, sGAG was measured in tissue disks at the end of the experiments (via the DMMB dye binding assay as described above), and sGAG released to the medium by treatment was also measured. To minimize any residual enzymatic activity after trypsin treatment during the uptake measurements, a protease inhibitor cocktail (Complete, Roche Applied Science, Indianapolis, IN) was added to the equilibration buffer containing ^{125}I-Pf-pep to inhibit serine, cysteine, and metallo- proteases as well as calpains.

Diffusive transport measurements. Real-time measurement of diffusive transport of the inhibitor into and through adult bovine cartilage slices (with intact superficial zone) was measured using a diffusion chamber consisting of two compartments, shown schematically in Fig. 2.1b [24, 29]. Groups of three 9-mm diameter cartilage slices were clamped in parallel by 3 pairs of O-rings positioned at the outer periphery of each disk; the disks were held between the two compartments in such a way that transport between compartments could only occur through the cartilage tissue. Both compartments were filled with 1×PBS supplemented with 0.1% BSA, 0.01% NaN_3 and protease inhibitors, and maintained at 20°C. Both chambers were magnetically stirred to minimize the effects of stagnant films on transport across the cartilage-buffer interfaces [30]. After addition of ^{125}I-Pf-pep to the upstream compartment, the downstream bath concentration of ^{125}I-Pf-pep was measured continuously by recirculating the bath through a gamma detector (A500 Radiomatic, Packard, Meriden, CT). To correct for any small labeled species (e.g., ^{125}I) that may have accumulated from degradation of ^{125}I-Pf-pep during diffusive transport experiments, we used experimental and analytical methods described in detail previously [27]. Aliquots from the baths were analyzed using Sephadex G10 chromatography before and after each experiment to determine the amount of any accumulated free ^{125}I. At the end of the experiment, free ^{125}I was injected into the upstream bath and the total radiolabel flux (attributed to the combination of ^{125}I-Pf-pep and free ^{125}I) was measured. Using an analytical expression for the total radiolabel flux (Eqn. (1) of [27]) in conjunction with chromatographic assessment of ^{125}I concentration, the contribution of any free ^{125}I present could be estimated for correction.

Statistical analysis. 2-way ANOVA was used to evaluate the effects of unlabeled Pf-pep concentration and tissue layer on the uptake ratio. Relationships among tissue sGAG

content, tissue hydration, and uptake ratio were tested by linear regression analysis. The effects of tissue layer on tissue sGAG density and tissue hydration were evaluated by t-test. The effects of removal of proteoglycans and ionic strength on uptake ratio were examined by 1-way ANOVA followed by post hoc Dunnett's test. For all statistical analyses, P values less than or equal to 0.05 were considered significant. Systat 12 software (Richmond, CA) was used to perform all analyses.

2.3 Results

Equilibrium uptake of ^{125}I-Pf-pep into adult bovine cartilage. The equilibrium uptake of ^{125}I-Pf-pep in the more superficial (L1) and middle-deep zone (L2) explants of adult bovine cartilage was measured. The uptake of ^{125}I-Pf-pep was significantly higher in L2 compared to L1 cartilage overall (2-way ANOVA, effect of the tissue layer, $p<0.0001$, Fig. 2.2). If ^{125}I-Pf-pep bound to sites in cartilage, we postulated that increasing amounts of unlabeled Pf-pep would compete with ^{125}I-Pf-pep for these binding sites, resulting in uptake of ^{125}I-Pf-pep that would vary with the concentration of unlabeled Pf-pep [18, 24]. However, the results of Fig. 2.2 show that there was no significant change in the uptake ratio of ^{125}I-Pf-pep with the concentration of unlabeled Pf-pep over the entire range tested for both L1 and L2 tissue (2-way ANOVA, no significant effect of the Pf-pep concentration or the interaction between tissue layer and concentration). These results suggest that there is little or no binding of Pf-pep to sites within the tissue (i.e., $N = 0$ in Eq. (1)). Under this assumption, these results suggest a ~ 2-4-fold upward partitioning of Pf-pep into adult bovine cartilage in a depth-dependent manner (with the partition coefficient, K, taken to be the measured R_U of Fig. 2.2).

As a positive control for the interpretation of concentration-dependent binding, we also measured the uptake ratio of ^{125}I-IGF-1 in both L1 and L2 explants using the same methods [18]. We observed that the uptake ratio of ^{125}I-IGF-1 in both L1 and L2 explants decreased dramatically by 30-fold as the bath concentration of unlabeled IGF-1 was increased from 10 nM to 100 nM (data not shown), consistent with the known binding of IGF-1 to IGF binding proteins (IGFBPs) located within the cartilage extracellular matrix (ECM) [18, 24].

For each of the 68 cartilage specimens that comprise the data-set of Fig. 2.2, we plotted the measured uptake ratio as a function of the specimen's individually measured sGAG content (Fig. 2.3a) and hydration (Fig. 2.3b, where hydration is defined here as water weight/dry weight [27, 31]). Uptake of Pf-pep increased with tissue sGAG content (Fig. 2.3a, linear regression, $r^2 = 0.637$, $p<0.0001$) and with decreasing tissue hydration (Fig. 2.3b, linear regression, $r^2 = 0.353$, $p<0.0001$). We also note that cartilage from the deeper region (L2) generally had higher GAG density (t-test, $p<0.0001$) and lower hydration (t-test, $p=0.00016$) than L1 tissue, consistent with previously reported trends for adult articular cartilage [32]. Therefore, L2 cartilage had higher fixed charge density (FCD) compared to the more superficial L1 tissue.

Uptake of ^{125}I-Pf-pep followed Donnan equilibrium partitioning. The data of Figs. 2.2 and 3 suggest that the uptake of the positively charged ^{125}I-Pf-pep was enhanced by the charge-charge interactions with the negative ECM. For small, positively charged species that do not to bind within cartilage tissue, such as Na^+ [15], partition coefficients in cartilage have been reported to be greater than 1, and to increase with FCD of the ECM in a manner that typically follows Donnan equilibrium [15]. To test whether the intratissue concentration of Pf-pep obeyed Donnan equilibrium, the net charge of Pf-pep was estimated by fitting the predictions

of Donnan theory to the data of Fig. 2.3a, and then compared to the known charge of +3. Donnan theory predicts that the partition coefficient of Pf-pep ($K_{pep} = \overline{C}_{pep} / C_{pep}$) is related to the partition coefficient of Na^+ ($K_{Na} = \overline{C}_{Na^+} / C_{Na^+}$) by a power law having the form,

$$\frac{\overline{C}_{pep}}{C_{pep}} = \left(\frac{\overline{C}_{Na^+}}{C_{Na^+}} \right)^Z \tag{2}$$

where Z is the net charge of Pf-pep, $\overline{C}_i$ is the intratissue concentration (mole per liter of intratissue water) and C_i is the bath concentration of the i^{th} species (see details of the theoretical model in the Appendix). By combining the laws of Boltzmann equilibrium and electroneutrality, we calculated the Donnan partitioning of bath Na^+ ions using the measured GAG density of each specimen (see Eq. A.5). The partition coefficient of ^{125}I-Pf-pep was assumed to be equal to the measured uptake ratio in Fig. 2.3. That is, all the radioactivity within the disks was assumed to be free (not bound) and assumed to be able to partition according to the Donnan equilibrium. Fig. 2.4 shows a plot of the calculated partition coefficients of ^{125}I-Pf-pep versus that of Na^+ for each individual cartilage disk; the solid lines are predicted theoretical curves for Pf-pep charge $Z = 1$ through $Z = 4$. To calculate the net charge of Pf-pep from these data, the partition coefficients of ^{125}I-Pf-pep and Na^+ were inserted into Eq. (2) and a robust nonlinear least squares method (MATLAB) was used to calculate the best fit value of Z; the bisquare function was used as the weighting function to reduce the effect of outliers. The resulting best fit $Z = +2.87$ ($r^2 = 0.763$) corresponds well to the known charge of the trivalent peptide, $Z = +3$, and is consistent with the assumption of Donnan partitioning and the assumption that all intratissue radioactivity is mobile and thus does not bind to sites that immobilize radioactive counts.

To further test the role of electrostatic interactions between the small peptide inhibitor and cartilage ECM, we examined the effect of loss of tissue GAG or screening GAG charge on the uptake of ^{125}I-Pf-pep into newborn bovine calf cartilage L2 disks. For GAG depletion studies, disks were incubated for 24 hours with 0.1 mg/ml trypsin at 4°C prior to the measurement of uptake of ^{125}I-Pf-pep. This trypsin treatment removed approximately 60% of the GAG from these L2 disks. For studies of the effects of charge screening, the NaCl concentration of the bath was increased to 1M at neutral pH [33]. Treated and control disks were then equilibrated with Pf-pep for 48-hours. Untreated control disks equilibrated in physiologic ionic strength (0.15M NaCl) showed significantly higher uptake of ^{125}I-Pf-pep than that observed in either trypsin-treated explants in 0.15M NaCl or untreated explants in 1M NaCl bath (Fig. 2.5, data shown for L2 disks, 1-way ANOVA post hoc Dunnett's test, vs. control group "FS, 0.15 M", $p<0.0001$), indicating that electrostatic interactions between Pf-pep and ECM are primarily responsible for the enhanced uptake.

Diffusive transport of ^{125}I-Pf-pep across adult bovine cartilage. Using the transport cell arrangement of Fig. 2.1b, the diffusive flux of ^{125}I-Pf-pep within and across disks of adult bovine cartilage was measured in order to estimate the diffusivity of Pf-pep within cartilage ECM (Fig. 2.6). At time $t \sim 50$ min, ^{125}I-Pf-pep was introduced into the upstream bath, and, with rapid mixing, a concentration gradient was quickly established across the disks. Previous studies have shown that binding of solutes to sites within cartilage in this geometry can dramatically slow transport across the disks and into the downstream bath, consistent with a significant decrease in the solute's effective diffusivity. In contrast, in the absence of binding, the concentration gradient of Pf-pep across cartilage slices between the two compartments of Fig. 2.6 would generate only passive diffusive flux of ^{125}I-Pf-pep through cartilage, and a more

rapid emergence of the solute into the downstream bath. A typical result showing transport of ^{125}I-Pf-pep across a group of three cartilage disks is shown in Fig. 2.6; the measured downstream concentration of ^{125}I-Pf-pep was normalized to the upstream concentration. After an initial lag time of ~10 minutes, the slope from $t \sim 60$ minutes to $t \sim 720$ minutes represents the steady state flux of ^{125}I-Pf-pep.

The data of Fig. 2.6 were used to estimate the intratissue diffusivity of ^{125}I-Pf-pep using established methods [18]. Since the upstream concentration of ^{125}I-Pf-pep is much higher than the downstream concentration during the initial ~700 minutes in Fig. 2.6, the steady-state flux, Γ, of ^{125}I-Pf-pep across the cartilage disks is given by,

$$\Gamma = \phi KD\frac{C_U - C_D}{\delta} \cong \phi KD\frac{C_U}{\delta} \tag{3}$$

where ϕ is the tissue porosity, K is the partition coefficient, D is the diffusivity, C_U is the upstream concentration, C_D is the downstream concentration, and δ is the average thickness of the three tissue disks. The time derivative (slope) of the normalized downstream concentration (C_D/C_U) can be related to the steady-state flux by,

$$\frac{\partial}{\partial t}\left(\frac{C_D}{C_U}\right) = \frac{A\Gamma}{V_{DS}C_U} \cong \frac{\phi KDA}{\delta V_{DS}} \tag{4}$$

where A is the total exposed area of the cartilage-disks, and V_{DS} is the volume of downstream bath. The diffusivity was thereby calculated from the steady-state flux using Eq. (4) [18].

The presence of mobile ^{125}I that may have accumulated during a diffusion experiment would artifactually increase the estimated tracer flux into the downstream bath and thereby alter the estimate of the diffusivity of ^{125}I-Pf-pep [27]. Sephadex G10 chromatography showed that small labeled species (i.e., ^{125}I) constituted less than 10% of total radioactivity of the bath (data not shown). In addition, when ^{125}I was directly added to the upstream bath near the end of

the experiment (e.g., at $t \simeq 980$ minutes in Fig. 2.6), the steeper slope observed immediately after addition of ^{125}I gave a direct measurement of the effect of a known amount of ^{125}I on the calculated flux and the resulting diffusivity. (The diffusivity of ^{125}I was independently measured to be ~ 3×10^{-6} cm^2/s). These results were combined with the independently measured partition coefficient of ^{125}I-Pf-pep (and unbound ^{125}I) to give a final estimate of the diffusivity of Pf-pep, using methods described previously [27]. The diffusion coefficients for L1 and L2 disks were 1.6×10^{-6} cm^2/s and 0.95×10^{-6} cm^2/s, respectively.

Finally, given an estimate of the diffusivity of Pf-pep, we can estimate the time needed to reach equilibrium in the uptake experiments of Figs. 2.2-5. The characteristic time constant τ for 1-dimensional diffusion of a solute into a disk of thickness δ given by $\delta^2/(\pi^2 D)$, where δ is the disk thickness and D is the solute diffusivity [34]. Using a value of D measured in L1 and L2 disks ~ 1×10^{-6} cm^2/s and δ = 400 μm, the calculated diffusion time constant is τ ~ 2.7 min, and diffusion equilibrium would be attained by 3-5 time constants [34]. Therefore, in the uptake experiments of Figs. 2.2-5, the concentration of Pf-pep within the tissue would certainly reach equilibrium by 24-48 hours.

2.4 Discussion

The results of this study indicate that Pf-pep, a small positively charged peptide inhibitor of PACE4, did not show measurable binding to the negatively charged GAG chains in cartilage; however, charge-charge interactions were critically important in determining the intratissue distribution of Pf-pep, which had a higher concentration in the tissue compared to

the bath. Partitioning correlated significantly with tissue GAG density, supporting a major role for matrix composition in the uptake of Pf-pep.

The equilibrium distribution of Pf-pep between cartilage and the surrounding bath followed Donnan equilibrium (Fig. 2.4), which resulted in a partition coefficient $K > 1$ (Fig. 2.2). This enhanced uptake of Pf-pep was associated with tissue GAG density (Fig. 2.3a), but was not due to intratissue binding (Fig. 2.2). The uptake of Pf-pep was lower in the surface zone (L1) than deeper (L2) tissue (Fig. 2.2), consistent with the lower GAG density and higher hydration of L1 tissue (Fig. 2.3). One caveat in comparing the uptake ratio in L1 and L2 is that L2 disks have one more cut surface than L1 tissue, which could affect the uptake ratio due to altered tissue hydration. Eisenberg [35] measured the swelling properties of middle zone (L2) adult bovine femoropatellar groove cartilage by changing the ionic strength of the bath, and found that this tissue showed minimal (< 3%) changes in swelling under hypotonic conditions (0.01M NaCl). This suggests that the additional cut surface of L2 disks would likely not affect tissue hydration.

Furthermore, depletion of GAG and the concomitant lowering of tissue fixed charge density following trypsin treatment dramatically decreased uptake of Pf-pep (Fig. 2.5), which is notable since trypsin treatment has been used to mimic certain aspects of cartilage degradation [36-40]. Taken together, we suggest that there would be less uptake of Pf-pep in areas of cartilage undergoing aggrecan loss as observed in OA. Compared to normal cartilage, OA cartilage has lower GAG content and higher hydration than healthy tissue [32], especially in the superficial zone. Thus, the beneficial effect of electrostatic interactions on uptake of Pf-pep would be lessened with progression of disease.

While uptake of this 760 Da peptide appeared dominated by Donnan equilibrium, steric exclusion may also be important to consider as the size of the solute increases. Maroudas included the effects of steric exclusion for larger solutes by incorporating Ogston's theory for the partitioning of spherical molecules into a hydrated matrix of linear fibers [41-44]. Based on the values of the solute radius and inter-fiber spacing, Ogston's theory would predict a decrease in the partition coefficient of a given neutral solute with increasing cartilage GAG density, rather than the increase in partition coefficient with GAG density observed here for Pf-pep. Modeling of the combined effects of steric exclusion and electrostatic partitioning for charged solutes has not been well studied in cartilage. For the general case of charged gels, Johnson and Deen extended Ogston's model by introducing a Boltzmann factor for the electrostatic partitioning of a spherical charged solute within a charged fiber matrix [45]. Using this model, ongoing studies are focused on including the role of excluded volume on intratissue partitioning of solutes having a range of effective radii.

In the absence of binding interactions, non-equilibrium transport of smaller solutes (e.g., Pf-pep) across cartilage is dominated by passive diffusion (Fig. 2.6). The characteristic time lag, τ, for diffusive penetrating into a tissue of thickness, L, is $\tau = L^2/6D$ [34], where D is the solute diffusivity. Using a value of D on the order of that measured in L2 tissue ($\sim 1\times10^{-6}$ cm^2/s), $\tau \sim 27$ min for $L = 1$mm. This is consistent with the order of magnitude time lag observed in Fig. 2.6 (~10 min) starting after the addition of Pf-pep at $t \sim 50$ min. Thus, Pf-pep can quickly diffuse into the cartilage, which would be a desired property for an intra-articular OA therapeutic. However, when a therapeutic agent is introduced into the synovial fluid and is intended for targets within cartilage, the synovial fluid concentration must be maintained to enable accumulation of the agent at its needed concentration within the tissue. If clearance from

the synovial fluid by the circulation is rapid [46], and the agent does not bind to sites and thereby remain at high enough concentration near the intended target (e.g., cell receptors, proteases or in the present case, PACE4), then such a small solute could quickly diffuse out of the cartilage without a sustained inward concentration gradient. For example, intra-articularly injected small non-steroidal anti-inflammatory drugs such as paracetamol (151 Da), diclofenac (296 Da), and salicylate (413 Da), were cleared from synovial fluid in 1-5 hrs; the rate of clearance depended on the size of molecules and their binding to albumin [47]. For comparison, the diffusive loss of Pf-pep from cartilage can be predicted using the estimated diffusivity (Fig. 2.6), which would then motivate the choice of an appropriate dosing frequency for intra-articular therapy. Assuming that the thickness of cartilage is of order ~1 mm, and that a ~10 mM concentration of Pf-pep could be quickly achieved in the cartilage after an initial intra-articular dose, the intratissue concentration of Pf-pep would fall below the IC_{50} of 2 μM by ~10 hrs, suggesting that daily treatment would be necessary. For Pf-pep, the effect of its positive charge was limited to enhancing partitioning (Fig. 2.2), but not to altered diffusive transport rates (Fig. 2.6) since Pf-pep did not bind to GAG chains. While the absence of binding to GAGs or other non-specific sites beneficial for achieving fast inward diffusion, there would be no long-term "sustained delivery" from such intratissue binding sites to the desired intratissue target (e.g., PACE4).

The diffusivity of ^{125}I-Pf-pep (~1×10^{-6} cm^2/s) was consistent with values found previously for similarly sized small molecules. For example, diffusivities of ^{3}H-thymidine (242 Da), ^{3}H-L696,418 (476 Da) and ^{3}H-raffinose (594 Da), in adult bovine cartilage were 3.2×10^{-6} cm^2/s, 0.72×10^{-6} cm^2/s and 2.9×10^{-6} cm^2/s, respectively [29]. It is well documented that the intratissue diffusivity of large solutes in cartilage is greatly affected by GAG density which, in

turn, is a function of tissue depth [42, 48], static compression [16, 49-51], and enzymatic degradation [36, 52, 53]. While fluid convection caused by dynamic compression is also well known to affect the transport of large solutes, diffusive transport dominates convection for small solutes [29, 54-56]. There is mixed evidence on the dependence of small solute diffusivity on the matrix density. Diffusivities of urea (60 Da) and glucose (180 Da) did not vary significantly with tissue depth [42]; static compression, however, which increases solid volume fraction, reduced the diffusivities of Na^+ and SO_4^{2-} ions [16] and tetramethylrhodamine (TMR, 430 Da) [49, 50]. Removal of proteoglycans using trypsin did not affect the diffusion coefficient of glucose [36], but did change that of gadolinium-DTPA (530 Da) [39]. These differences may be associated with the different methods used in these various studies. It is possible, therefore, that the diffusivity of Pf-pep could also be affected by changes in matrix density associated with compositional variations, compression or degradation.

Our diffusion experiments were carried out at room temperature for practical reasons: since the diffusion chamber was connected to a large flow-through gamma detector, it would be extremely difficult to control the temperature of the entire setup at 37°C. In order to calculate the diffusivity that would be found at 37°C, several previous investigators have found that the Stokes-Einstein relation gives an appropriate estimate for the effects of temperature on diffusivity in this temperature range [57, 58]. Assuming that intratissue diffusion of Pf-pep follows the Stokes-Einstein relation, the diffusion coefficient of Pf-pep would increase by a factor of ~1.4.

In summary, our results with Pf-pep suggest that a small, positively charged molecule will have a higher concentration within cartilage than in the surrounding synovial fluid; however, they may not be retained within the tissue unless there is additional specific binding

to intratissue substrates that can maintain enhanced concentration. Since small non-binding solutes have a higher diffusivity, such solutes can quickly penetrate and diffuse into cartilage and achieve an intratissue concentration that is enhanced by Donnan partitioning. However, they can also diffuse back out to the synovial fluid at the same rate due to nonequilibrium diffusion unless their intratissue concentration is maintained. Extensive loss of negatively charged GAG chains due to OA can lead to the loss of enhanced uptake of a positively charged therapeutic, even though such GAG loss, along with increased tissue hydration, would increase solute diffusivity.

2.5 Figures

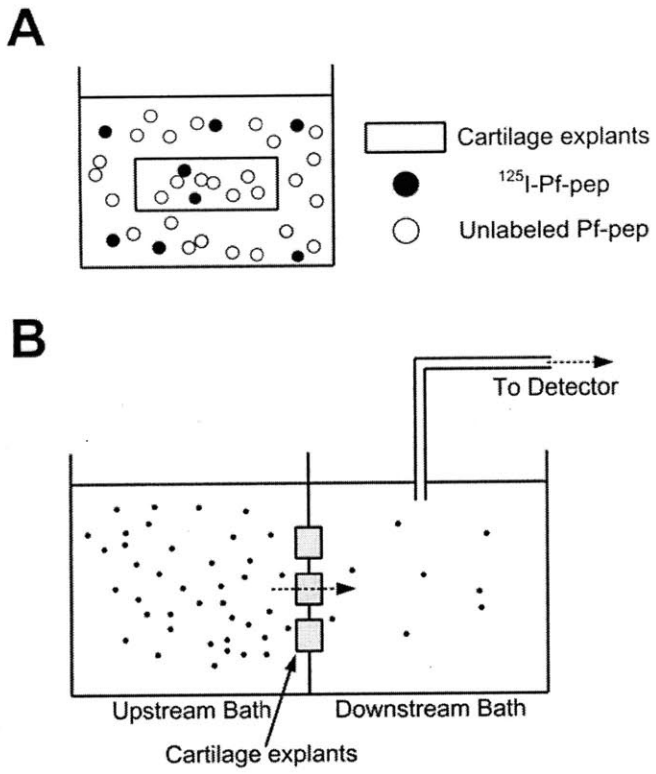

Figure 2.1 (a) Schematic diagram showing incubation of cartilage explants with labeled and unlabeled Pf-pep in the bath. (b) Transport chamber consisting of two compartments, upstream bath and downstream bath. Solutes only could transport through three 9-mm diameter cartilage slices clamped between two compartments. The downstream bath was recirculated through the detector to measure the radioactivity of downstream in real-time.

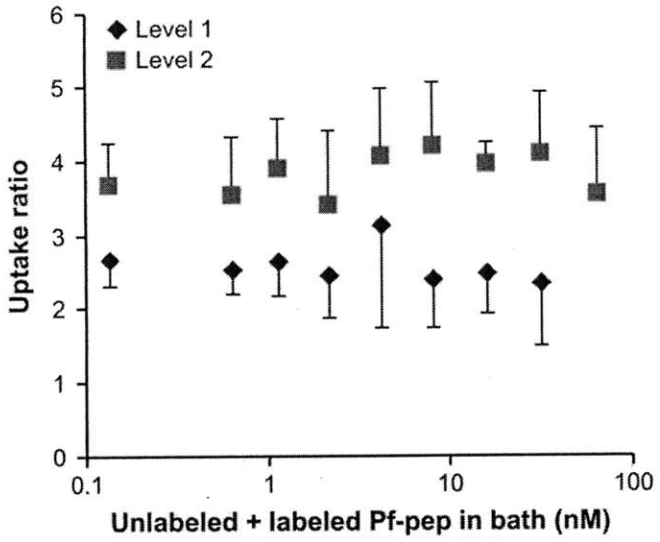

Figure 2.2 Concentration-dependent uptake ratio of ^{125}I-Pf-pep in adult bovine cartilage after 48 hr at 4°C in 1×PBS buffer. Graded amount of unlabeled Pf-pep was added with fixed amount of ^{125}I-Pf-pep (< 1 nM). The uptake ratio of ^{125}I-Pf-pep did not vary significantly with the concentration of unlabeled Pf-pep over the entire range of concentration for both L1 and L2 tissue (1-way ANOVA, $p = 0.825$ with L1, $p = 0.831$ with L2). The uptake of ^{125}I-Pf-pep was significantly higher in L2 compared to L1 cartilage overall (2-way ANOVA, $p < 0.0001$). Mean ± SD (n = 4 disks per condition)

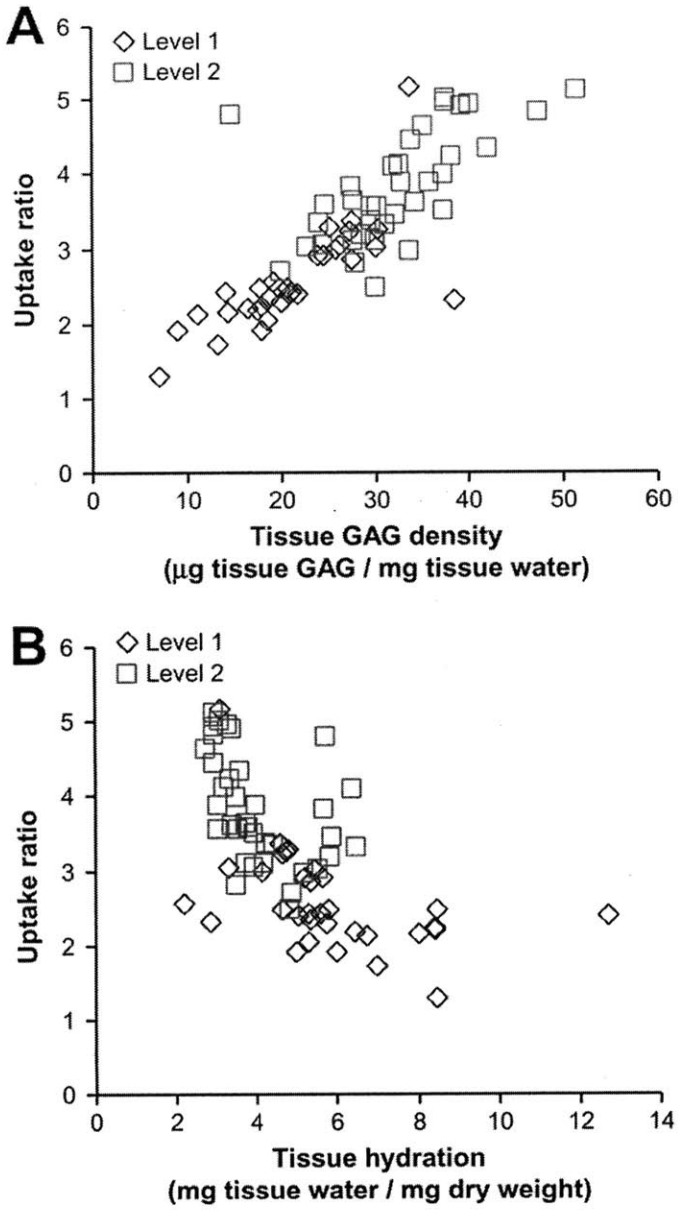

Figure 2.3 Dependence of the uptake ratio of ^{125}I-Pf-pep on (a) tissue GAG density (µg GAG content / mg tissue water) and (b) tissue hydration (mg tissue water / mg dry weight). Uptake of ^{125}I-Pf-pep increased with increasing tissue sGAG content and with decreasing tissue hydration (linear regression, $p < 0.0001$). Cartilage from the deeper region (L2) generally had higher GAG density (t-test, $p < 0.0001$) and lower hydration (t-test, $p = 0.00016$) than L1 tissue. Each data point represents one of the 68 cartilage specimens that comprise the data-set of Fig. 2.2.

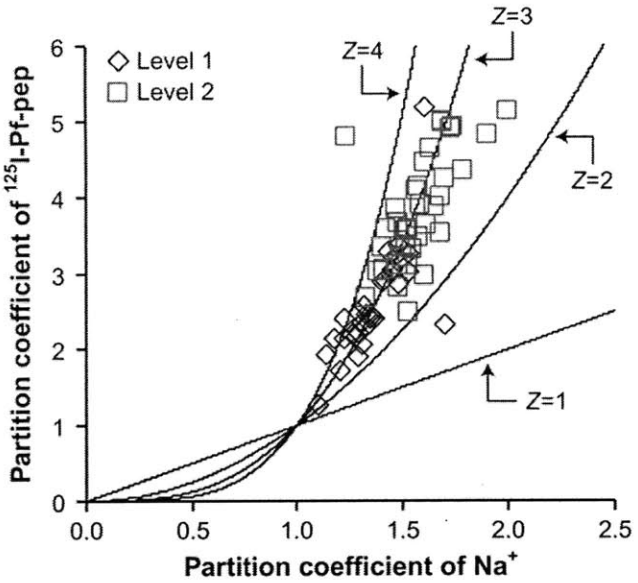

Figure 2.4 Estimate of the net charge (Z) of Pf-pep using Donnan equilibrium theory. Donnan theory predicts that the partition coefficient of ^{125}I-Pf-pep will follow the power-law relation with the partition coefficient of Na^+ by the exponent Z. The partition coefficient of Na^+ was calculated from the measured GAG density of each individual specimen (A.5) and the partition coefficient of ^{125}I-Pf-pep was assumed to be equal to the measured uptake ratio in Fig 2.3. The solid lines are the predicted theoretical curves for Pf-pep charge (Z = 1-4). The best fit value of Z was + 2.87, which corresponds well to the known charge of Pf-pep (+3). Each data point represents one of the 68 cartilage specimens that comprise the data-set of Fig. 2.2.

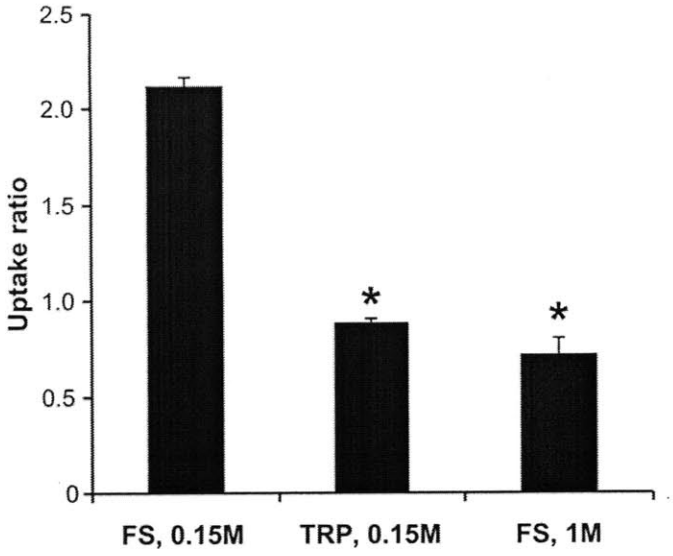

Figure 2.5 Effects of trypsin depletion of GAG (TRP, 0.15M NaCl) or screening of GAG electrostatic interactions (FS, 1M NaCl) on the uptake of ^{125}I-Pf-pep in L2 bovine calf cartilage disks. Untreated control disks in physiological ionic strength (FS, 0.15M NaCl) showed significantly higher partition coefficients compared to the two treated groups (*$p<0.0001$ by 1-way ANOVA post hoc Dunnett's test, vs. control group "FS, 0.15 M"). Mean ± SEM (n = 3 disks per condition)

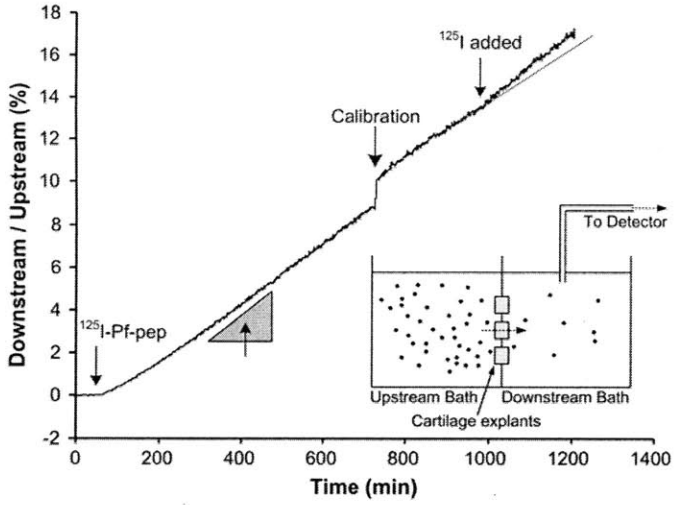

Figure 2.6 Non-equilibrium diffusion of ^{125}I-Pf-pep across groups of three adult bovine cartilage disks (data shown for L1 disks), plotted as the measured downstream concentration versus time, normalized to the applied upstream concentration. At t = 50 minutes, ^{125}I-Pf-pep was introduced to the upstream bath. The diffusivity of Pf-pep was calculated from the measured diffusive flux of ^{125}I-Pf-pep (i.e., the slope of the concentration vs. time data as shown). At t = 728 minutes, a 300 µl aliquot from the upstream bath (20 ml) was transferred to the downstream bath (20 ml) to calibrate the concentration. At t = 980 minutes, unbound ^{125}I was added to the upstream bath to estimate the contribution of unbound ^{125}I to the total flux and to correct for the presence of such ^{125}I in the calculated diffusivity of ^{125}I-Pf-pep. The solid line at the end of experiment shows the predicted flux which would be present if ^{125}I were not added.

2.6 References

[1] Malfait AM, Arner EC, Song RH, Alston JT, Markosyan S, Staten N, Yang Z, Griggs DW, Tortorella MD. Proprotein convertase activation of aggrecanases in cartilage in situ. Arch Biochem Biophys 2008;478:43-51.
[2] Tortorella MD, Burn TC, Pratta MA, Abbaszade I, Hollis JM, Liu R, Rosenfeld SA, Copeland RA, Decicco CP, Wynn R, Rockwell A, Yang F, Duke JL, Solomon K, George H, Bruckner R, Nagase H, Itoh Y, Ellis DM, Ross H, Wiswall BH, Murphy K, Hillman MC, Jr., Hollis GF, Newton RC, Magolda RL, Trzaskos JM, Arner EC. Purification and cloning of aggrecanase-1: a member of the ADAMTS family of proteins. Science 1999;284:1664-6.
[3] Abbaszade I, Liu RQ, Yang F, Rosenfeld SA, Ross OH, Link JR, Ellis DM, Tortorella MD, Pratta MA, Hollis JM, Wynn R, Duke JL, George HJ, Hillman MC, Jr., Murphy K, Wiswall BH, Copeland RA, Decicco CP, Bruckner R, Nagase H, Itoh Y, Newton RC, Magolda RL, Trzaskos JM, Hollis GF, Arner EC, Burn TC. Cloning and characterization of ADAMTS11, an aggrecanase from the ADAMTS family. J Biol Chem 1999;274:23443-50.
[4] Tortorella MD, Arner EC, Hills R, Gormley J, Fok K, Pegg L, Munie G, Malfait AM. ADAMTS-4 (aggrecanase-1): N-terminal activation mechanisms. Arch Biochem Biophys 2005;444:34-44.
[5] Wang P, Tortorella M, England K, Malfait AM, Thomas G, Arner EC, Pei D. Proprotein convertase furin interacts with and cleaves pro-ADAMTS4 (Aggrecanase-1) in the trans-Golgi network. J Biol Chem 2004;279:15434-40.
[6] Caterson B, Flannery CR, Hughes CE, Little CB. Mechanisms involved in cartilage proteoglycan catabolism. Matrix Biol 2000;19:333-44.
[7] Tortorella MD, Pratta M, Liu RQ, Austin J, Ross OH, Abbaszade I, Burn T, Arner E. Sites of aggrecan cleavage by recombinant human aggrecanase-1 (ADAMTS-4). J Biol Chem 2000;275:18566-73.
[8] Lark MW, Gordy JT, Weidner JR, Ayala J, Kimura JH, Williams HR, Mumford RA, Flannery CR, Carlson SS, Iwata M, Sandy JD. Cell-mediated catabolism of aggrecan. Evidence that cleavage at the "aggrecanase" site (Glu373-Ala374) is a primary event in proteolysis of the interglobular domain. J Biol Chem 1995;270:2550-6.
[9] Arner EC, Hughes CE, Decicco CP, Caterson B, Tortorella MD. Cytokine-induced cartilage proteoglycan degradation is mediated by aggrecanase. Osteoarthr Cartilage 1998;6:214-28.
[10] Sandy JD, Flannery CR, Neame PJ, Lohmander LS. The structure of aggrecan fragments in human synovial fluid. Evidence for the involvement in osteoarthritis of a novel proteinase which cleaves the Glu 373-Ala 374 bond of the interglobular domain. J Clin Invest 1992;89:1512-6.
[11] Lohmander LS, Neame PJ, Sandy JD. The structure of aggrecan fragments in human synovial fluid. Evidence that aggrecanase mediates cartilage degradation in inflammatory joint disease, joint injury, and osteoarthritis. Arthritis Rheum 1993;36:1214-22.
[12] Glasson SS, Askew R, Sheppard B, Carito B, Blanchet T, Ma HL, Flannery CR, Peluso D, Kanki K, Yang Z, Majumdar MK, Morris EA. Deletion of active ADAMTS5 prevents cartilage degradation in a murine model of osteoarthritis. Nature 2005;434:644-8.
[13] Maroudas A. Physicochemical properties of cartilage in light of ion exchange theory. Biophys J 1968;8:575-95.

[14] Buckwalter JA, Mankin HJ, Grodzinsky AJ. Articular cartilage and osteoarthritis. Instr Course Lect 2005;54:465-80.
[15] Maroudas A. Physicochemical properties of articular cartilage. 2nd ed., Pitman, Tunbridge Well, England, 1979.
[16] Nimer E, Schneiderman R, Maroudas A. Diffusion and partition of solutes in cartilage under static load. Biophys Chem 2003;106:125-46.
[17] Schneiderman R, Snir E, Popper O, Hiss J, Stein H, Maroudas A. Insulin-like growth factor-I and its complexes in normal human articular cartilage: Studies of partition and diffusion. Arch Biochem Biophys 1995;324:159-72.
[18] Garcia AM, Szasz N, Trippel SB, Morales TI, Grodzinsky AJ, Frank EH. Transport and binding of insulin-like growth factor I through articular cartilage. Arch Biochem Biophys 2003;415:69-79.
[19] Tokunou T, Miller R, Patwari P, Davis ME, Segers VF, Grodzinsky AJ, Lee RT. Engineering insulin-like growth factor-1 for local delivery. Faseb J 2008;22:1886-93.
[20] Miller R, Grodzinsky AJ, Cummings K, Lee RT, Patwari P. Intra-articular injection of HB-IGF-1 sustains delivery of IGF-1 to cartilage through binding to chondroitin sulfate. 56th Annual Meeting of the Orthopaedic Research Society, New Orleans, LA. March 6–9, 2010.
[21] van den Berg WB, van de Putte LBA, Zwarts WA, Joosten LA. Electrical charge of the antigen determines intraarticular antigen handling and chronicity of arthritis in mice. J Clin Invest 1984;74:1850-9.
[22] van den Berg WB, van de Putte LBA. Electrical charge of the antigen determines its localization in the mouse knee joint deep penetration of cationic bovine serum albumin in hyaline articular cartilage. Am J Pathol 1985;121:224-34.
[23] van den Berg WB, van Lent PLEM, van de Putte LBA, Zwarts WA. Electrical charge of hyaline articular cartilage: its role in the retention of anionic and cationic proteins. Clin Immunol Immunopathol 1986;39:187-97.
[24] Bhakta NR, Garcia AM, Frank EH, Grodzinsky AJ, Morales TI. The insulin-like growth factors (IGFs) I and II bind to articular cartilage via the IGF-binding proteins. J Biol Chem 2000;275:5860-6.
[25] Bennett GL, Horuk R. Iodination of chemokines for use in receptor binding analysis. Methods Enzymol 1997;288:134-48.
[26] Sah RLY, Kim YJ, Doong JYH, Grodzinsky AJ, Plaas AHK, Sandy JD. Biosynthetic response of cartilage explants to dynamic compression. J Orthop Res 1989;7:619-36.
[27] Garcia AM, Lark MW, Trippel SB, Grodzinsky AJ. Transport of tissue inhibitor of metalloproteinases-1 through cartilage: contributions of fluid flow and electrical migration. J Orthop Res 1998;16:734-42.
[28] Nussbaum JH, Grodzinsky AJ. Proton diffusion reaction in a protein poly-electrolyte membrane and the kinetics of electro-mechanical forces. J Membrane Sci 1981;8:193-219.
[29] Garcia AM, Frank EH, Grimshaw PE, Grodzinsky AJ. Contributions of fluid convection and electrical migration to transport in cartilage: Relevance to loading. Arch Biochem Biophys 1996;333:317-25.
[30] Maroudas A, Bullough P, Swanson SAV, Freeman MAR. The Permeability of Articular Cartilage Human. J Bone Joint Surg Br 1968;50B:166-77.
[31] Basser PJ, Schneiderman R, Bank RA, Wachtel E, Maroudas A. Mechanical properties of the collagen network in human articular cartilage as measured by osmotic stress technique. Arch Biochem Biophys 1998;351:207-19.

[32] Venn M, Maroudas A. Chemical composition and swelling of normal and osteoarthrotic femoral-head cartilage. 1. Chemical composition. Ann Rheum Dis 1977;36:121-9.
[33] Frank EH, Grodzinsky AJ. Cartilage electromechanics. 1. Electrokinetic transduction and the effects of electrolyte pH and ionic-strength. J Biomech 1987;20:615-27.
[34] Crank J. The mathematics of diffusion. 2nd ed., Clarendon Press, Oxford, 1979.
[35] Eisenberg SR, Grodzinsky AJ. Swelling of articular-cartilage and other connective tissues: electromechanochemical forces. J Orthop Res 1985;3:148-59.
[36] Torzilli PA, Arduino JM, Gregory JD, Bansal M. Effect of proteoglycan removal on solute mobility in articular cartilage. J Biomech 1997;30:895-902.
[37] Frank EH, Grodzinsky AJ, Koob TJ, Eyre DR. Streaming potentials: a sensitive index of enzymatic degradation in articular cartilage. J Orthop Res 1987;5:497-508.
[38] Burstein D, Gray ML, Hartman AL, Gipe R, Foy BD. Diffusion of small solutes in cartilage as measured by nuclear-magnetic-resonance (NMR) spectroscopy and imaging. J Orthop Res 1993;11:465-78.
[39] Foy BD, Blake J. Diffusion of paramagnetically labeled proteins in cartilage: Enhancement of the 1-D NMR imaging technique. J Magn Reson 2001;148:126-34.
[40] Xia Y, Farquhar T, Burtonwurster N, Verniersinger M, Lust G, Jelinski LW. Self-diffusion monitors degraded cartilage. Arch Biochem Biophys 1995;323:323-8.
[41] Maroudas A. Biophysical chemistry of cartilaginous tissues with special reference to solute and fluid transport. Biorheology 1975;12:233-48.
[42] Maroudas A. Distribution and diffusion of solutes in articular cartilage. Biophys J 1970;10:365-79.
[43] Maroudas A. Transport of solutes through cartilage: permeability to large molecules. J Anat 1976;122:335-47.
[44] Ogston AG. The spaces in a uniform random suspension of fibres. Trans Faraday Soc 1958;54:1754-7.
[45] Johnson EM, Deen WM. Electrostatic effects on the equilibrium partitioning of spherical colloids in random fibrous media. J Colloid Interf Sci 1996;178:749-56.
[46] Simkin PA, Nilson KL. Trans-synovial exchange of large and small molecules. Clin Rheum Dis 1981;7:99-129.
[47] Owen SG, Francis HW, Roberts MS. Disappearance kinetics of solutes from synovial fluid after intra-articular injection. Br J Clin Pharmacol 1994;38:349-55.
[48] Leddy HA, Guilak F. Site-specific molecular diffusion in articular cartilage measured using fluorescence recovery after photobleaching. Ann Biomed Eng 2003;31:753-60.
[49] Quinn TM, Kocian P, Meister JJ. Static compression is associated with decreased diffusivity of dextrans in cartilage explants. Arch Biochem Biophys 2000;384:327-34.
[50] Quinn TM, Morel V, Meister JJ. Static compression of articular cartilage can reduce solute diffusivity and partitioning: implications for the chondrocyte biological response. J Biomech 2001;34:1463-9.
[51] Evans RC, Quinn TM. Solute diffusivity correlates with mechanical properties and matrix density of compressed articular cartilage. Arch Biochem Biophys 2005;442:1-10.
[52] Lotke PA, Granda JL. Alterations in the permeability of articular cartilage by proteolytic enzymes. Arthritis Rheum 1972;15:302-8.
[53] Lotke PA, Granda JL. Changes in the permeability of human articular cartilage in early degenerative osteoarthritis. Surg Forum 1971;22:449-50.

[54] Evans RC, Quinn TM. Solute convection in dynamically compressed cartilage. J Biomech 2006;39:1048-55.
[55] Evans RC, Quinn TM. Dynamic compression augments interstitial transport of a glucose-like solute in articular cartilage. Biophys J 2006;91:1541-7.
[56] O'hara BP, Urban JPG, Maroudas A. Influence of cyclic loading on the nutrition of articular cartilage. Ann Rheum Dis 1990;49:536-9.
[57] Torzilli PA. Effects of temperature, concentration and articular surface removal on transient solute diffusion in articular cartilage. Med Biol Eng Comput 1993;31:S93-S8.
[58] Serrat MA, Williams RM, Farnum CE. Temperature alters solute transport in growth plate cartilage measured by in vivo multiphoton microscopy. J Appl Physiol 2009;106:2016-25.
[59] Buschmann MD, Grodzinsky AJ. A molecular model of proteoglycan-associated electrostatic forces in cartilage mechanics. J Biomech Eng 1995;117:179-92.

2.7 Supplementary Data

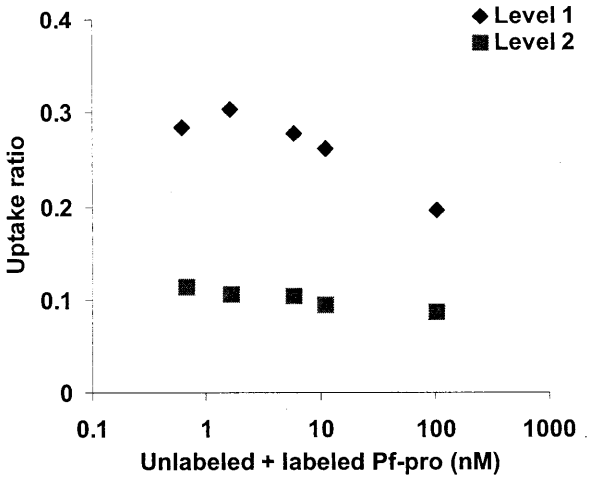

Figure 2S.1 Concentration-dependent uptake ratio of ^{125}I-Pf-pro (22 kDa, pI = 5.1) in adult bovine cartilage after 48 hr at 4°C in 1×PBS buffer. Graded amount of unlabeled Pf-pro was added with fixed amount of ^{125}I-Pf-pro (~ 0.6 nM). For each condition, disks (n = 7-8) were incubated in the same well and pooled together during radioactivity counting. Total radioactivity and total mass from pooled disks were collected to calculate uptake ratio. The uptake ratio of ^{125}I-Pf-pro did not vary significantly with the concentration of unlabeled Pf-pro over the entire range of concentration for L2 tissue. The uptake ratio in L1 decreased with increasing amount of unlabeled Pf-pro. The uptake of ^{125}I-Pf-pro was lower in L2 compared to L1 cartilage overall.

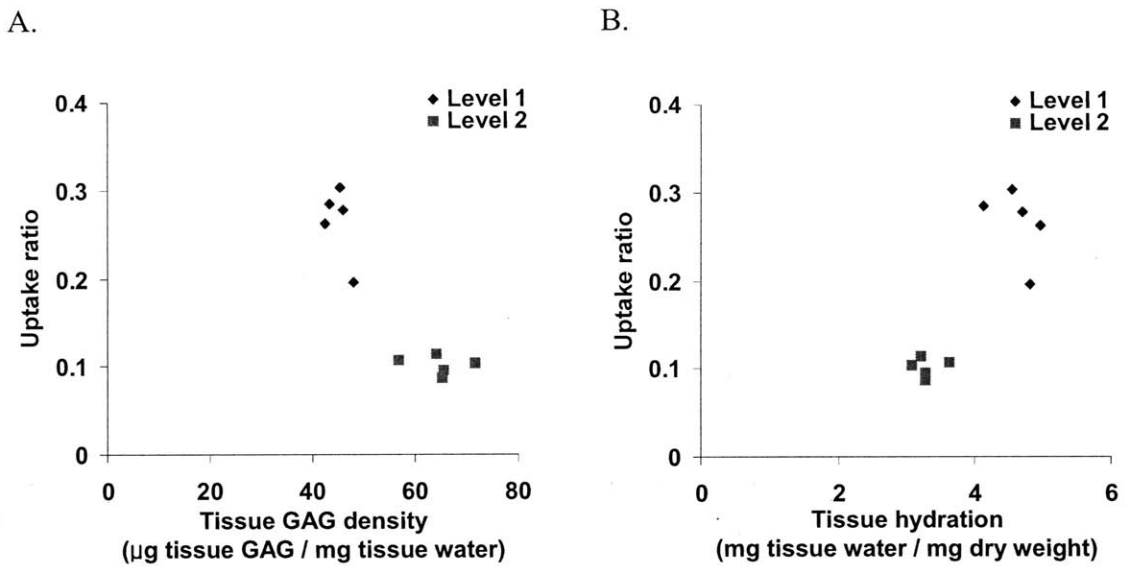

Figure 2S.2 Dependence of the uptake ratio of ^{125}I-Pf-pro (22 kDa, pI = 5.1) on (A) tissue GAG density (µg GAG content / mg tissue water) and (B) tissue hydration (mg tissue water / mg dry weight). Uptake of ^{125}I-Pf-pro decreased with increasing tissue sGAG content and with decreasing tissue hydration. Cartilage from the deeper region (L2) generally had higher GAG density and lower hydration than L1 tissue. Each data point represents one data point of Fig. 2S.1.

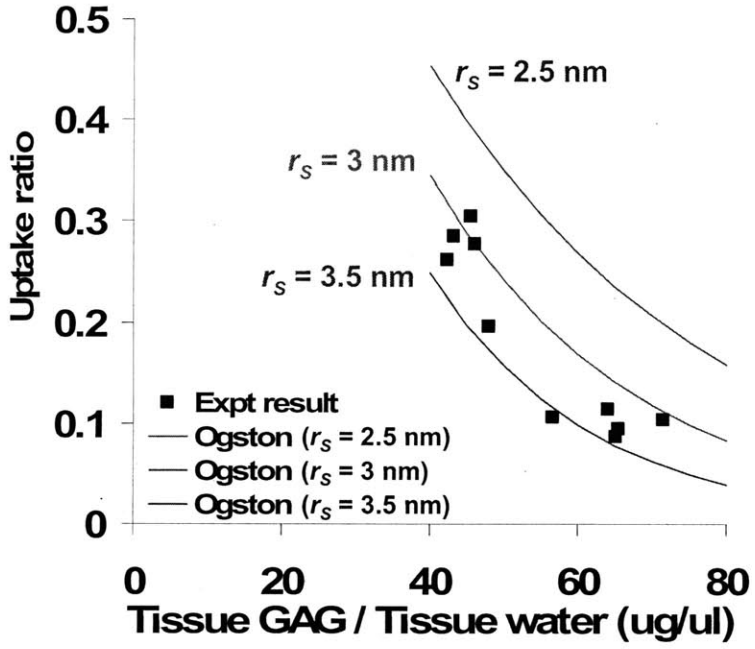

Figure 2S.3 Comparison of experimental results with Ogston's theory. Ogston's theory is based on the probability of finding space in uniform random suspension of fibers (Ogston, Trans Faraday Soc, 1958). Partition coefficient of Pf-pro, K_{Ogston}, given by Ogston is

$$K_{Ogston} = \exp\left[-\phi\left(1+\frac{r_s}{r_f}\right)^2\right],$$

where, Φ is fiber volume fraction, r_s is solute radius, and r_f is fiber radius. For this case, Φ can be regarded as PG volume fraction, which is given by (Total GAG ×Partial specific volume) / (Volume of extrafibrillar water) (Nimer, Biophys Chem, 2003). Total GAG was experimentally measured. We assumed that partial specific volume was 0.55 ml/g (Hascall, J Biol Chem, 1970). Volume of extrafibrillar water was given by (Volume of tissue water – Volume of intrafibrillar water), where intrafibrillar water = 1 g / g collagen (Maroudas, Biochim Biophys Acta, 1991). We assumed that r_f is 0.55 nm (Quinn, J Biomech, 2001). Since the radius of Pf-pro is not known, radii of similar sized molecules are used to define the range of r_s that we can plug into the model. For example, radii of SM22 (22 kDa; Lees-Miller, J Biol Chem, 1987), GFP (27 kDa; Terry, Biochem Bioph Res Co, 1995), and ovalbumin (45 kDa; Maroudas, J Anat, 1976) were 2.55 nm, 2.82 nm, and 2.8 nm, respectively.

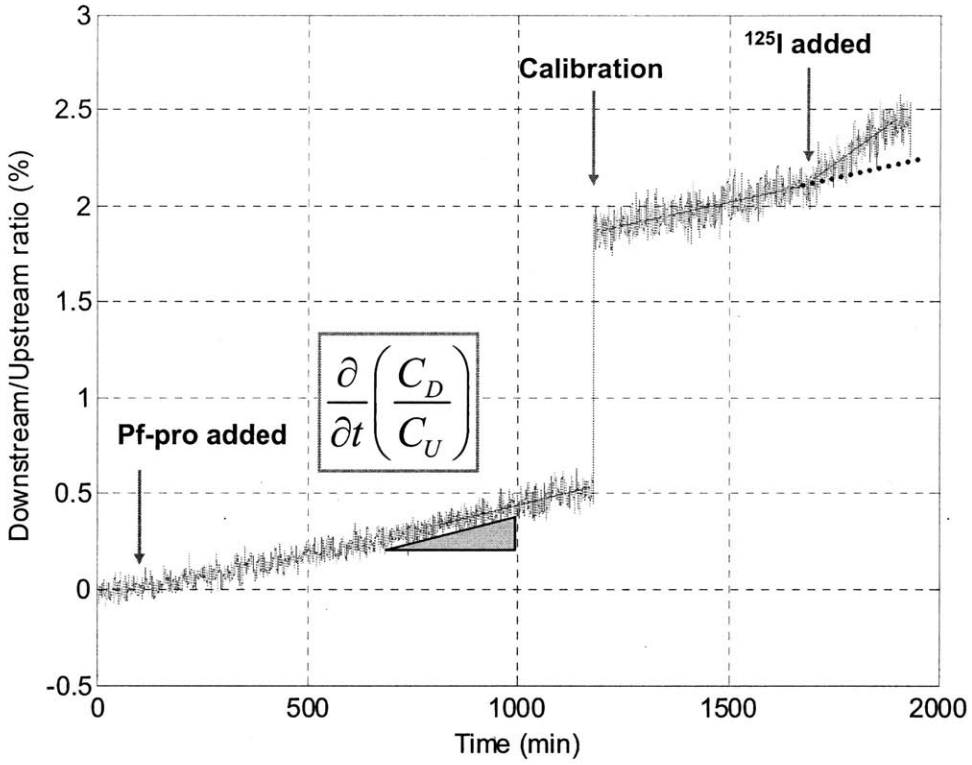

Figure 2S.4 Non-equilibrium diffusion of ^{125}I-Pf-pro (22 kDa, pI = 5.1) across groups of three adult bovine cartilage disks (data shown for L1 disks), plotted as the measured downstream concentration versus time, normalized to the applied upstream concentration. At t = 96 minutes, ^{125}I-Pf-pro was introduced to the upstream bath. The diffusivity of Pf-pro was calculated from the measured diffusive flux of ^{125}I-Pf-pro (i.e., the slope of the concentration vs. time data as shown). At t = 1179 minutes, a 300 µl aliquot from the upstream bath (20 ml) was transferred to the downstream bath (20 ml) to calibrate the concentration. At t = 1681 minutes, unbound ^{125}I was added to the upstream bath to estimate the contribution of unbound ^{125}I to the total flux and to correct for the presence of such ^{125}I in the calculated diffusivity of ^{125}I-Pf-ro. The solid line at the end of experiment shows the predicted flux which would be present if ^{125}I were not added. The diffusion coefficients for L1 disks was 0.82×10^{-8} cm^2/s.

2.8 Appendix

Donnan equilibrium predicts the distribution of Pf-pep with charge, Z, to be related to Na and Cl ion concentrations by,

$$\left(\frac{\overline{C}_{pep}}{C_{pep}}\right)^{\frac{1}{Z}} = \frac{\overline{C}_{Na^+}}{C_{Na^+}} = \frac{C_{Cl^-}}{\overline{C}_{Cl^-}}, \qquad \text{(A.1)}$$

where $\overline{C}_{pep}$, $\overline{C}_{Na^+}$, and $\overline{C}_{Cl^-}$ are intratissue concentration of Pf-pep, Na^+, and Cl^-, respectively, and C_{pep}, C_{Na^+}, and C_{Cl^-} are bath concentration of Pf-pep, Na^+, and Cl^-, respectively. Since the bath was PBS buffer with physiological ionic strength, the bath concentration of Na^+ and Cl^- are given by

$$C_0 = C_{Na^+} = C_{Cl^-} = 0.15\ M\,. \qquad \text{(A.2)}$$

Charge neutrality requires the sum of all charges becomes net zero as given by

$$\rho + \overline{C}_{Na^+} - \overline{C}_{Cl^-} + \overline{C}_{pep} = 0\,, \qquad \text{(A.3)}$$

where ρ is the fixed charge density, which has a negative value in cartilage. We can safely neglect $\overline{C}_{pep}$ in Eq. (A. 3), since Pf-pep is a minor carrier compared to Na^+ or Cl^-. Combining Eq. (A. 1) and Eq. (A. 2) to eliminate $\overline{C}_{Cl^-}$ in Eq. (A. 3) gives

$$\rho + \overline{C}_{Na^+} - \frac{C_0^2}{\overline{C}_{Na^+}} = 0\,. \qquad \text{(A.4)}$$

Eq. (A. 4) is quadratic equation for $\overline{C}_{Na^+}$ and the solution is given by

$$\overline{C}_{Na^+} = \frac{-\rho + \sqrt{\rho^2 + 4C_0^2}}{2}, \qquad \text{(A.5)}$$

where only one solution is valid since $\overline{C}_{Na^+}$ cannot be negative. The charge density, ρ, can be converted from the GAG density by assuming −2 moles of charge per 1 mole of disaccharide unit in GAG chains. Then ρ (mol/L) is given by,

$$\rho = -2 \cdot \frac{\text{GAG content (μg)}}{MW_{GAG} \cdot \text{Tissue water (μl)}}, \tag{A.6}$$

where MW_{GAG} is 458 g/mol [59]. Rearranging Eq. (A.1) gives

$$Z = \frac{\log\left(\frac{\overline{C}_{pep}}{C_{pep}}\right)}{\log\left(\frac{\overline{C}_{Na^+}}{C_{Na^+}}\right)}, \tag{A.7}$$

and Z can be computed for individual explants using the known partition ratios on the right side of Eq. (A.7). The average value of Z calculated from the 68 explants was +3.07 ± 0.74 (SD). The best fit value of Z corresponding to the 68 specimen population was obtained from a robust nonlinear least squares method (MATLAB) used to iteratively calculate the value of Z which minimized the least squares error from an initial guess; the bisquare function was used to down weight large residuals. The resulting best fit was Z = +2.87 (r^2 = 0.763).

CHAPTER 3

Effects of Mechanical Injury and Exogenous Cytokines on Transport of Fab fragments into Articular Cartilage*

* This chapter is a manuscript in preparation for submission

3.1 Introduction

Articular cartilage is a load-bearing tissue found at the end of long bones within the synovial joints. Degradation of the extracellular matrix (ECM) of the articular cartilage is the key feature of osteoarthritis (OA) pathogenesis, which reflects an imbalance between the anabolic and catabolic activities of chondrocytes [1]. Traumatic joint injury is a major risk factor of development of secondary OA, though the mechanism by which the joint injury results in disease development is not fully understood. The pathomechanisms of traumatic injury leading to cartilage degeneration have been widely investigated using in vitro models including mechanical injury and exogenous cytokines [2-9]. Abnormal compressive loading resulted in tissue swelling, loss of proteoglycan, denatured collagen, decreasing mechanical integrity, cell death, and altered regulation of gene expression. In addition, interactions between exogenous cytokines and mechanical injury caused synergistic loss of proteoglycan.

Adult cartilage is avascular and alymphatic, and therefore, essential nutrients, signaling molecules, metabolites, and waste products must be delivered to or removed from chondrocytes through the ECM [10]. Since solute transport primarily depends on the properties of the ECM, damage to the matrix following injury, inflammation, or abnormal chondrocyte activity can potentially alter the transport of important proteins essential for cellular activities, as well as protein therapeutics. Although the pathway by which injury leads to abnormal cell activity is not well understood, chondrocyte metabolism is reported to be largely affected by mechanical and physiochemical properties of the surrounding matrix network [11]. Also, the concentrations of biological molecules and therapeutic agents, and the rate of transport of degraded or newly

synthesized matrix molecules are key factors which mediate the fate of cellular metabolic activities [12-15].

However, changes in the transport behavior of articular cartilage caused by mechanical injury or inflammatory cytokines have not been studied in detail. The effects of cyclic impact loading on canine cartilage explants were studied by Farquhar et al., who reported an increased self-diffusion of water molecules [16]. Cartilage specimens treated with trypsin have been used as a model of matrix degradation by several groups [17-21]. Treatment with trypsin generally increased the intratissue diffusivity and partition coefficient of solutes. Although trypsin treatment may mimic certain aspects of matrix degradation, it is hard to predict the effects of tissue- and cell-level response to injury on transport properties, since trypsin non-specifically degrades matrix molecules.

As an effort to prevent the progression of OA, therapeutic interventions such as disease-modifying osteoarthritis drugs (DMOADs) are being developed based on understanding of the pathophysiology of the disease [22]. Inflammatory mediators and matrix degrading enzymes are under study as promising future targets. To attack such targets that may be secreted by the chondrocytes or upregulated within the surrounding tissue in response to injury or cytokines, an appropriate concentration of pharmacological agents must be transported into cartilage tissue. However, there is a lack of understanding of the transport of therapeutic agents against OA that have specific physiochemical properties. Due to the ECM of cartilage, the accessibility of pharmacological agents to chondrocytes is limited, especially when the size of a drug molecule is large [23]. Therefore, to evaluate, predict, and optimize the availability of drugs in cartilage tissue, it is important to characterize the uptake and retention of agents in the cartilage. By combining knowledge of the effects of injury and cytokines on transport, we will be able to

elaborate drug delivery strategies for joint injury depending on the severity of the trauma to cartilage.

Therefore, to understand the extent of altered transport of large therapeutic protein solutes caused by traumatic injury to the cartilage, our objectives were to characterize and quantify changes in the kinetics and extent of protein uptake following injury and inflammatory cytokine treatment.

3.2 Materials and Methods

Tissue harvest. Cartilage explants were harvested from the femoropatellar grooves of 1-2 weeks old calves (Research 87, Marlborough, MA) [24]. Briefly, 9-mm diameter cartilage-bone cylinders were cored, mounted on a microtome and either removed top superficial layer to obtain 1 mm-thick middle zone slices or sliced sequentially from the top surface to divide explants into level-1 (L1, ~800 μm with superficial zone intact) and level-2 (L2, ~800 μm below L1). Four or five disks (3 mm-diameter, 1 mm-thick) were cored from each slice using a dermal punch. All cartilage specimens were equilibrated either in serum-free medium (low-glucose DMEM (1 g/L) supplemented with 1% insulin-transferrin-selenium (10 μg/mL insulin, 5.5 μg/mL transferrin, 5 ng/mL selenium, Sigma), 10 mM HEPES buffer, 0.1 mM nonessential amino acids, 0.4 mM proline, 20 μg/mL ascorbic acid, 100 units/mL penicillin G, 100 μg/mL streptomycin, and 0.25 μg/mL amphotericin B in a 37°C, 5% CO2 incubator or in 1× phosphate buffered saline (PBS) supplemented with 0.1% bovine serum albumin (BSA), 0.01% sodium azide (NaN_3) and protease inhibitors (Complete, Roche Applied Science, Indianapolis, IN) at 4°C prior to experiments.

Solute preparation. An iodinated 48 kDa Fab fragment (^{125}I-Fab) and a 150 kDa monoclonal antibody (^{125}I-mAb), both raised against the inflammatory cytokine, IL-6, were kindly provided by Centocor, Johnson and Johnson, as part of a collaborative study of the efficacy of blocking IL-6 in osteoarthritic disease. Before all experiments using ^{125}I-Fab or ^{125}I-mAb, Sephadex G50 chromatography was used to separate and remove any small ^{125}I-species that may have resulted from degradation of iodinated proteins, (0.7 × 50 cm columns using an elution buffer of 1×PBS buffer with 0.1% BSA and 0.01% NaN_3, and the void volume collected for the desired ^{125}I-Fab or ^{125}I-mAb) [24].

Injurious compression. Cartilage disks to be injured were placed individually between impermeable platens of a polysulfone chamber (50 % strain, 100%/s strain rate), in a radially unconfined compression configuration [3]. During injury loading, disks were compressed to 50% strain with a constant velocity of 1mm/second and immediately released with the same rate (50 % strain, 100%/s strain rate). This injury protocol typically resulted in a peak stress of ~ 20 MPa, which is known to produce ECM damage and approximately 10-20% cell death.

Measurement of protein uptake ratio. Disks were incubated with a fixed amount of labeled solutes with or without unlabeled solutes. The buffer consisted of 1×PBS supplemented with 0.1% BSA, 0.01% NaN_3 and protease inhibitors at 4°C or DMEM supplemented with 1% ITS, and 0.1% BSA at 37°C. At selected time points, disks were removed from the bath and briefly rinsed in fresh PBS buffer. The surface of each disk was quickly blotted with Kimwipes and the wet weight was measured. The ^{125}I-radioactivity of each cartilage disk and aliquots of the equilibration baths were quantified individually using a gamma counter. Disks were then lyophilized and the dry weight was measured; the water weight of each disk was calculated from the tissue wet and dry weights. The *uptake ratio* was calculated as the concentration of the

^{125}I-Fab or ^{125}I-mAb in the cartilage disks (per intratissue water weight) normalized to the concentration of ^{125}I-Fab or ^{125}I-mAb in the equilibration bath. The disks were then digested with proteinase-K (Roche Applied Science, Indianapolis, IN) and the sulfated glycosaminoglycan (sGAG) content of each disk was measured using the dimethylmethylene blue (DMMB) dye binding assay [25]. Samples from the baths were again analyzed by Sephadex G50 chromatography to determine whether any small labeled species (e.g., ^{125}I) may have accumulated from degradation of ^{125}I-Fab or ^{125}I-mAb during each experiment. The uptake ratio was corrected to take into account the presence of any such small labeled species, assuming the small species to be ^{125}I [26]. In a separate control experiment, the uptake ratio of ^{125}I alone was measured to calibrate the correction factor, which was ~ 0.6.

To investigate the possibility that Fab or mAb may bind to specific sites within the cartilage tissue, disks were incubated with a fixed amount of labeled solutes with graded amounts of unlabeled solutes, and we compared the measured uptake ratio to a theoretical model as described in 2.2 Materials and Methods in Chapter 2.

Ring-Core transport studies. Plugs were compressed to ~ 10% final strain between impermeable platens of a polysulfone plastic loading chamber to prevent diffusion from the top and bottom surfaces. This slight static compression would thereby only allow the flux in the radial direction. At selected time points after adding radiolabeled or unlabeled solutes, disks were briefly rinsed, and a 2-mm diameter core was punched from the center of a 3 mm diameter plug. The uptake ratios in the annular ring and inner core were separately measured as described above.

Effects of exogenous cytokines combined with mechanical injury. To test the effect of exogenous cytokines combined with mechanical injury, explants were subjected to no

treatment (control), mechanical injury, exogenous TNFα, or a combination of injury and TNFα. The ring-core experimental setup was used to carry out subsequent experiments. Normal or injured 3 mm-diameter × 1 mm-thick disks were compressed to ~ 900 μm in loading chambers and incubated with ^{125}I-Fab, unlabeled Fab (10 μg/ml), and with or without TNFα (2.5 ng/ml for day 0~2, 25 ng/ml for day 2~6). The medium was replaced every 2 days and saved for further analysis. At day 2, 4, and 6, disks were collected and processed as described in "Ring-Core transport study".

3.3 Results

Anti-IL-6 Fab fragment (48 kDa) was able to penetrate into bovine cartilage explants. The transient uptake of ^{125}I-Fab was measured up to 9 days in middle zone explants from bovine calf cartilage to evaluate the ability of these fragments to penetrate into cartilage by simple diffusion. Diffusion of such solutes can be slow as previously reported due to their size [23]. It took ~ 4 days for ^{125}I-Fab to penetrate and reach partial equilibrium within cartilage disks at 4°C and 37°C (Fig. 3.1). For this reason, in subsequent experiments requiring equilibrium, the duration of incubation was at least 5 days. In addition, the uptake ratio at 37°C was significantly higher than that measured at 4°C.

To determine whether these Fab fragments may bind to specific sites within the tissue, graded amounts of unlabeled Fab were added to the baths during incubation and the uptake ratio was measured at day 5. Adding unlabeled Fab up to 1 μM did not significantly change the uptake of ^{125}I-Fab at 37°C and 4°C (Fig. 3.2), indicating negligible amount of competitive binding between the labeled and unlabeled Fab under these conditions. The same experiment

was repeated with two different animals and showed that animal-to-animal variation was not significant (data not shown).

Anti-IL-6 Fab fragment (48 kDa) was not evenly distributed across the thickness of explants by 3-days. To visualize spatial distribution of ^{125}I-Fab within the cartilage disks, autoradiography images of human knee explants incubated with ^{125}I-Fab were taken (collaborated with Dr. Ernst Hunziker at the University of Bern, Switzerland). Human knee cartilage disks including the intact superficial layer were incubated with ^{125}I-Fab without unlabeled Fab at 37°C for 3 days. Autoradiography revealed that ^{125}I-Fab fully penetrated throughout the tissue though marked gradients in grain density suggested that complete equilibrium had not yet been reached (Fig. 3.3 and 3.4). The ^{125}I-Fab grain density was higher in the superficial layer than the deeper layer, suggesting that the spatial distribution of Fab count not be reflected in the uptake ratio.

Injurious compression and exogenous TNFα altered transport of anti-IL-6 Fab fragments into bovine knee cartilage. A single injurious compression cycle induced a significant increase in the uptake ratio of ^{125}I-Fab compared to uninjured controls (2-way ANOVA, Fig. 3.5a). In untreated free-swelling disks, the uptake ratio decreased with the tissue GAG density (linear regression, $p=0.009$, $r^2=0.709$). However, in injured tissue, the change in the uptake ratio did not show a significant linear relationship with the GAG density (Fig. 3.5b). Although no statistical significance was observed, the average GAG density in the injured tissue was higher than that measured in the normal tissue. Furthermore, higher strains and strain rates during the injurious loading resulted in higher uptake ratios, accompanied by the lower GAG density and higher tissue hydration of explants (Fig. 3.6, Fig. 3S.3). These results consistently demonstrated that the simple mechanical insult on the cartilage tissue was enough

to change the accessibility of large proteins and that the extent of change depended on the severity of injury.

In addition, we tested the effect of the exogenous cytokine, TNFα, combined with the mechanical injury on the uptake of ^{125}I-Fab. Treatment with the mechanical injury, TNFα, and combination of injury and TNFα significantly increased the uptake ratio of ^{125}I-Fab, and the combined effect of injury and TNFα induced the largest increase (Fig. 3.7a). The GAG release to medium also showed a trend similar to the uptake ratio, suggesting that the decrease in cartilage GAG content was related to the higher uptake ratio (Fig. 3.7b).

To further relate the increase in the uptake and tissue degradation, the GAG density, tissue hydration, and uptake ratio in the ring and core regions was separately quantified (Fig. 3.8, Fig 3S.4). The uptake ratio in the core region was ~ 0.1 – 0.2, indicating that ^{125}I-Fab was able to penetrate to the core, consistent with the autoradiography images. In each condition, the uptake ratio of ^{125}I-Fab in the ring was higher than core. Interestingly, the change in the uptake ratio by the treatment was present in both the ring and core regions in all treatment groups (injury, TNFα, injury with TNFα), where the combination of injury and TNFα induced the largest increase in the uptake ratio measured in the ring. With the combination of TNFα and injury, the uptake ratio in the ring was > 1, suggesting that the binding of ^{125}I-Fab to matrix sites was present.

Treatments with TNFα alone, and the combination of injury and TNFα caused a temporal decrease in the GAG density but control and injury did not show the temporal change in the GAG content (Fig. 3.8b, 2-way ANOVA with factors of time and region, p-values for time-factor were 0.46, 0.275, 0.006, and 0.068 for control, injury, TNFα, and TNFα with injury, respectively). The decrease in the GAG density due to TNFα alone or TNFα combined with

injury was well matching to the increased GAG loss to media (Fig. 3.7b). Adding exogenous TNFα induced the decrease in GAG density in both the ring and core regions over time but the GAG density in the ring showed more decrease than that in the core.

GAG depletion or long term incubation with normal tissue induced the uptake ratio above 1. The combination of injury and TNFα resulted in the highest uptake ratio in the annular ring, which was above 1 (Fig. 3.8a). For large proteins such as the Fab (48 kDa), the uptake ratio above 1 cannot be solely explained by an enhanced partitioning of unbound solutes inside the tissue. Although incubation with graded amounts of unlabeled Fab did not suggest the presence of significant binding of Fab to sites within the tissue (Fig. 3.2), we were not able to completely rule out the possibility of binding given the results of Fig. 3.8. To examine whether additional matrix degradation induces more uptake, explants were enzymatically degraded to remove proteoglycans. Then, the uptake of ^{125}I-Fab was measured while the trypsin-treated explants were compressed to 10% strain in the loading chambers. The measured uptake ratio was ~ 5 in the ring and ~ 3 in the core at day 6 (Fig. 3.9a). Treatment with chondroitinase ABC generated similar results to trypsinized disks when the explants were under compression (Fig. 3.9b). If chondroitinase ABC-treated explants were kept free-swelling, the uptake ratio of ^{125}I-Fab was ~ 22 in the ring and ~ 14 in the core at day 4 (Fig. 3.9), suggesting that Fab may bind to the matrix or the outer surface of the explants.

We also observed that the uptake ratio in the normal tissue could be above 1 if we lengthen the duration of incubation. When normal explants were incubated wit ^{125}I-Fab for 15 days under 10% strain compression, the uptake ratio was ~ 5 in the ring and ~ 2 in the core (Fig. 3.10), which was similar to the uptake measured in GAG-depleted explants with the shorter incubatoin. The possibility of degradation of ^{125}I-Fab during the long term incubation was

tested with SDS-PAGE, which compared the Fab fresh out of the stock with the Fab incubated for 2-week at 37°C. There was no significant difference between two species (Fig. 3S.5).

Anti-IL-6 mAb (150 kDa) was mostly excluded from interstitial space of normal human cartilage. Penetration of ^{125}I-mAb into human knee cartilage including intact superficial layer was examined by observing the uptake ratio and autoradiography images from normal and trypsin-treated explants incubated with ^{125}I-mAb and with or without 50 μM unlabeled mAb. For all conditions, adding unlabeled mAb significantly decreased the uptake ratio of ^{125}I-mAb (Fig 3.11). In addition, the trypsin treatment increased the uptake of ^{125}I-mAb. The durations of incubation, 3 days and 8 days, did not play a major role in affecting the uptake ratio. Interestingly, in most conditions, the uptake ratio was above 1, suggesting binding of mAb to certain sites in the tissue. However, as suggested from the autoradiography images of ^{125}I-Fab, the uptake ratio is the average from bulk tissue measurement and cannot demonstrate the spatial distribution.

Autoradiography images revealed that the tissue depth, the addition of unlabeled mAb, and trypsin treatment significantly affected the local distribution of ^{125}I-mAb in the human tissue. In normal tissue, many more grains were located at the superficial layer and only small amount or background-level of grains were detected at the deep region (Fig. 3.12). In the trypsin treated tissue, the distribution of grains was more uniform than that observed in the normal tissue. In the tissue incubated without unlabeled mAb, densely-concentrated grains were co-localized with cells, indicating significant binding of ^{125}I-mAb to cells or the matrix around cells (Fig 3S.10). These dense grains around the cell were significantly reduced by adding unlabeled mAb (data not shown). Distribution of fluorescent-tagged mAb observed in bovine cartilage was consistent with results from autoradiography (Fig. 3.13). In the untreated

tissue, mAb was only located at the outer surface and no penetration into the deeper region was detected. However, in the GAG-depleted tissue, mAb was detected throughout the tissue, confirming the significant role of steric exclusion on mAb by GAG chains.

3.4 Discussion

Our results suggest that Fab fragments (48 kDa) can diffuse throughout the depth of cartilage tissue even though the spatial distribution was not uniform with depth by day 3. However, mAb (150 kDa) could penetrate only the superficial layer and was excluded from the deeper regions of the cartilage. We also found out that there can be a greater accessibility of large solutes into the cartilage after the direct mechanical injury or inflammatory cytokine treatment to the tissue, where the increase in the uptake was related with the severity of matrix damage and loss. The combination of mechanical injury and TNFα induced the most dramatic increase in the uptake, suggesting the joint injury accompanied by the inflammatory response can disrupt the normal transport process.

Although full-penetration of ^{125}I-Fab throughout the thickness was observed in autoradiography images, the spatial distribution was not uniform and depended on the depth of the explants. Significant penetration of ^{125}I-Fab was detected at the more hydrated surface region and a less amount at the middle or deep region of the tissue. Presumably the spatial distribution of ^{125}I-Fab would be more uniform by days 6-8 after further equilibration would be reached. The effect of the steric exclusion by the tissue matrix was more dramatic with ^{125}I-mAb, which was only detectable at the surface layer. These results suggest that Fab can reach intra-tissue targets located beyond the superficial layer, whereas mAb can only affect the

surface layer. It is interesting to note that Fab and mAb would diffuse more freely within the tissue when the matrix is subjected to severe degradation. Large mAb would be able to penetrate into the deeper region after the matrix degeneration, suggesting mAb can be effective against targets located at the deep region when the cartilage undergoes a significant degradation.

Mechanical injury as used in the present study induced tissue swelling, which was indicated by the increased tissue hydration. Such tissue swelling is likely caused by damage to the collagen fibril network, which provides the tensile stiffness of the cartilage tissue and thereby restricts the osmotic swelling pressure generated by highly charged GAG chains [27]. The increased hydration or lowered GAG density following the mechanical injury would allow large solutes to move with less hindrance within the cartilage, resulting in an increased partition coefficient. Interestingly, due to the different local mechanical properties along the depth, the damage on the local matrix following injury will also vary with the depth of the tissue. Therefore, combined with the depth-dependent distribution of solutes, the amount of changes in the uptake caused by mechanical injury will vary with depth, which may result in zone-dependent cellular responses to joint trauma.

There is ample evidence supporting the notion that tissue hydration and GAG density play a major role in restricting the penetration of large solutes within the cartilage. Maroudas showed that partition coefficient of large solutes exponentially decreased with the increasing fixed charge density in adult human cartilage [23]. Quinn et al. reported that static compression reduced the diffusivity and partition coefficient of fluorescent tracers in adult bovine cartilage, and the effect of static compression was partially attributed to the increased matrix GAG density [28]. In addition, enzymatic degradation of proteoglycans significantly increased the diffusivity and partitioning of radiolabeled solutes in adult bovine cartilage, and the increase

was more dramatic for larger molecules (dextran 70 kDa) [29]. Human ankle cartilage, which generally shows higher GAG density than human knee cartilage, exhibited a lower partition coefficient of 70 kDa dextran [30].

TNFα treatment further increased the change in the uptake, suggesting that the inflammatory response following joint injury can play a critical role in altering the transport property of the damaged cartilage. Increase in the uptake was accompanied by the GAG loss at the each region, where the largest change was observed in the tissue with the most severe GAG loss, confirming the regulatory role of GAG on the uptake. Although the change in the uptake was present at both regions for treated explants, the combination of injury and TNFα caused the largest change at the ring, which was the front end contacting inflammatory cytokine, TNFα. This suggests that severely damaged region at the articular surface due to the injury and inflammation will be subjected to substantial changes in the uptake of such solutes.

Proteoglycan depletion and long term incubation revealed that ^{125}I-Fab bound to certain sites in the tissue, which contradicted the result from the competitive binding experiment, which showed no change in the uptake ratio with the graded amount of unlabeled Fab up to 1 μM. Binding sites of Fab were not removed by trypsin, suggesting collagen molecules would be one of the candidates for binding. Binding of Fab became detectable after the trypsin treatment or long term incubation, suggesting proteoglycan molecules were possibly restricting the binding interaction between ^{125}I-Fab and binding sites. Ongoing study focuses on finding binding sites and extending the study to understand how the binding would change the effect of injury and cytokine on transport properties.

The present study suggests that mechanical injury and inflammatory cytokines may mediate cellular activity via altering the transport properties of cartilage. Although our study of

the effect of injury and cytokines on transport was limited to the 48 kDa Fab fragment of the antibody, it is possible to predict that the transport of similarly-sized proteins, including growth factors, cytokines, and matrix molecules, would be modified by a similar traumatic injury. Therefore, cellular activities that require such solutes would be affected by joint injury, resulting in significant changes in transport properties. Furthermore, since chondrocytes are ultimately responsible for detecting changes in the integrity of the ECM and for remodeling of the matrix, alterations in the rate of movement of newly synthesized or degraded matrix molecules would be critical aspect that perturbs cell metabolism.

3.5 Figures

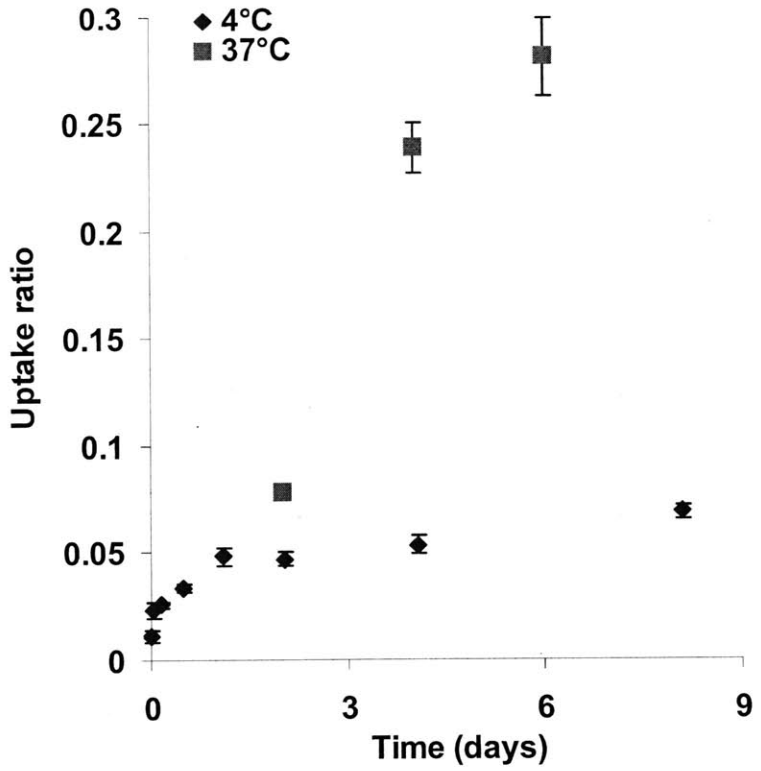

Figure 3.1 Uptake ratio of ^{125}I-Fab in the bovine calf cartilage measured at different time points. Cartilage disks (3 mm-diameter, 1 mm-thick) were incubated with ^{125}I-Fab either at 4°C under free-swelling condition or at 37°C under 10% offset static compression. For the measurement at 4°C, disks were incubated without unlabeled Fab in 1×PBS with 0.1% BSA, 0.01% sodium azide, and protease inhibitors. For measurement at 37°C, disks were incubated with 10 μg/ml (= 66.7 nM) unlabeled Fab in DMEM with 0.1% BSA, and 1% ITS. No unlabeled Fab was added for both cases. Mean ± SEM, n = 6 for 4°C and n = 5 for 37°C.

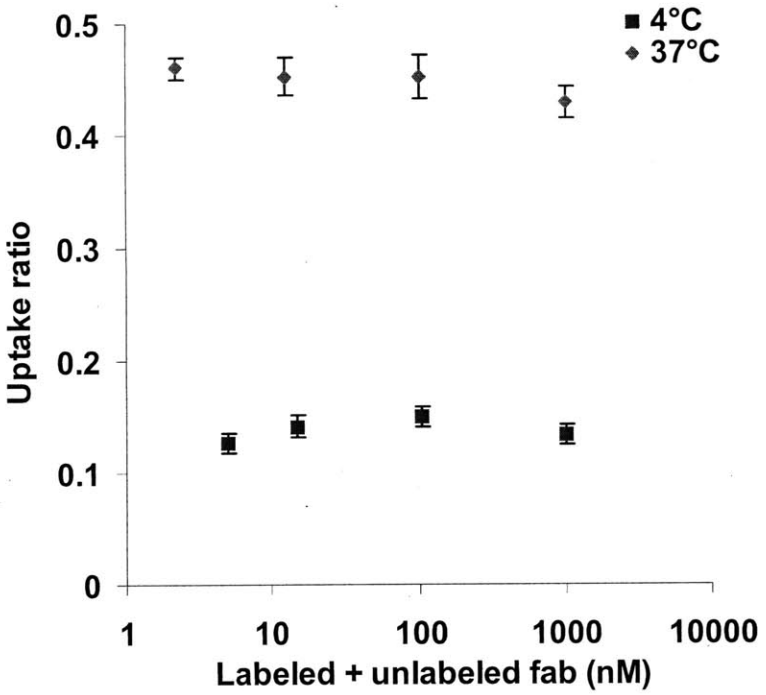

Figure 3.2 Uptake ratio of ^{125}I-Fab with graded amounts (0, 10, 100, and 1000 nM) of unlabeled Fab in the bovine calf cartilage. Free-swelling cartilage disks (3 mm-diameter, 1 mm-thick) were incubated with ^{125}I-Fab either at 4°C in 1×PBS with 0.1% BSA, 0.01% sodium azide, and protease inhibitors or at 37°C in DMEM with 0.1% BSA, and 1% ITS. The concentration of ^{125}I-Fab was fixed to 5.01 nM and 2.21 nM for the measurement at 4°C and 37°C, respectively. Mean ± SEM, n = 4 for 4°C and n = 5 for 37°C.

A.

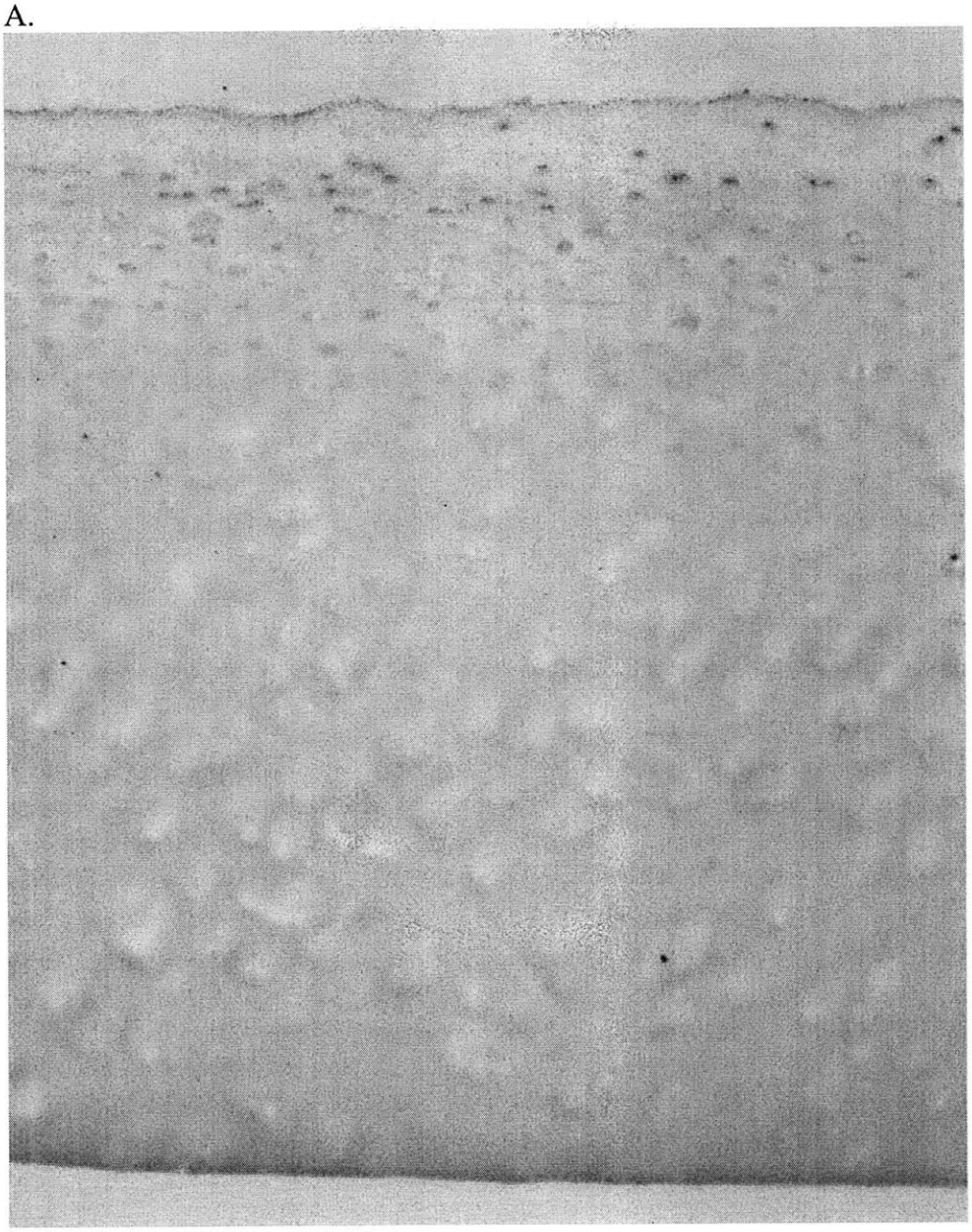

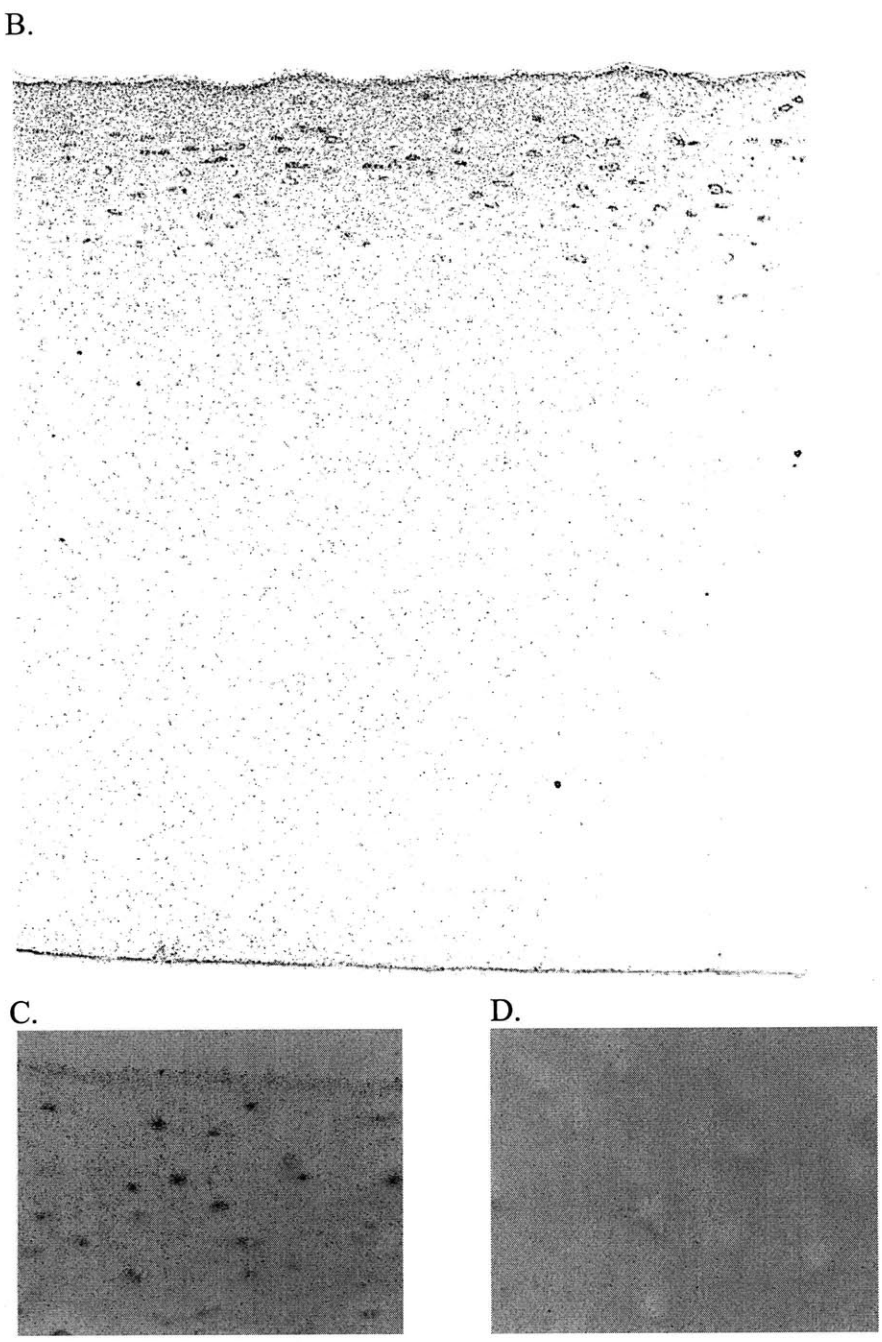

Figure 3.3 Autoradiography images of ^{125}I-Fab in human knee cartilage. Disks were harvested from first ~ 700 μm layer of grade 0 - 1 human knee cartilage including the intact superficial zone. The donor was a 26-year old female. Free-swelling cartilage disks were incubated with ^{125}I-Fab without unlabeled Fab at 37°C for 3 days in 1×PBS with 0.1% BSA, 0.01% sodium azide, and protease inhibitors. **A.** Images from ×10 objective. **B.** The image from A was adjusted to enhance grains and remove background color using Photoshop (Adobe, San Jose, CA). **C.** Images from ×40 objective, showing surface region. **D.** Images from ×40 objective, showing deeper region.

A.

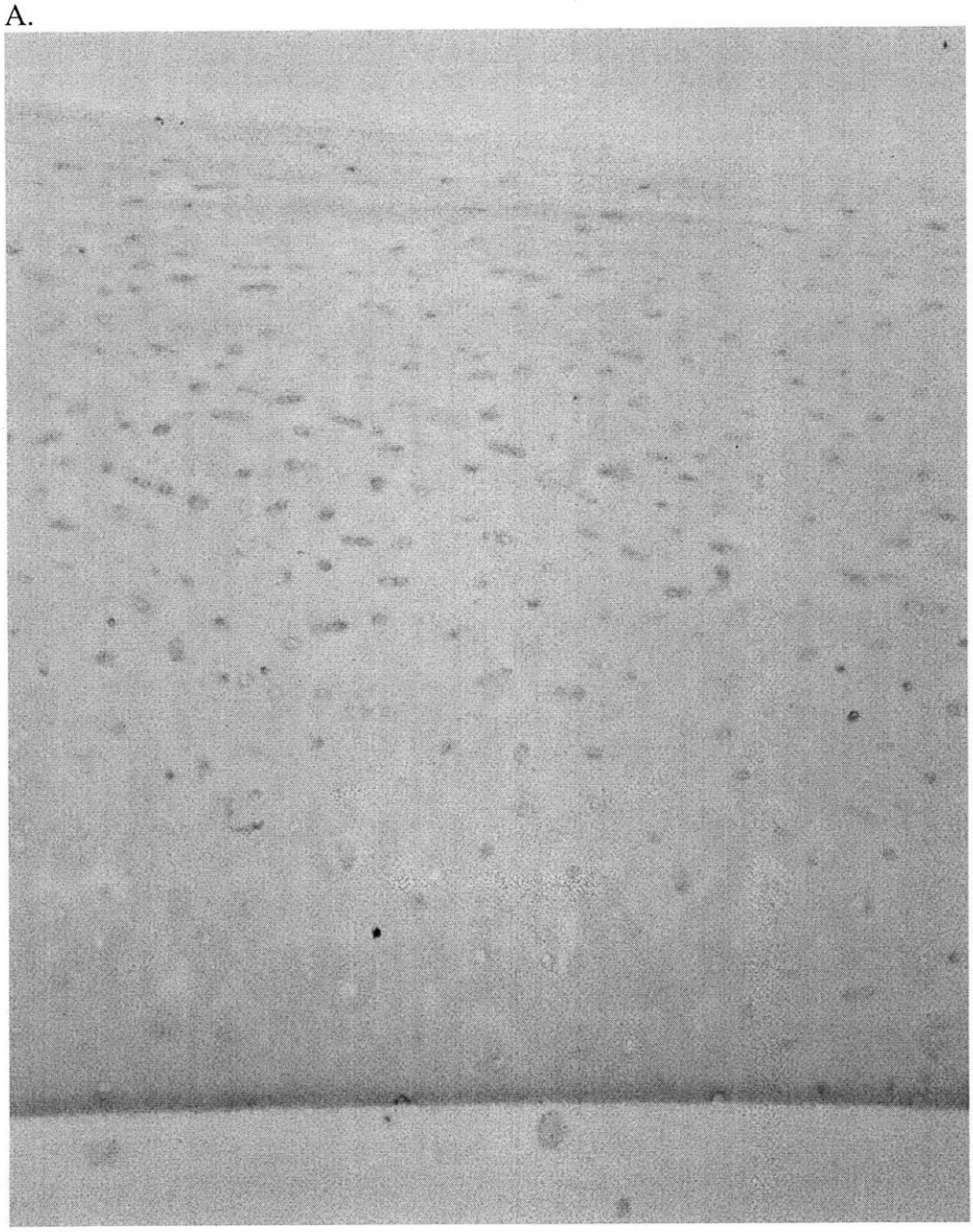

B.

C.

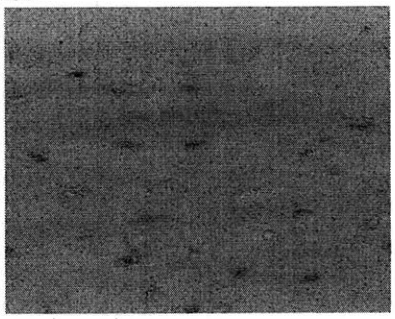

D.

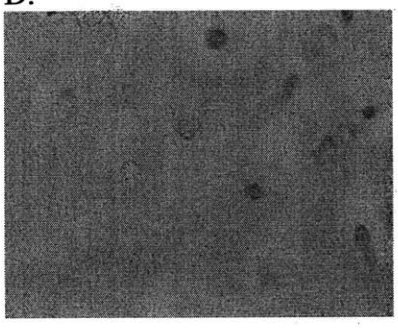

Figure 3.4 Autoradiography images of ^{125}I-Fab in human knee cartilage. Disks were harvested from first ~ 700 μm layer of grade 0 - 1 human knee cartilage including the intact superficial zone. The donor was a 26-year old female. Free-swelling cartilage disks were incubated with ^{125}I-Fab without unlabeled Fab at 37°C for 3 days in 1×PBS with 0.1% BSA, 0.01% sodium azide, and protease inhibitors. **A.** Images from ×10 objective. **B.** The image from A was adjusted to enhance grains and remove background color using Photoshop (Adobe, San Jose, CA). Binary images converted from A. **C.** Images from ×40 objective, showing surface region. **D.** Images from ×40 objective, showing deeper region.

A.

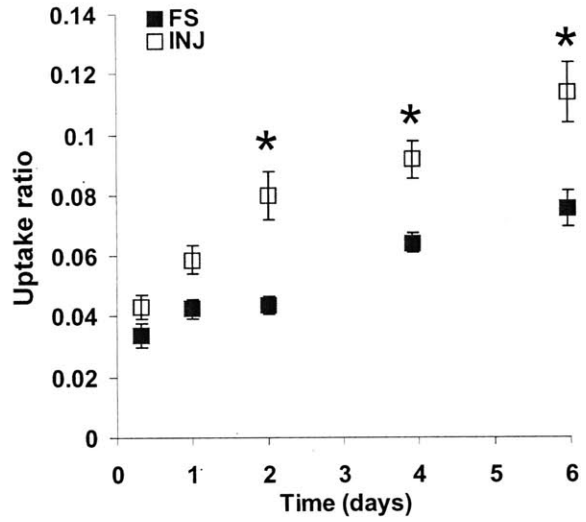

B.

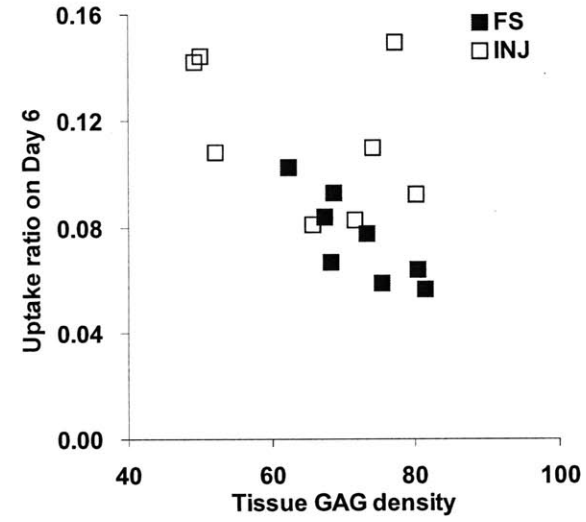

Figure 3.5 Effect of the mechanical injury on the uptake of ^{125}I-Fab in the bovine calf cartilage. **A.** Uptake ratio ^{125}I-Fab in the normal and injured cartilage was measured up to 6 days. Disks were incubated with ^{125}I-Fab without unlabeled Fab at 4°C in 1×PBS with 0.1% BSA, 0.01% sodium azide, and protease inhibitors. Mean ± SEM, n = 8. *$p<0.05$ Tukey pairwise, 2-way ANOVA (time and injury). **B.** Uptake ratio of ^{125}I-Fab on day 6 relative to the tissue GAG density. In free-swelling tissue, the GAG density and uptake ratio showed a significant linear relationship ($r^2=0.709$).

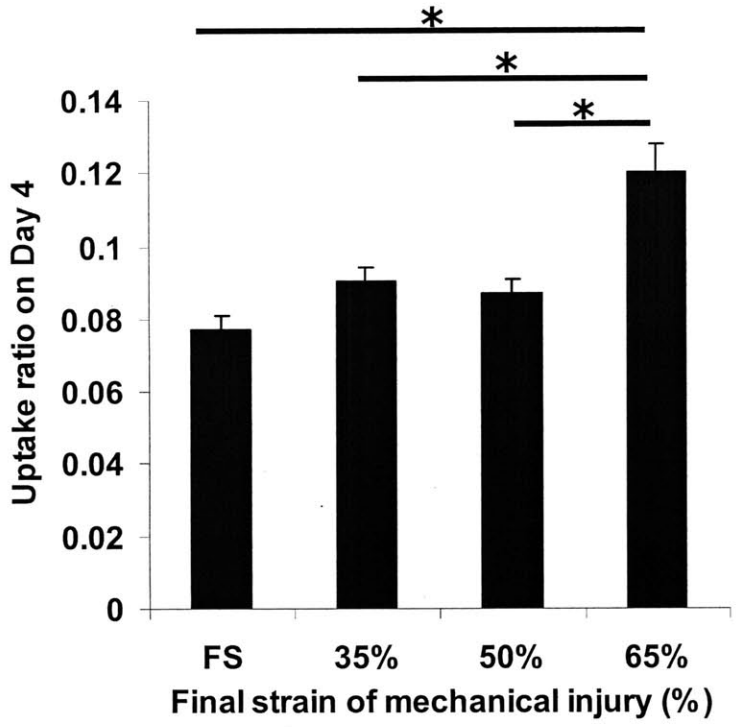

Figure 3.6 Effect of the final strain and strain rate of the mechanical injury on the uptake ratio of ^{125}I-Fab in the bovine calf cartilage ("FS" = free swelling; "35%" = 35% final strain, 70%/s strain rate; "50%" = 50% final strain, 100%/s strain rate; "65%" = 65% final strain, 130%/s strain rate). Uptake ratio ^{125}I-Fab in the normal and injured cartilage was measured on day 4. Disks were incubated with ^{125}I-Fab without unlabeled Fab at 4°C in 1×PBS with 0.1% BSA, 0.01% sodium azide, and protease inhibitors. Mean ± SEM, n = 15. *$p<0.05$ Tukey pairwise, 1-way ANOVA.

A.

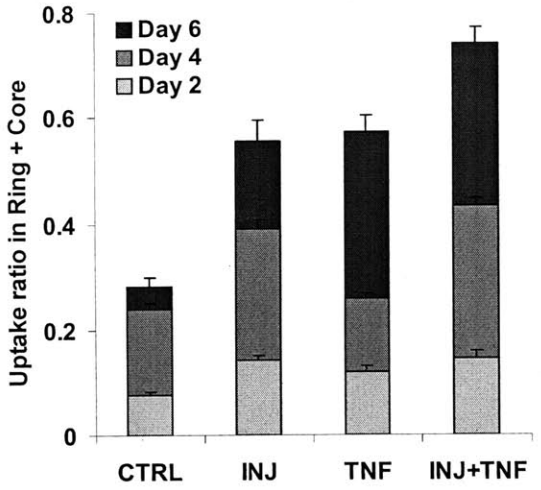

B.

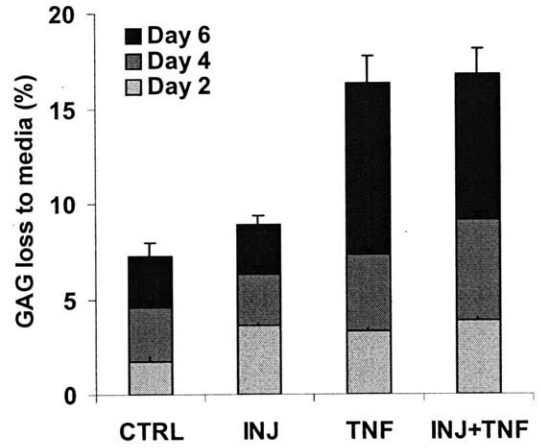

Figure 3.7 Effect of the mechanical injury and exogenous cytokine on the uptake ratio of ^{125}I-Fab and the GAG release to media. Disks were incubated at 37°C with ^{125}I-Fab and 10 μg/ml (= 66.7 nM) unlabeled Fab in DMEM with 0.1% BSA, and 1% ITS under 10% offset static compression. **A.** Uptake ratio of ^{125}I-Fab. **B.** GAG release to media. Mean ± SEM, n = 4 - 5.

A.

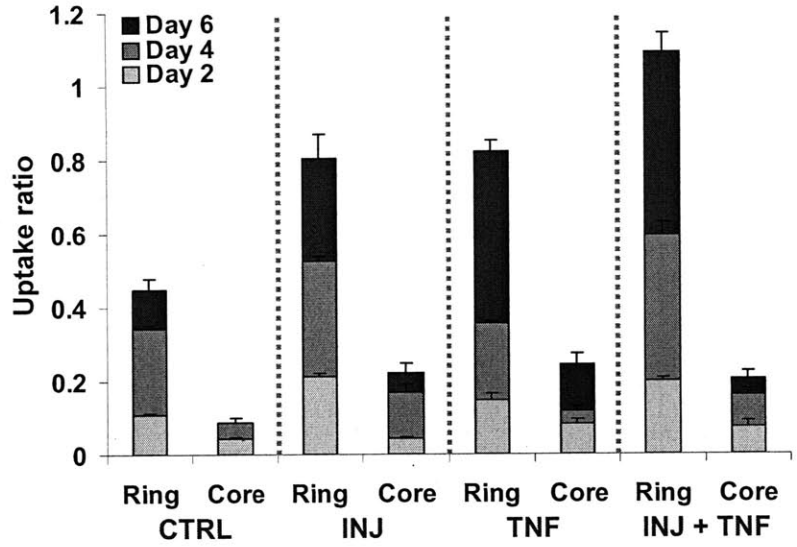

B.

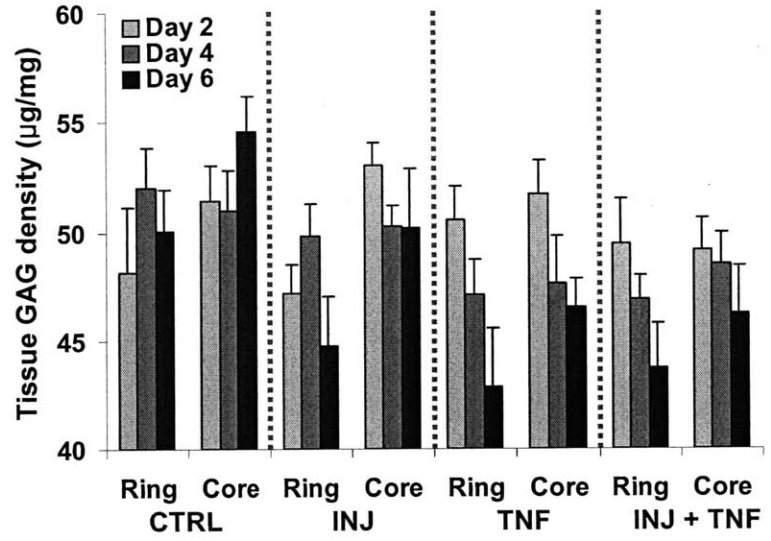

Figure 3.8 Effect of the mechanical injury and exogenous cytokine on the uptake ratio of ^{125}I-Fab and the tissue GAG density, which were separately measured in the ring and core regions. Disks were incubated at 37°C with ^{125}I-Fab and 10 µg/ml (= 66.7 nM) unlabeled Fab in DMEM with 0.1% BSA, and 1% ITS under 10% offset static compression. **A.** Uptake ratio of ^{125}I-Fab. **B.** Tissue GAG density. Mean ± SEM, n = 4 - 5.

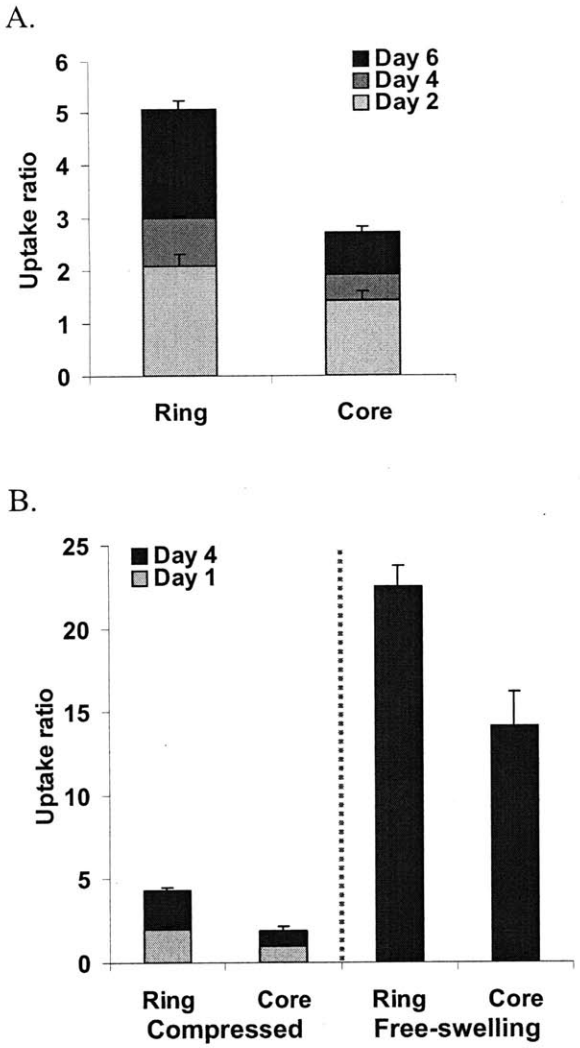

Figure 3.9 Effect of the enzymatic digestion of ECM on the uptake ratio of ^{125}I-Fab. **A.** Uptake ratio in the trypsinized disks, which were separately measured in the ring and core regions. 1 mm-thick × 3 mm-diameter disks were treated with 0.1 mg/ml trypsin for 24 hrs at 37°C. Disks were incubated at 37°C with ^{125}I-Fab and 10 μg/ml (= 66.7 nM) unlabeled Fab in DMEM with 0.1% BSA, and 1% ITS under 10% offset static compression. Mean ± SEM, n = 4 - 5. **B.** Uptake ratio in the chondroitinase ABC-treated disks, which were measured either separately in the ring and core regions or in the whole disks. 0.5 mm-thick × 3 mm-diameter were treated with 0.4 U/ml chondroitinase ABC for 3 days at 37°C. Disks were incubated at 37°C with ^{125}I-Fab but without unlabeled Fab in 1×PBS, with 0.1% BSA, 0.01% sodium azide, and protease inhibitors either under 10% offset static compression or free-swelling condition. Mean ± SEM, n = 3.

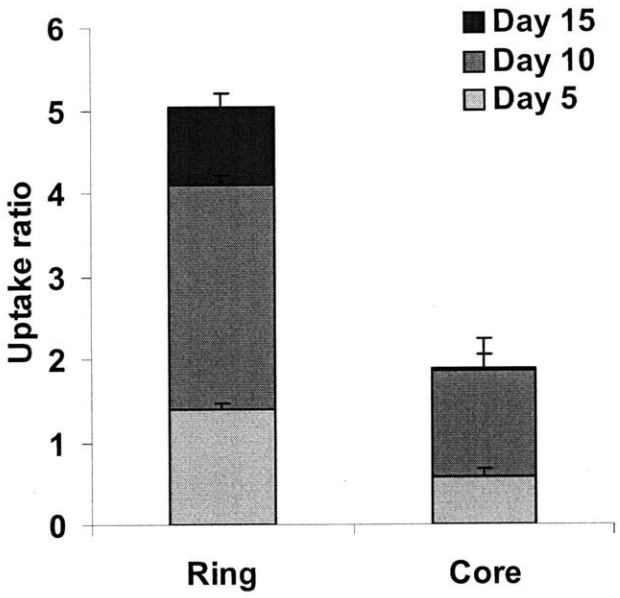

Figure 3.10 Uptake ratio of ^{125}I-Fab in long-term incubation, which were separately measured in the ring and core regions. 1 mm-thick × 3 mm-diameter disks were incubated at 37°C with ^{125}I-Fab and 100 nM unlabeled Fab in 1×PBS, with 0.1% BSA, 0.01% sodium azide, and protease inhibitors under 10% offset static compression. The equilibrating buffer was changed every 2.5 days. Mean ± SEM, n = 5.

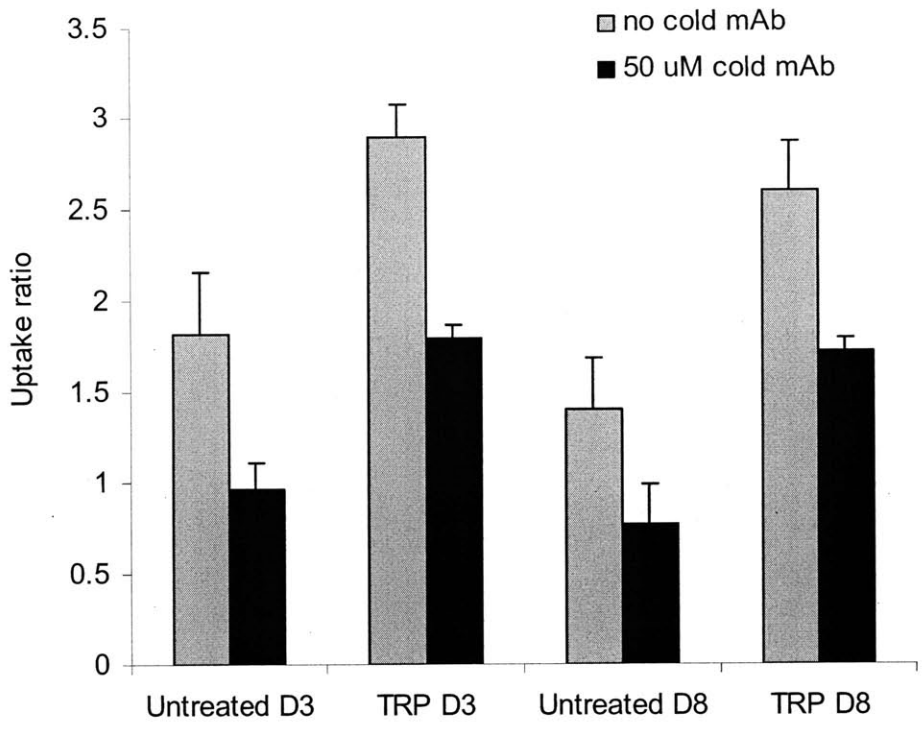

Figure 3.11 Uptake ratio of ^{125}I-mAb in normal and trypsin-treated human cartilage explants incubated with or without unlabeled mAb. 0.7 mm-thick × 3 mm diameter human knee explants (male, 28-year old, overweight, grade 0) were either kept free-swelling or treated with 0.1 mg/ml trypsin for 24 hrs at 37°C. Both groups of explants were incubated with ^{125}I-mAb with or without 50 μM unlabeled mAb in 1×PBS, with 0.1% BSA, 0.01% sodium azide, and protease inhibitors at 37°C for 3 days or 8 days. At the selected time points, disks were collected, briefly rinsed for 10 sec and then rinsed for four times for 15 min in fresh PBS. Mean ± SEM, n = 4.

A.

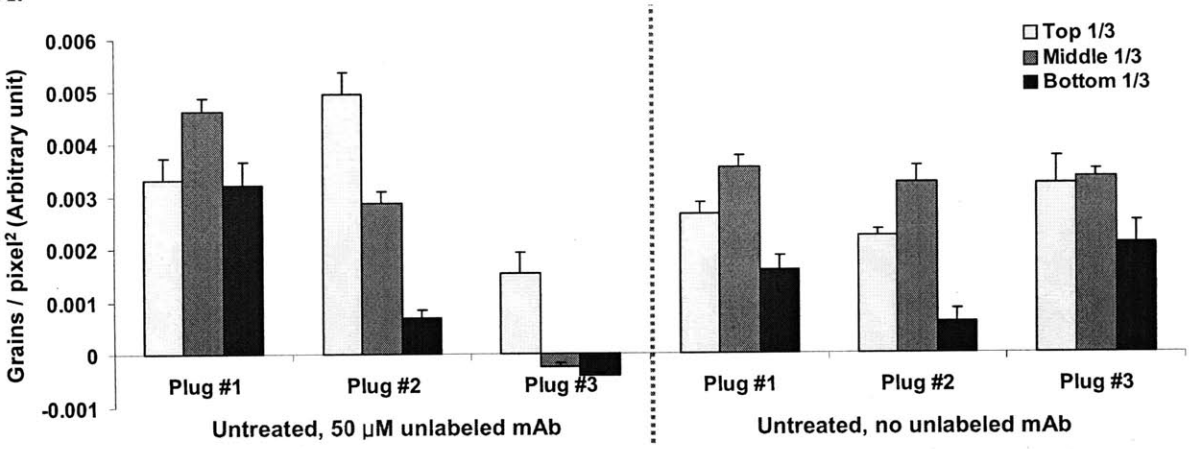

B.

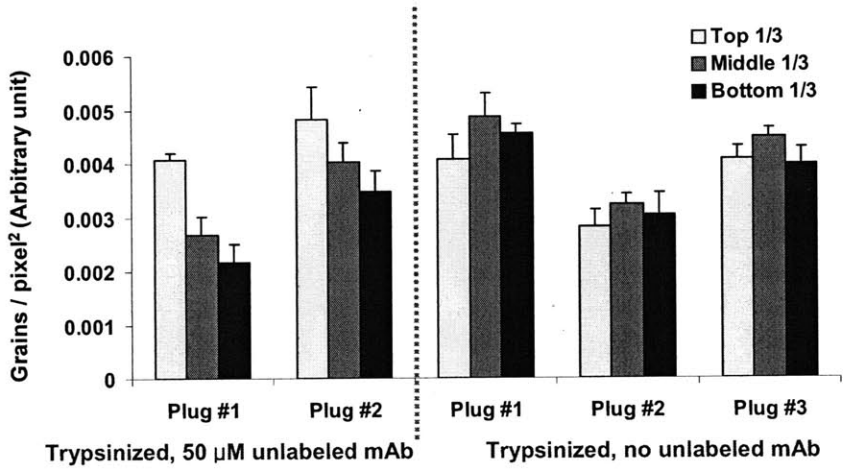

Figure 3.12 Grain density of ^{125}I-mAb measured in autoradiography images from human knee explants (see Fig. 3S.10). Cartilage disks were prepared as described in Fig. 3.11. Each slice was divided into 3 sections along the depth (top, middle, and bottom), and grains in each section was counted separately. Background grains existing outside of the tissue was counted and this background grains were subtracted from the grain number counted within the tissue. **A.** Grain density in untreated explants incubated with or without 50 µM unlabeled mAb for 8 days. **B.** Grain density in trypsinized explants incubated with or without 50 µM unlabeled mAb for 8 days.

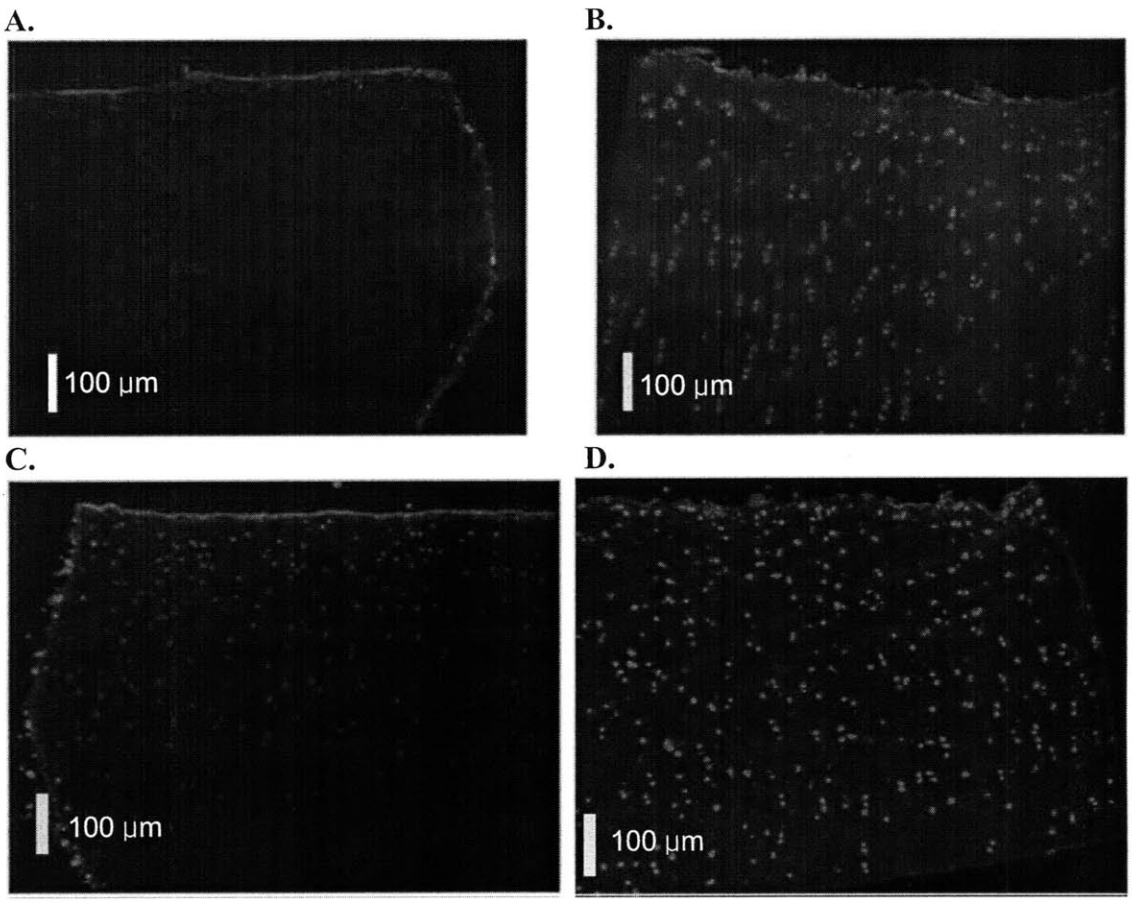

Figure 3.13 Distribution of AlexaFluor-568 conjugated anti-IL-6 mAb in bovine cartilage (collaborator: Karl Kavalkovich, Centocor). Untreated or GAG-depleted bovine cartilage disks were incubated with fluorescent-tagged mAb for 24 hrs or 6 days. GAG depletion was carried out by incubating explants with IL-1 and OSM for 14 days prior to the experiment.
A. Untreated tissue incubated for 24 hrs. **B.** GAG-depleted tissue incubated for 24 hrs.
C. Untreated tissue incubated for 6 days. **D**. GAG-depleted tissue incubated for 6 days.

3.6 References

[1] Buckwalter JA, Mankin HJ, Grodzinsky AJ. Articular Cartilage and Osteoarthritis. Instr Course Lect 2005;54:465-80.
[2] Loening AM, James IE, Levenston ME, Badger AM, Frank EH, Kurz B, Nuttall ME, Hung HH, Blake SM, Grodzinsky AJ, Lark MW. Injurious mechanical compression of bovine articular cartilage induces chondrocyte apoptosis. Arch Biochem Biophys 2000;381:205-12.
[3] Kurz B, Jin M, Patwari P, Cheng DM, Lark MW, Grodzinsky AJ. Biosynthetic response and mechanical properties of articular cartilage after injurious compression. Journal of Orthopaedic Research 2001;19:1140-6.
[4] Patwari P, Cook MN, DiMicco MA, Blake SM, James IE, Kumar S, Cole AA, Lark MW, Grodzinsky AJ. Proteoglycan degradation after injurious compression of bovine and human articular cartilage in vitro: interaction with exogenous cytokines. Arthritis Rheum 2003;48:1292-301.
[5] DiMicco MA, Patwari P, Siparsky PN, Kumar S, Pratta MA, Lark MW, Kim YJ, Grodzinsky AJ. Mechanisms and kinetics of glycosaminoglycan release following in vitro cartilage injury. Arthritis and Rheumatism 2004;50:840-8.
[6] Kurz B, Lemke AK, Fay J, Pufe T, Grodzinsky AJ, Schunke M. Pathomechanisms of cartilage destruction by mechanical injury. Annals of Anatomy-Anatomischer Anzeiger 2005;187:473-85.
[7] Lee JH, Fitzgerald JB, Dimicco MA, Grodzinsky AJ. Mechanical injury of cartilage explants causes specific time-dependent changes in chondrocyte gene expression. Arthritis Rheum 2005;52:2386-95.
[8] Sui Y, Lee JH, Dimicco MA, Vanderploeg EJ, Blake SM, Hung HH, Plaas AH, James IE, Song XY, Lark MW, Grodzinsky AJ. Mechanical injury potentiates proteoglycan catabolism induced by interleukin-6 with soluble interleukin-6 receptor and tumor necrosis factor alpha in immature bovine and adult human articular cartilage. Arthritis Rheum 2009;60:2985-96.
[9] Stevens AL, Wishnok JS, White FM, Grodzinsky AJ, Tannenbaum SR. Mechanical injury and cytokines cause loss of cartilage integrity and upregulate proteins associated with catabolism, immunity, inflammation, and repair. Mol Cell Proteomics 2009;8:1475-89.
[10] Maroudas A. Physicochemical Properties of Cartilage in Light of Ion Exchange Theory. Biophys J 1968;8:575-95.
[11] Grodzinsky AJ, Levenston ME, Jin M, Frank EH. Cartilage tissue remodeling in response to mechanical forces. Annual Review of Biomedical Engineering 2000;2:691-+.
[12] Quinn TM, Grodzinsky AJ, Buschmann MD, Kim YJ, Hunziker EB. Mechanical compression alters proteoglycan deposition and matrix deformation around individual cells in cartilage explants. Journal of Cell Science 1998;111:573-83.
[13] Quinn TM, Morel V, Meister JJ. Static compression of articular cartilage can reduce solute diffusivity and partitioning: implications for the chondrocyte biological response. J Biomech 2001;34:1463-9.
[14] Buschmann MD, Kim YJ, Wong M, Frank E, Hunziker EB, Grodzinsky AJ. Stimulation of aggrecan synthesis in cartilage explants by cyclic loading is localized to regions of high interstitial fluid flow. Arch Biochem Biophys 1999;366:1-7.
[15] Kim YJ, Sah RL, Grodzinsky AJ, Plaas AH, Sandy JD. Mechanical regulation of cartilage biosynthetic behavior: physical stimuli. Arch Biochem Biophys 1994;311:1-12.

[16] Farquhar T, Xia Y, Mann K, Bertram J, BurtonWurster N, Jelinski L, Lust G. Swelling and fibronectin accumulation in articular cartilage explants after cyclical impact. Journal of Orthopaedic Research 1996;14:417-23.
[17] Torzilli PA, Arduino JM, Gregory JD, Bansal M. Effect of proteoglycan removal on solute mobility in articular cartilage. J Biomech 1997;30:895-902.
[18] Frank EH, Grodzinsky AJ, Koob TJ, Eyre DR. Streaming Potentials - a Sensitive Index of Enzymatic Degradation in Articular-Cartilage. J Orthop Res 1987;5:497-508.
[19] Burstein D, Gray ML, Hartman AL, Gipe R, Foy BD. Diffusion of Small Solutes in Cartilage as Measured by Nuclear-Magnetic-Resonance (Nmr) Spectroscopy and Imaging. J Orthop Res 1993;11:465-78.
[20] Foy BD, Blake J. Diffusion of paramagnetically labeled proteins in cartilage: Enhancement of the 1-D NMR imaging technique. J Magn Reson 2001;148:126-34.
[21] Xia Y, Farquhar T, Burtonwurster N, Verniersinger M, Lust G, Jelinski LW. Self-Diffusion Monitors Degraded Cartilage. Arch Biochem Biophys 1995;323:323-8.
[22] Pelletier J-P, Martel-Pelletier J. DMOAD developments: present and future. Bull NYU Hosp Jt Dis 2007;65:242-8.
[23] Maroudas A. Transport of Solutes through Cartilage - Permeability to Large Molecules. Journal of Anatomy 1976;122:335-47.
[24] Garcia AM, Szasz N, Trippel SB, Morales TI, Grodzinsky AJ, Frank EH. Transport and binding of insulin-like growth factor I through articular cartilage. Arch Biochem Biophys 2003;415:69-79.
[25] Sah RLY, Kim YJ, Doong JYH, Grodzinsky AJ, Plaas AHK, Sandy JD. Biosynthetic Response of Cartilage Explants to Dynamic Compression. J Orthop Res 1989;7:619-36.
[26] Garcia AM, Lark MW, Trippel SB, Grodzinsky AJ. Transport of tissue inhibitor of metalloproteinases-1 through cartilage: contributions of fluid flow and electrical migration. J Orthop Res 1998;16:734-42.
[27] Maroudas A. Balance between Swelling Pressure and Collagen Tension in Normal and Degenerate Cartilage. Nature 1976;260:808-9.
[28] Quinn TM, Morel V, Meister JJ. Static compression of articular cartilage can reduce solute diffusivity and partitioning: implications for the chondrocyte biological response. Journal of Biomechanics 2001;34:1463-9.
[29] Torzilli PA, Arduino JM, Gregory JD, Bansal M. Effect of proteoglycan removal on solute mobility in articular cartilage. Journal of Biomechanics 1997;30:895-902.
[30] Fetter NL, Leddy HA, Guilak F, Nunley JA. Composition and transport properties of human ankle and knee cartilage. Journal of Orthopaedic Research 2006;24:211-9.

3.7 Supplementary Data

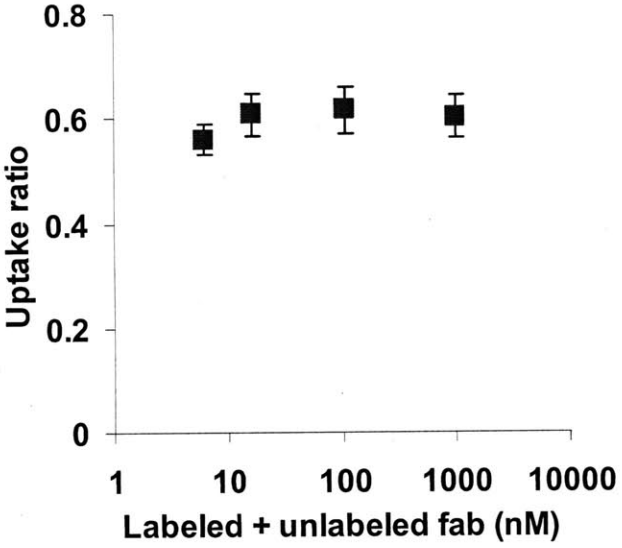

Figure 3S.1 Uptake ratio of ^{125}I-Fab with graded amount (0, 10, 100, and 1000 nM) of unlabeled Fab in bovine calf cartilage. Free-swelling cartilage disks (3 mm-diameter, 1 mm-thick) were incubated with ^{125}I-Fab at 37°C in 1×PBS with 0.1% BSA, 0.01% sodium azide, and protease inhibitors. Concentration of ^{125}I-Fab was fixed to 6.20 nM. Mean ± SEM, n = 5.

A.

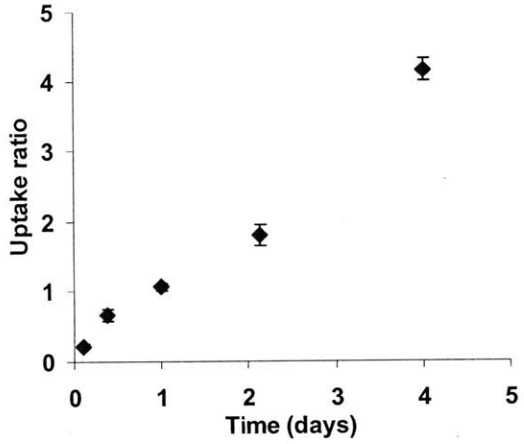

B.

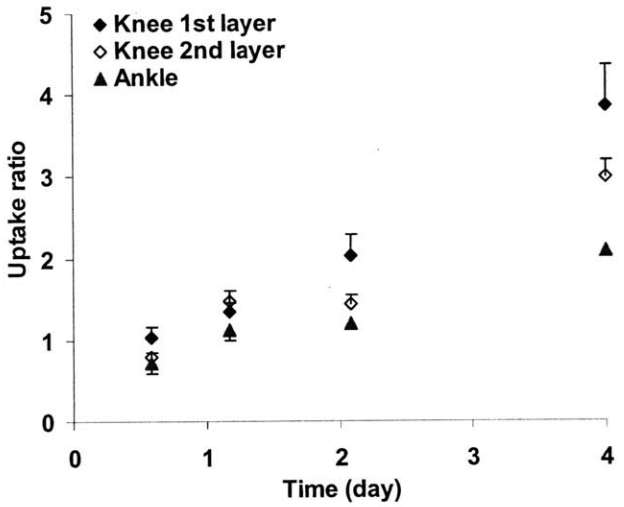

Figure 3S.2 Uptake ratio of ^{125}I-Fab in adult human cartilage. **A.** Cartilage disks were harvested from first ~ 700 μm layer of grade 0 human knee cartilage (condyle and patellar groove). Donor was 43-year old male. Free-swelling cartilage disks were incubated with ^{125}I-Fab without unlabeled Fab at 37°C in 1×PBS with 0.1% BSA, 0.01% sodium azide, and protease inhibitors. Mean ± SEM, n = 4. **B.** Cartilage disks were harvested from grade 0 human knee (condyle and patellar groove) and ankle cartilage. Donor was 28-year old male. Free-swelling cartilage disks were incubated with ^{125}I-Fab with 10 μg/ml (= 66.7 nM) unlabeled Fab at 37°C in DMEM with 0.1% BSA, and 1% ITS. Mean ± SEM, n = 5.

A.

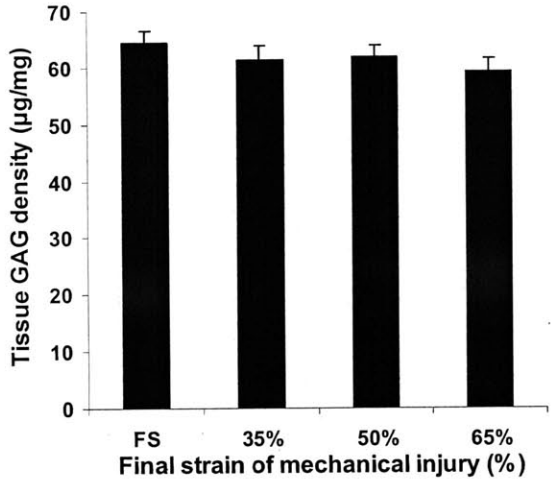

B.

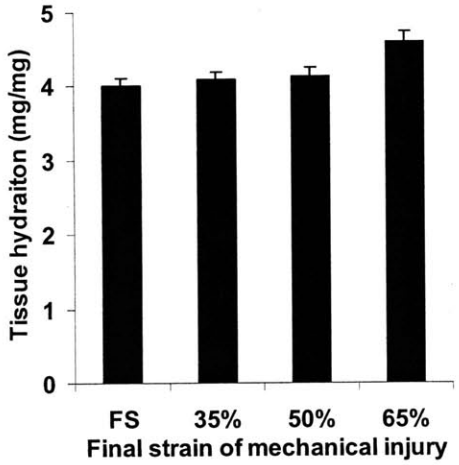

Figure 3S.3 Effect of the final strain and strain rate of mechanical injury on the tissue GAG density and tissue hydration in bovine calf cartilage ("FS" = free swelling; "35%" = 35% final strain, 70%/s strain rate; "50%" = 50% final strain, 100%/s strain rate; "65%" = 65% final strain, 130%/s strain rate). Same data sets from Figure 3.6 were used. **A.** Tissue GAG density. **B.** Tissue hydration.

A.

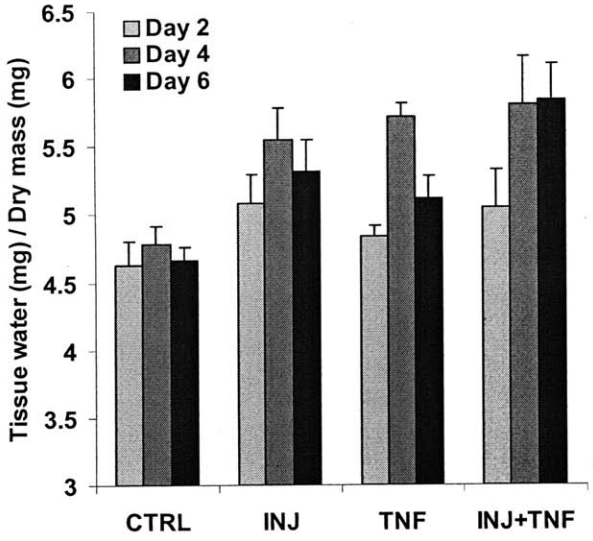

B.

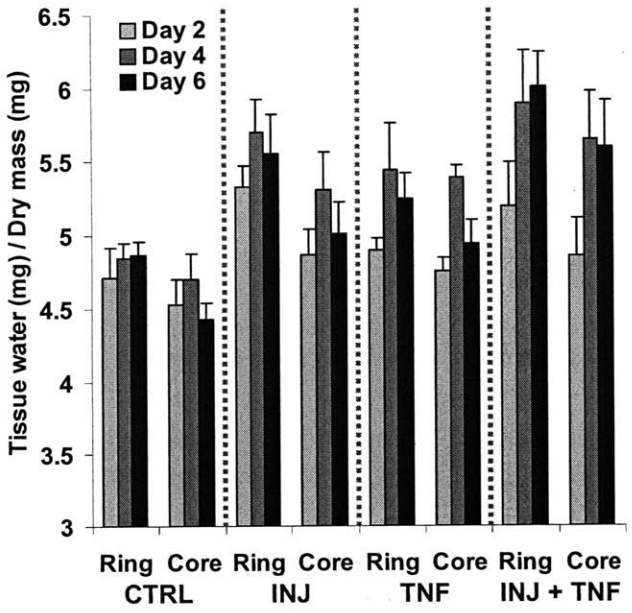

Figure 3S.4 Effect of the mechanical injury and exogenous cytokine on the tissue hydration. Disks were incubated at 37°C with ^{125}I-Fab and 10 μg/ml (= 66.7 nM) unlabeled Fab in DMEM with 0.1% BSA, and 1% ITS under 10% offset static compression. **A.** Tissue hydration of 3 mm diameter × 1-mm thick disk. **B.** Tissue hydration separately measured in the ring and core regions. Mean ± SEM, n = 4 - 5.

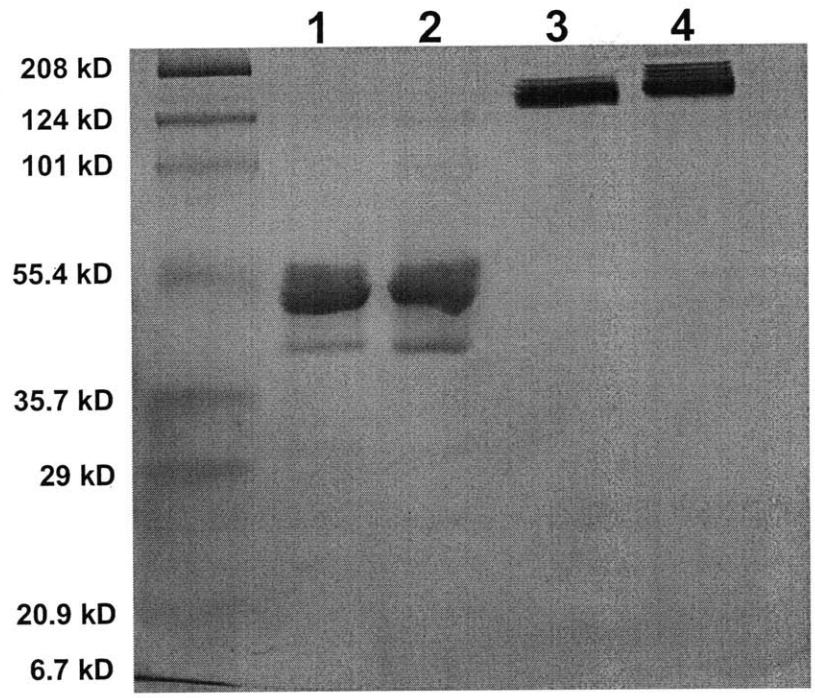

Figure 3S.5 SDS-PAGE analysis of Fab and mAb in non-reducing condition, detected by Coomassie Blue staining. **Lane 1:** Fab fresh out of stock. **Lane 2:** Fab incubated for 2 weeks at 37°C. **Lane 3:** mAb fresh out of stock. **Lane 4:** mAb incubated for 2 weeks at 37°C.

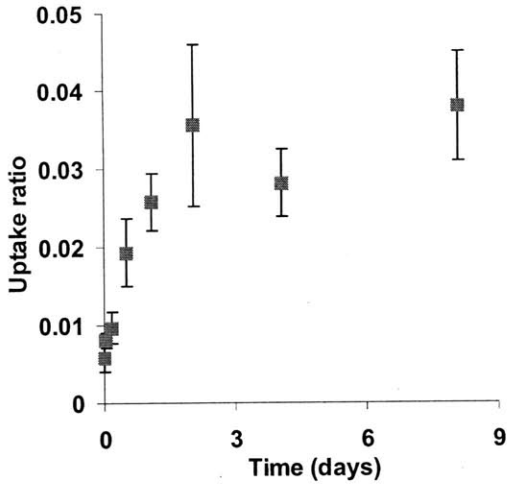

Figure 3S.6 Uptake ratio of ^{125}I-mAb in bovine calf cartilage measured at different time points. Cartilage disks (3 mm-diameter, 1 mm-thick) were incubated with ^{125}I-mAb at 4°C under free-swelling condition. Disks were incubated without unlabeled mAb in 1×PBS with 0.1% BSA, 0.01% sodium azide, and protease inhibitors. Mean ± SEM, n = 6.

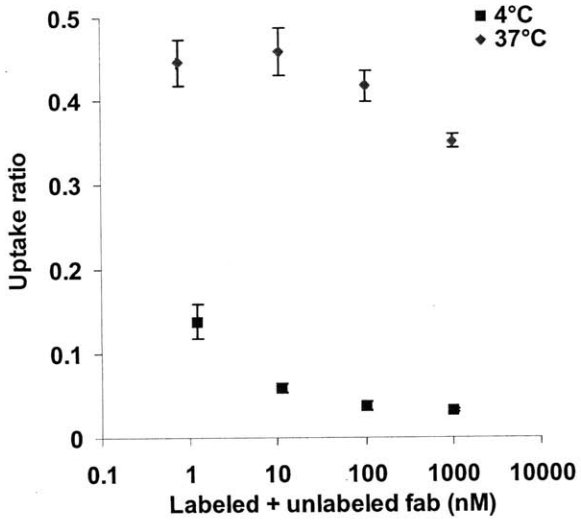

Figure 3S.7 Uptake ratio of ^{125}I-mAb with graded amount (0, 10, 100, and 1000 nM) of unlabeled mAb in bovine calf cartilage. Free-swelling cartilage disks (3 mm-diameter, 1 mm-thick) were incubated with ^{125}I-mAb either at 4°C in 1×PBS with 0.1% BSA, 0.01% sodium azide, and protease inhibitors or at 37°C in DMEM with 0.1% BSA, and 1% ITS. Concentration of ^{125}I-mAb was fixed to 1.23 nM and 0.76 nM for measurement at 4°C and 37°C, respectively. Mean ± SEM, n = 5 for 4°C and n = 5 for 37°C. 1-way ANOVA showed significant effect of concentration factor on the uptake at both temperatures ($p < 0.0001$ at 4°C, $p = 0.016$ at 37°C).

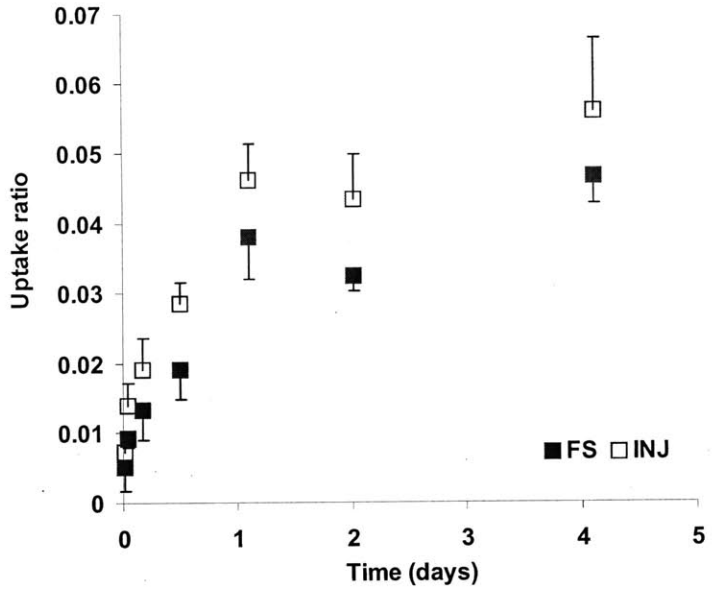

Figure 3S.8 Effect of mechanical injury on the uptake of ^{125}I-mAb in bovine calf cartilage. Uptake ratio ^{125}I-mAb in normal and injured cartilage was measured up to 4 days. Disks were incubated with ^{125}I-mAb without unlabeled mAb at 4°C in 1×PBS with 0.1% BSA, 0.01% sodium azide, and protease inhibitors. Mean ± SEM, n = 6. 2-way ANOVA (time and injury) showed significant effect of injury on the uptake ($p = 0.01$).

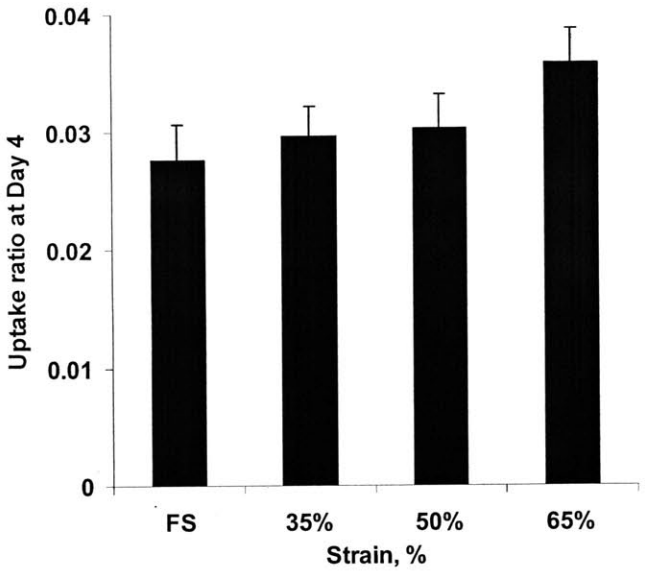

Figure 3S.9 Effect of the final strain and strain rate of mechanical injury on the uptake ratio of ^{125}I-mAb in bovine calf cartilage ("FS" = free swelling; "35%" = 35% final strain, 70%/s strain rate; "50%" = 50% final strain, 100%/s strain rate; "65%" = 65% final strain, 130%/s strain rate). Uptake ratio ^{125}I-mAb in normal and injured cartilage was measured on day 4. Disks were incubated with ^{125}I-mAb without unlabeled mAb at 4°C in 1×PBS with 0.1% BSA, 0.01% sodium azide, and protease inhibitors. Mean ± SEM, n = 16. 1-way ANOVA did not show significant effect of injury on uptake.

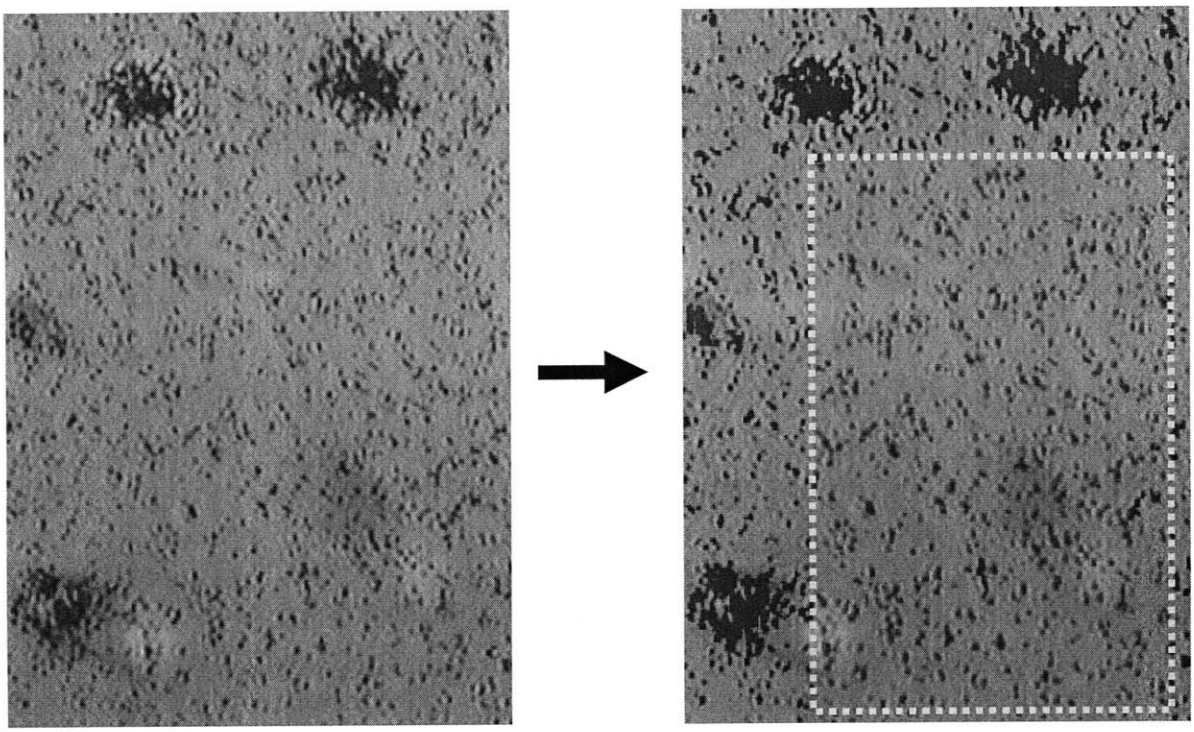

Figure 3S.10 Quantitative analysis of autoradiography of ^{125}I-mAb in adult human cartilage. Samples were prepared using same method described in Fig. 3.11 Images taken from each slice were processed by IPLab (Scanalytics, Inc.) to count grains representing ^{125}I-mAb. To distinguish grains from background staining, a threshold blue value was chosen for each image. Rectangular region of interest (yellow box) was selected while avoiding cells. Number of grains in region of interest was counted and the grain density was presented as number of grains divided by size of region of interest (pixel × pixel) in arbitrary unit.

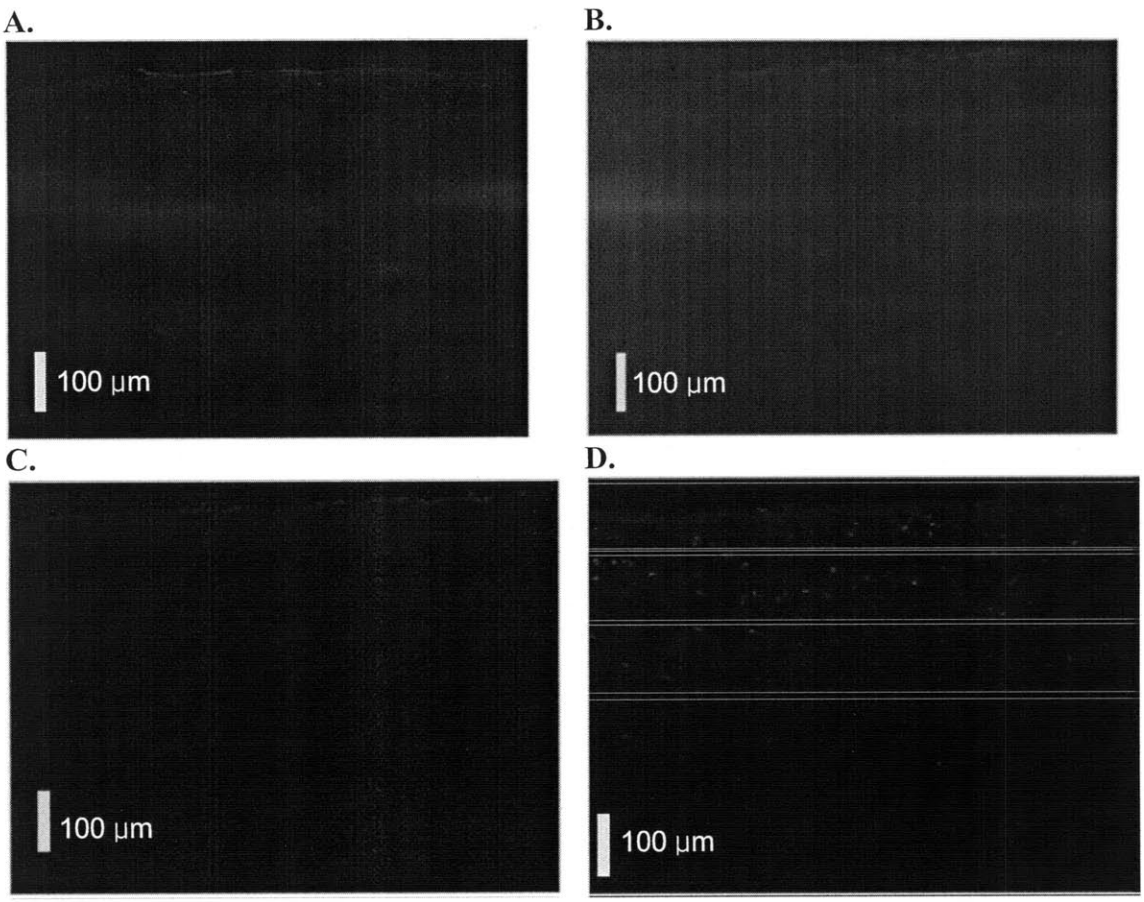

Figure 3S.11 Distribution of AlexaFluor-568 conjugated anti-IL-6 mAb in human cartilage (collaborator: Karl Kavalkovich, Centocor). Untreated or GAG-depleted human cartilage disks were incubated with fluorescent-tagged mAb for 24 hrs or 6 days. GAG depletion was carried out by incubating explants with IL-1 and OSM for 14 days prior to the experiment. **A.** Untreated tissue incubated for 24 hrs. **B.** GAG-depleted tissue incubated for 24 hrs. **C.** Untreated tissue incubated for 6 days. **D.** GAG-depleted tissue incubated for 6 days.

CHAPTER 4

Transport and Binding of Tumor Necrosis Factor-α to Matrix Sites in Articular Cartilage*

* This chapter is a manuscript in preparation for submission

4.1 Introduction

Tumor necrosis factor-α (TNFα) is a pro-inflammatory cytokine involved in cartilage matrix degradation and joint damage in OA [1]. In addition to other cytokines such as IL-1, TNFα is known as a major factor causing cartilage destruction in OA pathogenesis. TNFα stimulates the synthesis of catabolic enzymes, such as matrix metalloproteinases and aggrecanases, which are responsible for matrix degradation [1]. As a result, TNFα can induce a significant aggrecanase-mediated proteoglycan loss [2]. Interestingly, combined with mechanical injury [3] or other cytokines, such as IL-6 [4], TNFα caused a synergistic loss of GAG from cartilage explants. Also, TNFα inhibits cartilage biosynthesis [5] and increases the potency of IL-1 in stimulating chondrocytes to synthesize nitric oxide [6], which is a key catabolic mediator.

The bioactive form of TNFα is a 51 kDa trimer of 17.5 kDa monomer subunits [7, 8]; the monomers have a lower binding affinity to cell receptors and less cytotoxicity than trimers [8]. Trimer TNFα slowly dissociates to the monomer form at sub-nanomolar concentrations, but the trimer is relatively stable at the nanomolar range [7, 9]. Dissociated monomers can rapidly reassociate to trimers if an excess amount of TNFα is added [7]. However, the TNFα concentration in the synovial fluid from normal joints is < 5 pg/ml (= 0.29 pM) and increases significantly to ~40 pg/ml (= 2.4 pM) following joint injury [10-12], suggesting that, even in an abnormal joint state, the trimer TNFα would dissociate to monomers due to the low concentration of TNFα in the synovial fluid. Isoelectric point of TNFα is ~5.3, which suggests that TNFα is slightly negatively-charged in physiological pH [13].

The trimer-monomer conversion of TNFα raises interesting questions regarding the transport of TNFα to intra-tissue targets in the cartilage since the solute size significantly affects intra-tissue transport processes [14]. Since adult articular cartilage is avascular and alymphatic, solutes must be delivered through the extracellular matrix (ECM), and therefore steric hindrance between the ECM and solutes plays a key role in the transport for relatively large molecules [15]. In general, assuming that binding is not involved in transport, smaller solutes can diffuse faster than larger solutes, suggesting that the monomer TNFα could reach cell receptors faster than the trimer form. However, trimers, not monomers, are the bioactive form that can trigger cell responses.

In addition, the binding of certain proteins to sites within the ECM or, in general, to cell receptors, can change the transport kinetics through the cartilage. For example, a reversible binding of the anabolic growth factor, insulin-like growth factor-I (IGF-I), to its binding proteins sequestered within the ECM inhibited diffusion of IGF-I, and effectively increased the diffusion time of IGF-I through the adult bovine cartilage [16, 17]. Indeed, in many tissues, TNFα is known to bind to matrix molecules including heparin [18], fibronectin [19], laminin [20], decorin [21], biglycan [21], and dermatan sulfate [21] but not to chondroitin sulfate [21]. TNFα also weakly binds to collagen type I [19], type II [19], and type IV [22], which are major components of the cartilage matrix. A heparin-binding domain has also recently been identified [23]. Matrix-bound TNFα may have altered biological activity compared to soluble TNFα [19, 22, 24].

To better understand interactions between TNFα and the matrix, which may regulate the bioactivity and accessibility of TNFα to chondrocytes, our objectives were to characterize and

quantify equilibrium binding and transient transport kinetics of TNFα in cartilage, including the presence of the oligomeric as well as the monomeric forms of TNFα.

4.2 Materials And Methods

Tissue harvest. Cartilage explants were harvested from the femoropatellar grooves of 1-2 weeks old calves (Research 87, Marlborough, MA) [16]. Briefly, 9-mm diameter cartilage-bone cylinders were cored and mounted on a microtome. The top superficial layer was removed to obtain 0.5 mm-thick middle zone slices. Four or five disks (3 mm-diameter, 0.5 mm-thick) were cored from each slice using a dermal punch. All cartilage specimens were equilibrated either in the serum-free medium (low-glucose DMEM (1 g/L) supplemented with 1% insulin-transferrin-selenium (10 μg/mL insulin, 5.5 μg/mL transferrin, 5 ng/mL selenium, Sigma), 10 mM HEPES buffer, 0.1 mM nonessential amino acids, 0.4 mM proline, 20 μg/mL ascorbic acid, 100 units/mL penicillin G, 100 μg/mL streptomycin, and 0.25 μg/mL amphotericin B in a 37°C, 5% CO2 incubator or in the 1× phosphate buffered saline (PBS) supplemented with 0.1% bovine serum albumin (BSA), 0.01% sodium azide (NaN_3) and protease inhibitors (Complete, Roche Applied Science, Indianapolis, IN) at 4°C prior to experiments.

Solute preparation. Iodinated TNFα was purchased from PerkinElmer (Waltham, MA). Before all experiments using ^{125}I-TNFα, Sephadex G25 chromatography was used to separate and remove any small ^{125}I-species that may have resulted from degradation of iodinated proteins, (0.7 × 50 cm columns using an elution buffer of 1×PBS buffer with 0.1% BSA and 0.01% NaN_3, and the void volume collected for the desired ^{125}I-TNFα) [16].

Injurious compression. Cartilage disks to be injured were placed individually between impermeable platens of a polysulfone chamber (50 % strain, 100%/s strain rate), which generates radially unconfined compression [25]. During the injury loading, the disk was

compressed to 50% strain with a constant velocity of 1mm/second and immediately released with the same rate (50 % strain, 100%/s strain rate). This injury protocol usually resulted in a peak stress of ~ 20 MPa, which is known to produce ECM damage and cell death.

Measurement of uptake ratio. Disks were incubated with a fixed amount of labeled solutes with or without unlabeled solutes. The buffer consisted of 1×PBS supplemented with 0.1% BSA, 0.01% NaN_3 and protease inhibitors at 4°C or DMEM supplemented with 1% ITS, and 0.1% BSA at 37°C. At selected time points, disks were removed from the bath and briefly rinsed in fresh PBS buffer. The surface of each disk was quickly blotted with Kimwipes and the wet weight was measured. The ^{125}I-radioactivity of each cartilage disk and aliquots of the equilibration baths were quantified individually using a gamma counter. Disks were then lyophilized and the dry weight was measured; the water weight of each disk was calculated from the tissue wet and dry weights. The *uptake ratio* was calculated as the concentration of the ^{125}I-TNFα in the cartilage disks (per intra-tissue water weight) normalized to the concentration of ^{125}I-TNFα in the equilibration bath. The disks were then digested with proteinase-K (Roche Applied Science, Indianapolis, IN) and the sulfated glycosaminoglycan (sGAG) content of each disk was measured using the dimethylmethylene blue (DMMB) dye binding assay [26]. Samples from the baths were again analyzed by Sephadex G75 chromatography to determine whether any small labeled species (e.g., ^{125}I) may have accumulated from degradation of ^{125}I-TNFα during each experiment. The uptake ratio was corrected to take into account the presence of any such small labeled species, assuming the small species to be ^{125}I [27]. In a separate control experiment, the uptake ratio of ^{125}I alone was measured to calibrate the correction factor, which was ~ 0.6.

To investigate the possibility that TNFα may bind to specific sites within the cartilage tissue, disks were incubated with a fixed amount of labeled solutes with graded amounts of unlabeled solutes, and we compared the measured uptake ratio to a theoretical model as described in 2.2 Materials and Methods in Chapter 2.

Ring-Core transport study. Plugs were compressed to ~ 10% final strain between impermeable platens of a polysulfone plastic loading chamber to prevent diffusion from the top and bottom surfaces. Static compression would only allow the flux from the radial direction. At selected time points after adding radiolabeled or unlabeled solutes, disks were briefly rinsed, and a 2-mm diameter core was punched from the center of a 3 mm diameter plug. The uptake ratios in the annular ring and inner core were separately measured as described above.

Cross-linking TNFα. ^{125}I-TNFα or unlabeled TNFα was cross-linked with bifunctional reagent *Bis* -|| sulfone (BSOCOES, Pierce Chemical Co.) [8]. ^{125}I-TNFα in 1×PBS with 0.1% BSA or unlabeled TNFα in 1×PBS was reacted with 1 mM BSOCOES for 10 min at 4°C. To quench the reaction, 1 M glycine in 0.1 M sodium phosphate buffer, pH 7.5, was added to a final concentration of 100 mM glycine and incubated for at least 15 min at 4°C. To remove uncross-linked species, reacted ^{125}I-TNFα or unlabeled TNFα were passed through 30 kDa-cutoff centrifugal filter (Millipore, Billerica, MA) and retentates were collected. The concentration of cross-linked unlabeled TNFα was determined by BCA protein assay (Thermo Scientific, Rockford, IL).

4.3 Results

Timer-monomer distribution of TNFα was a function of TNFα concentration. To investigate the effect of TNFα concentration on the trimer-monomer conversion, ^{125}I-TNFα was

incubated with a graded amount of unlabeled TNFα for 24 hrs or 48 hrs at 4°C (Fig. 4.1). With added unlabeled TNFα, ^{125}I-TNFα formed the trimer with unlabeled TNFα, and a higher concentration of unlabeled TNFα induced a larger and sharper trimer peak. There was no significant difference between 24 hrs and 48 hrs incubation when unlabeled TNFα was added (Fig. 4.1b, c). However, without added unlabeled TNFα, more ^{125}I-TNFα existed as a monomer after 48 hrs compared to 24 hrs (Fig 4.1a).

Equilibrium and transient uptake ratio of ^{125}I-TNFα depended on the bath concentration of TNFα. The uptake ratio of ^{125}I-TNFα in both human and bovine cartilage was ~6-7 at low concentrations of unlabeled TNFα and decreased markedly with the addition of unlabeled TNFα (Fig. 4.2). The addition of sodium azide and protease inhibitors did not substantially alter the uptake ratio (Fig. 4.2a, Viable cells vs. Non-viable cells). A similar result was observed when the experiment was repeated using 1×PBS with 0.1% BSA at 4°C (Fig. 4S.3), indicating that cellular activity was not the major determinant of the equilibrium binding of TNFα within the tissue. GAG loss from explants during 48 hrs of TNFα incubation at all concentrations was <5.8% for media with azide (<11.5% for without azide, Fig. 4S.2).

One way to explain the decrease in the uptake ratio with added unlabeled TNFα is the competition for binding sites between ^{125}I- and unlabeled TNFα. For this case, we used a theoretical model based on a first-order, reversible, bimolecular reaction involving one dominant family of binding sites. This model treated monomeric and trimeric TNFα as the same molecule, hence having the same binding properties. The estimated binding parameters for the medium with sodium azide and protease inhibitors were $N_T = 10.8 \pm 0.63$ nM, $K_{eq} = 1.86 \pm 0.01$ nM, and $K = 0.99 \pm 0.03$ (1 nM ≡ 17 ng/ml). The theoretical curve of the uptake ratio (solid line, Fig. 4.2a) was constructed from these binding parameters. For comparison, the

TNFα cell receptor density is sub-nanomolar, significantly lower than the predicted site density, N_T, based on the known cell density [28] and the number of TNFα receptors per cell [29].

Measurements of the transient uptake ratio of ^{125}I-TNFα up to 2 days (Fig. 4.3a), combined with the equilibrium binding parameters (N_T, K_{eq}, K) from Fig. 4.2 and the transient diffusion-reaction theory [16], gave a diffusivity for ^{125}I-TNFα within cartilage of 9×10^{-8} cm^2/s without unlabeled TNFα, and a lower value, 1.2×10^{-8} cm^2/s, with 340 ng/mL of unlabeled TNFα. G75 chromatography (Fig. 4.3b) showed that ^{125}I-TNFα existed more as a monomer at the low TNFα concentration but formed the trimer at higher concentrations, as previously reported [7].

Equilibrium uptake ratio of cross-linked ^{125}I-TNFα was significantly lower than that of native ^{125}I-TNFα. A decrease in the uptake ratio with the unlabeled TNFα (Fig. 4.2) also can be explained by different binding properties for trimer and monomer. Svenson et al. showed a higher nonspecific binding of monomeric than of trimeric ^{125}1-TNFα to IgG [30]. To test whether the monomer and the trimer have different binding and uptake in the cartilage, we cross-linked TNFα to artificially generate a trimer-only TNFα. Using BSOCOES as a cross-linking agent, both ^{125}I-TNFα and unlabeled TNFα were successfully cross-linked to a trimeric form showing a higher molecular weight (Fig. 4.4). Cross-linked ^{125}I-TNFα remained in the trimer form at a sub-nanomolar concentration, at which untreated ^{125}I-TNFα spontaneously dissociates to the monomer (Fig. 4.4a). Native unlabeled TNFα appeared at three distinctive bands in the SDS-PAGE analysis, representing the trimer, dimer, and monomer (Fig. 4.4b), whereas cross-linked unlabeled TNFα showed a single band at the trimer location (Fig. 4.4b).

To test whether cross-linking disrupts the bioactivity of TNFα, the catabolic effect of cross-linked TNFα on the cartilage tissue was compared to that of native TNFα. Sulfate

incorporation rate was decreased by both native and cross-linked TNFα although only 100 ng/ml native TNFα showed a significant difference (Fig. 4.5a). Similarly, GAG loss to medium was increased by adding both native and cross-linked TNFα (Fig. 4.5b). Cross-linked TNFα showed similar catabolic effects on cartilage tissue, suggesting that cross-linking did not disrupt the TNFα-cell receptor binding.

The equilibrium uptake of cross-linked ^{125}I-TNFα was measured with and without cross-linked unlabeled TNFα. The uptake ratio of cross-linked ^{125}I-TNFα decreased from 0.8 to 0.47 with added cross-linked unlabeled TNFα and was significantly lower than that of native ^{125}I-TNFα (Fig. 4.6a), suggesting that the trimer exhibits less binding to matrix sites than the monomer. Unlike native ^{125}I-TNFα (Fig. 4.3b), cross-linked ^{125}I-TNFα remained as the trimer regardless of the presence of cross-linked unlabeled TNFα (Fig. 4.6b).

Equilibrium uptake of ^{125}I-TNFα was not affected by trypsin treatment. To examine and differentiate between possible binding sites in the matrix, the tissue was treated with trypsin, and the uptake ratio was measured. Trypsin is known to digest fibronectin [31], laminin [32], proteoglycan core proteins and other non-collagenous proteins. Interestingly, trypsin treatment did not significantly alter the uptake ratio of ^{125}I-TNFα regardless of the presence of unlabeled TNFα, suggesting that the binding sites were not removed by trypsin treatment (Fig. 4.7). Further treatment with chondroitinase ABC following trypsin treatment did not change the uptake ratio, which confirmed that chondroitin sulfate GAGs were not the major binding sites of TNFα (Fig. 4S.5).

^{125}I-TNFα was able to penetrate into the cartilage tissue. To test whether ^{125}I-TNFα is able to penetrate into the cartilage and not just sticking to the outer surface of the cartilage, the uptake ratio was separately measured in the ring and core regions using a static compression

chamber. Although the uptake ratio measured in the ring was significantly higher than that in the core, ^{125}I-TNFα did show certain amount of penetration into the core (Fig 4.8a). Trypsin treatment significantly increased the uptake ratio in the core compared to the uptake measured in the core of normal disks at the same time point, indicating the depletion of GAG decreased the steric hindrance and facilitated the diffusive transport into the core region. As a result, unlike the normal tissue, trypsin treated disks showed similar values of the uptake ratio for the ring and core. Adding unlabeled TNFα reduced uptake ratios in both ring and core regions for normal and trypsinized disks. The distribution of trimer-monomer forms of ^{125}I-TNFα was well preserved until the end of experiment (Fig. 4.8b-c).

4.4 Discussion

Predicted binding site density from the fit of biomolecular reaction model was ~10 nM, significantly higher than the TNFα cell receptor density, which is sub-nanomolar [28, 29]. The results of this study suggest that TNFα binds to sites within the cartilage matrix, resulting in the TNFα concentration higher in the tissue than the bath. The monomeric form of TNFα showed stronger binding than the trimer TNFα. As a result, the trimer-monomer conversion of TNFα played a key role in regulating the binding of TNFα. Trypsin treatment of explants did not change the extent of binding of TNFα, indicating that binding sites were not removed by trypsin treatment.

The equilibrium uptake ratio decreased markedly with addition of graded amounts of unlabeled TNFα, suggested that there was significant binding of TNFα to the tissue matrix. Interestingly, the fit of the equilibrium binding isotherm and the transient uptake theory to their respective data were consistent with the reversible binding of TNFα to a single, dominant

family of binding sites within the matrix. However, this model was based on the bimolecular reaction model which assumed that the trimer and the monomer had the same partition coefficient, binding site density, dissociation constant.

Svenson et al. suggested that the TNFα monomer had a higher binding affinity to a human immunoglobulin than the trimer [30]. Our study with the cross-linked TNFα, indeed, showed that the trimeric TNFα exhibited significantly less binding than the monomer, in contrast to our model that assumed the bimolecular reaction with the same binding constants for both species. One caveat in understanding the result using cross-linked TNFα is that cross-linking process might change the structure of TNFα and disrupt its native binding property. This concern was also raised from Smith et al. and they showed that cross-linked TNFα had a weaker binding to cell receptors. As a result, in order to elicit the same level of cytotoxicity, more cross-linked TNFα was needed than the native TNFα [8]. However, although the activity from the cross-linked TNFα was weaker than the native TNFα, the receptor binding was not completely lost [8]. Our observation of GAG loss and the reduction in the biosynthesis induced by the cross-linked TNFα in the cartilage also suggested that the binding to receptors on chondrocytes was not significantly disrupted by cross-linking. This suggested that the TNFα structure was not severely disturbed after cross-linking, although the binding mechanism to cell receptors may be different from that to matrix binding sites.

The monomer form of TNFα can travel faster than the trimer in the tissue due to its smaller size, but the binding of monomer TNFα will effectively slow down the diffusion of monomer. The TNFα concentration in the synovial fluid is in the picomolar range, suggesting that the soluble TNFα trimer will slowly dissociate to monomers. Once TNFα is dissociated to monomers, TNFα monomers will bind to the matrix, which will hinder the diffusion of TNFα

in the cartilage even though the monomers have a higher diffusivity than the trimers. Additionally, the TNFα monomers have to reassociate to the trimer in order to bind cell receptors since the trimer is the bioactive form. These additional steps will reduce the ability of the TNFα monomer to stimulate chondrocytes within the cartilage tissue. If the trimer TNFα can maintain its trimeric form until it reaches to cell receptors during the transport through the matrix, the trimer will diffuse with less binding than the monomer although the diffusion of trimer is slower than the monomer. It is important to note that the local TNFα concentration is not an only factor that governs the availability of TNFα around the cells. The trimer-to-monomer conversion, according to the local concentration of TNFα, along with different binding affinities of the trimer and the monomer to matrix sites can also play a major role in regulating the availability and bioactivity of TNFα.

If there is no other mechanism that prevents the dissociation of trimeric TNFα to the monomer form within the synovial fluid or cartilage tissue, a significant portion of TNFα will be in monomeric due to its low concentration. As described above, considering binding and inferior bioactivity, the monomer TNFα will possess reduced ability to stimulate chondrocytes compared to the trimer. A further complication is the presence of soluble forms of TNFα receptor (sTNFR), which are well known to inhibit the effect of TNFα [1]. However, Aderka et al. showed that sTNFR can augment the effect of TNFα by stabilizing the structure of TNFα when sTNFR exists at low concentrations [33]. This suggests that sTNFR can function as a carrier of TNFα, maintaining the trimeric form of TNFα during transport. However, molecular weights of receptor-ligand complexes are 75 kDa and 100 kDa with sTNFR-I and sTNFR-II, respectively [34], indicating the complex will be largely excluded from the interstitial space.

Trypsin treatment of cartilage did not significantly change the uptake ratio of TNFα, suggesting that the binding site(s) were not removed by trypsin. Trypsin is known to degrade proteoglycan core proteins, suggesting that collagen may be one of the candidates for binding. In the cartilage, collagen type II is most abundant form and collagen types IX, XI, VI, and X, are present in relatively smaller amounts. Considering relative abundance, collagen type II is a major candidate for binding sites. Indeed, TNFα is known to bind weakly to collagen type I, II, and IV [19, 22]. TNFα is not the only cytokine or growth factor that is known to bind to collagen molecules. There are other growth factors known to bind collagens, including transforming growth factor-β that binds to collagen type VI and platelet derived growth factor that binds to collagen type I, II, III, IV, V, and VI. [35]. Ongoing studies are focusing on the further identification of the matrix molecules and proteins that bind TNFα.

In summary, our results suggest that TNFα monomers bind to matrix sites, which can significantly slow the transient transport of TNFα within cartilage. In addition, since the local concentration of TNFα can affect the trimer-to-monomer conversion, cartilage matrix can play a major role in regulating the local concentration and bioactivity of TNFα. In turn, TNFα stimulation of cells can upregulate matrix remodeling and degradation. Identifying the matrix binding sites and its binding mechanism will help us to better understand the feedback between cytokine stimulation and matrix remodeling.

4.5 Figures

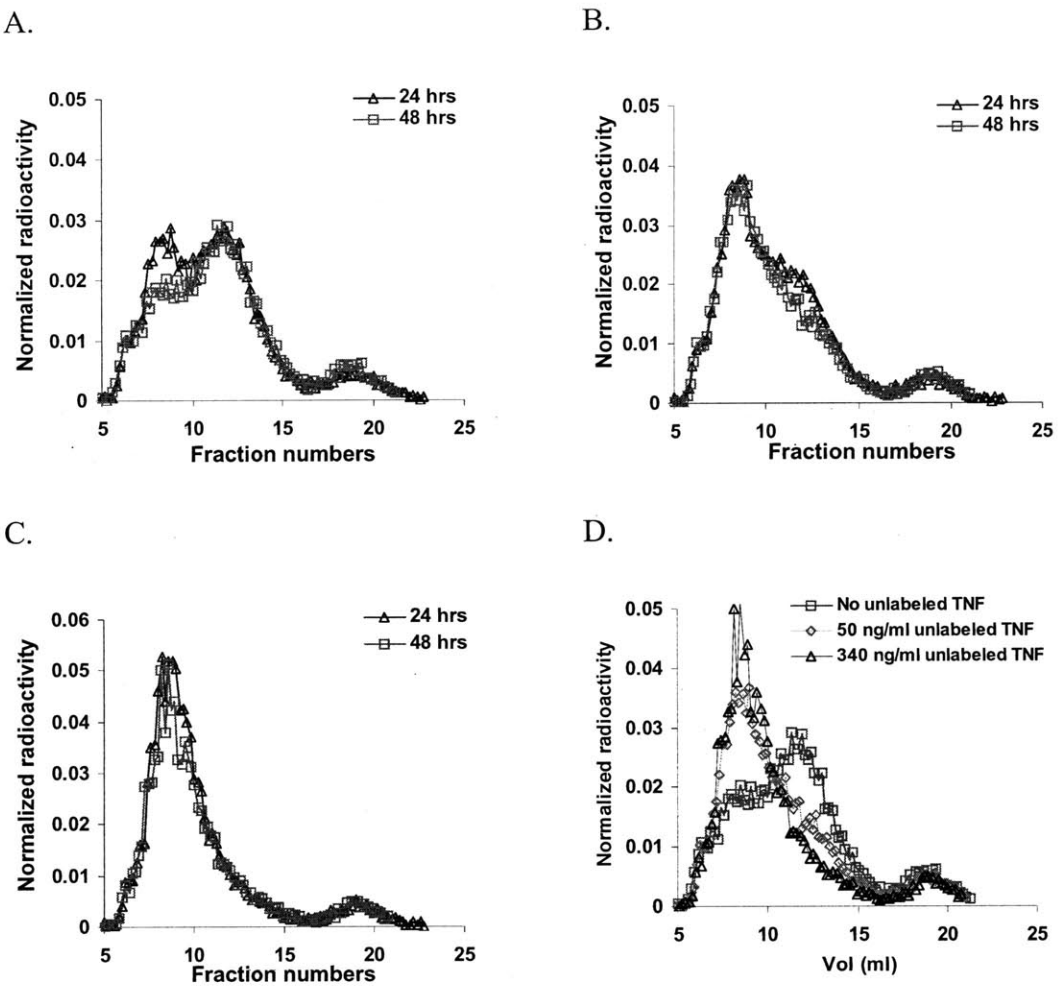

Figure 4.1 Effects of concentration of TNFα on the distribution of monomeric and oligomeric forms. A fixed amount of ^{125}I- TNFα (2.55 ng/ml = 0.15 nM) was incubated with a graded amount of unlabeled TNFα for 24 hrs or 48 hrs at 4°C. Samples were analyzed by Sephadex G75 gel filtration chromatography. **A.** No unlabeled TNFα was added. **B.** 50 ng/ml (2.94 nM) unlabeled TNFα was added. **C.** 340 ng/ml (20 nM) unlabeled TNFα was added. **D.** Results from A ~ C at 48 hrs were plotted together.

A.

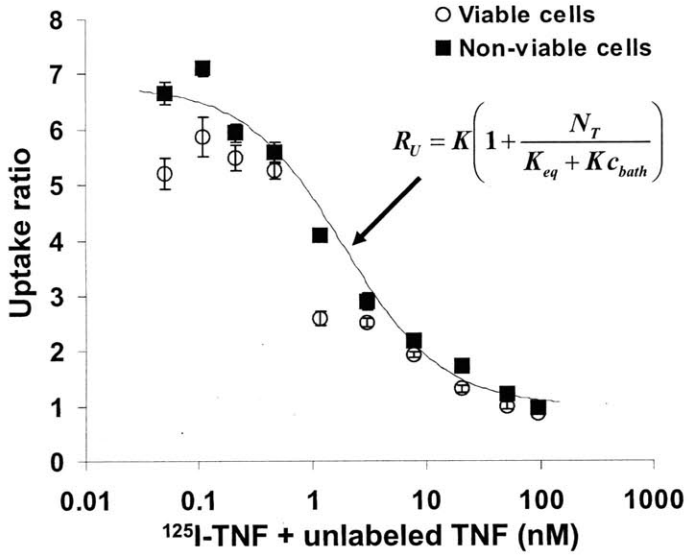

B.

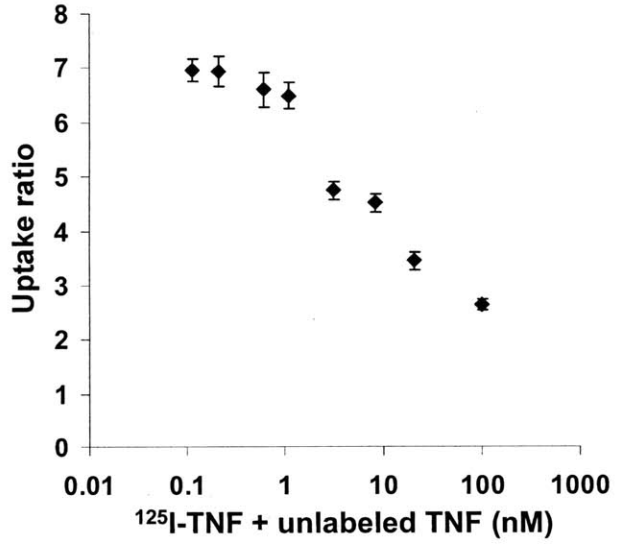

Figure 4.2 **A.** Equilibrium uptake ratio of ^{125}I-TNFα (0.838 ng/ml = 0.0492 nM) in bovine calf cartilage. Disks were incubated in DMEM with 1% ITS, and 0.1% BSA at 37°C for 48 hrs in the presence (closed square, non-viable cell) or absence (open circle, viable cell) of 0.01% sodium azide (NaN_3) + protease inhibitors. Solid line shows theoretical prediction for the medium with sodium azide assuming a dominant single family of binding sites. (n = 6, mean ± SEM). The uptake ratio decreased with addition of graded amounts of unlabeled TNFα. **B.** Equilibrium uptake ratio of ^{125}I-TNFα (1.91 ng/ml = 0.112 nM) in adult human cartilage (grade 0 tissue from patellar groove, 44 yr, male, normal weight). Disks were incubated in 1×PBS with 0.1% BSA, protease inhibitors, and 0.01% NaN_3 at 37°C for 48 hrs (n = 8, mean ± SEM). The uptake ratio decreased with a graded amount of unlabeled TNFα.

A.

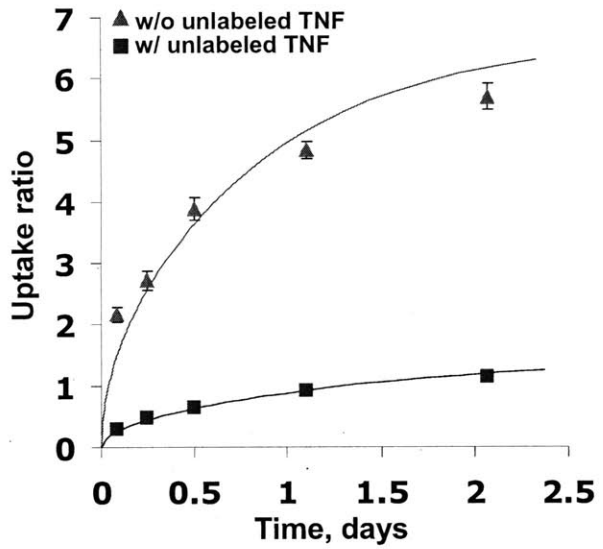

B.

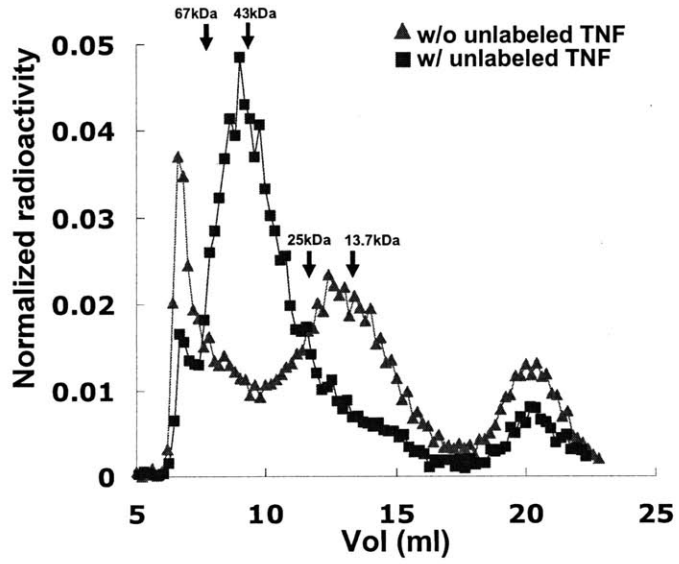

Figure 4.3 **A.** Transient transport of ^{125}I-TNFα (0.838 ng/ml = 0.0492 nM) with or without unlabeled TNFα (340 ng/ml = 20 nM) into bovine calf cartilage. Disks were incubated in DMEM with 1% ITS, and 0.1% BSA at 37°C. Solid lines are prediction of diffusion-reaction theory (n = 6, mean ± SEM). **B.** Sephadex G75 chromatograms of equilibration baths. Arrows indicate the elution volumes of molecular weight standards (kDa).

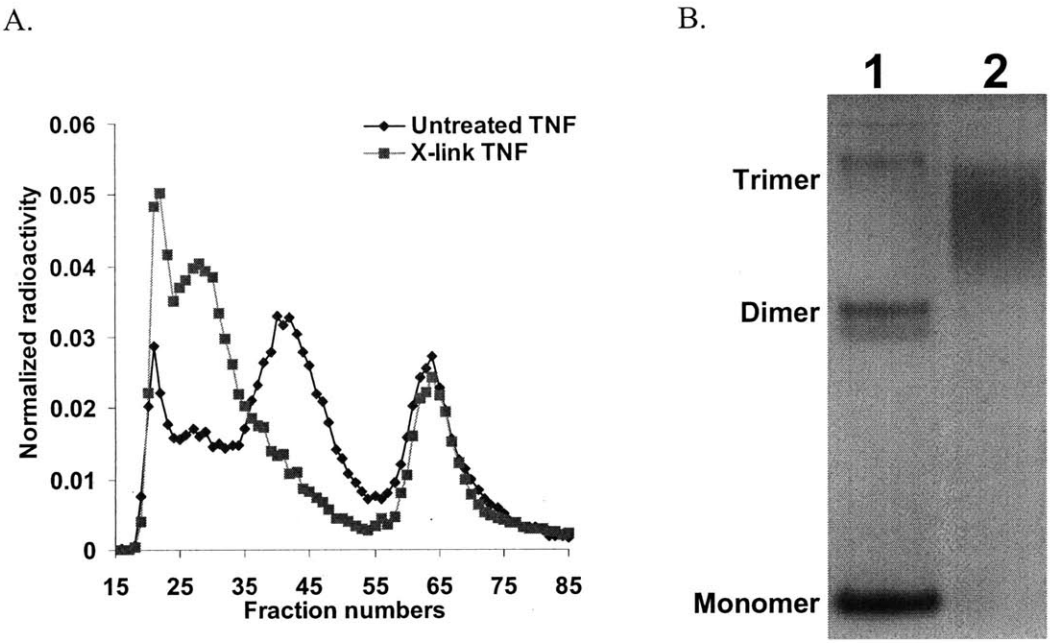

Figure 4.4 **A.** Sephadex G75 chromatography of native ^{125}I-TNFα and cross-linked ^{125}I-TNFα. ^{125}I-TNFα (5 nM) was either cross-linked or untreated, and then diluted to a final concentration of 0.1 nM. After 24 hrs at 37°C, each sample was run through a G75 column. **B.** SDS-PAGE analysis of native (lane 1) and cross-linked (lane 2) unlabeled TNFα, detected by silver staining. Unlabeled TNFα was either cross-linked or kept untreated. Cross-linked TNFα was passed through 30 kDa-cutoff centrifugal filter to remove uncross-linked monomers and to only retain trimer TNFα. Native TNFα was also filtered using the same method to test whether the ultrafiltration step would disrupt the structure of TNFα. Collected retentates from filtration were run through SDS-PAGE (10% Bis-Tris gel) under non-reducing condition and detected by silver staining. Cross-linked TNFα showed a single trimer band. However, native TNFα showed three bands representing trimer, dimer, and monomer since non-covalently linked TNFα trimer retained after filtration was dissociated into dimer and monomer during SDS-PAGE.

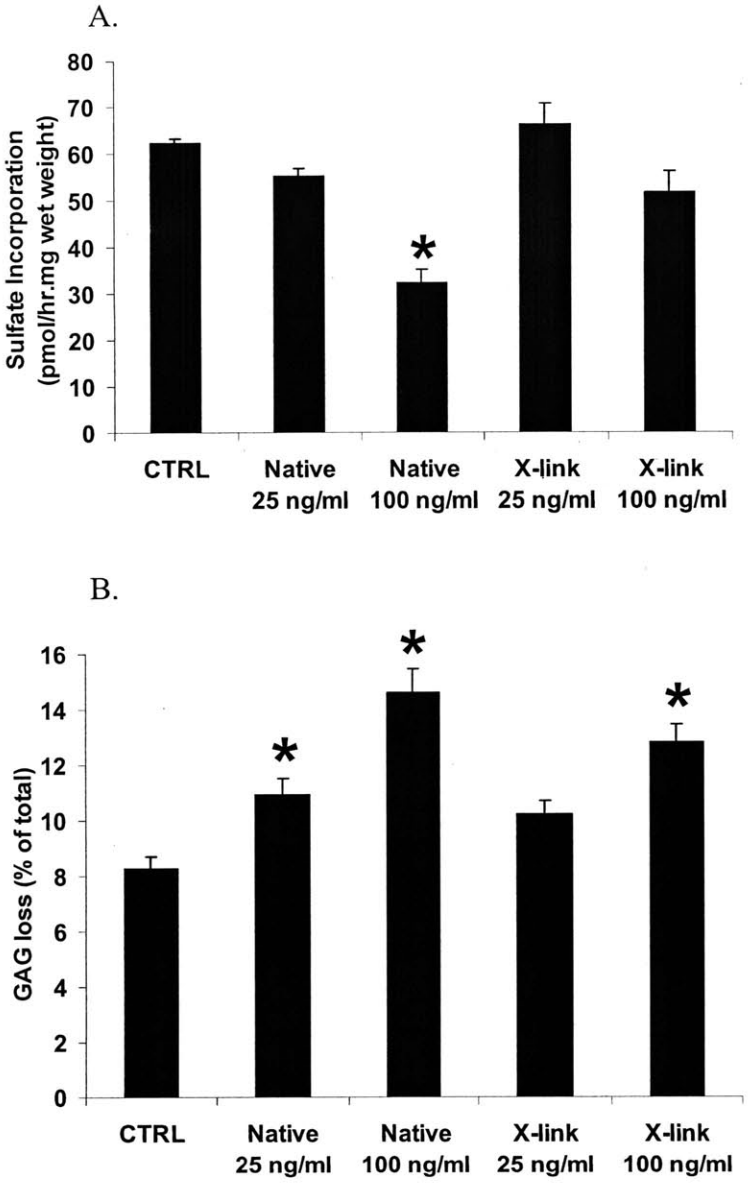

Figure 4.5 Bioactivity of cross-linked TNFα was compared to native TNFα. **A.** Sulfate incorporation rate during last 48 hrs of 6-day incubation. **B.** GAG loss to media during 6-day incubation. n = 6, mean ± SEM, *p<0.05, 1-way ANOVA, post-hoc Dunnett's test with CTRL as a reference.

A.

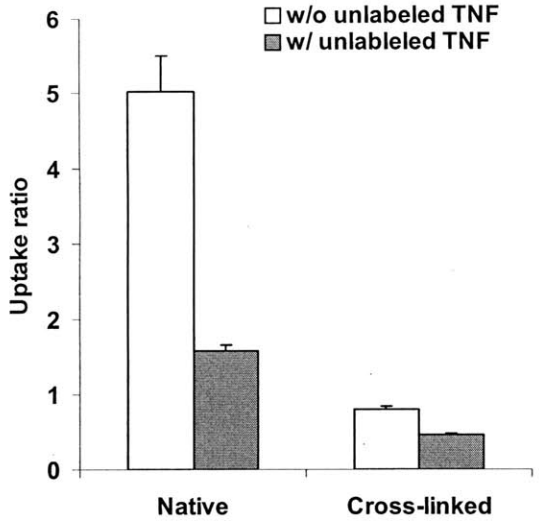

B.

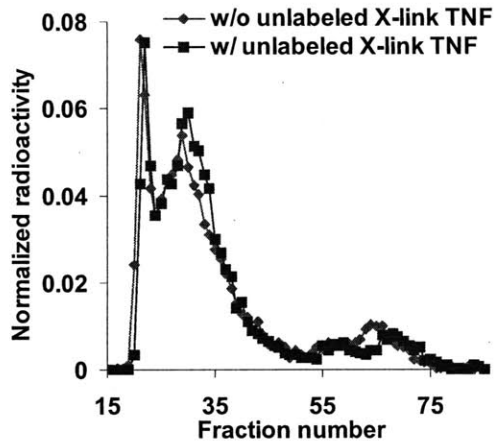

Figure 4.6 **A.** Uptake ratio of native and cross-linked ^{125}I-TNFα. Native ^{125}I-TNFα (23 pM) was incubated with or without 20 nM native unlabeled TNFα for 24 hrs at 4°C. Cross-linked ^{125}I-TNFα (81 pM) was incubated with or without 20 nM cross-linked unlabeled TNFα for 24 hrs at 37°C. **B.** Sephadex G75 chromatography of cross-linked ^{125}I-TNFα (81 pM) with or without 20 nM cross-linked unlabeled TNFα.

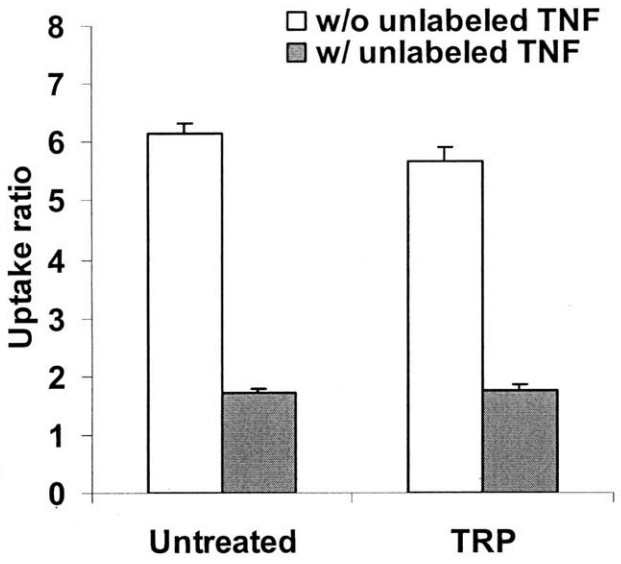

Figure 4.7 Effect of trypsin treatment on the equilibrium uptake of ^{125}I-TNFα in the bovine calf cartilage with the presence or absence of unlabeled TNFα (340 ng/ml = 20 nM). Disks were either free swelled (Untreated) or treated with 0.1 mg/ml trypsin for 48 hrs at 37°C (TRP). Disks were incubated with ^{125}I-TNFα (0.39 ng/ml = 0.023 nM) and unlabeled TNFα (0 or 20 nM) for 48 hrs in 1×PBS with 0.1% BSA, protease inhibitors, and 0.01% NaN_3 at 37°C (n = 5, mean ± SEM).

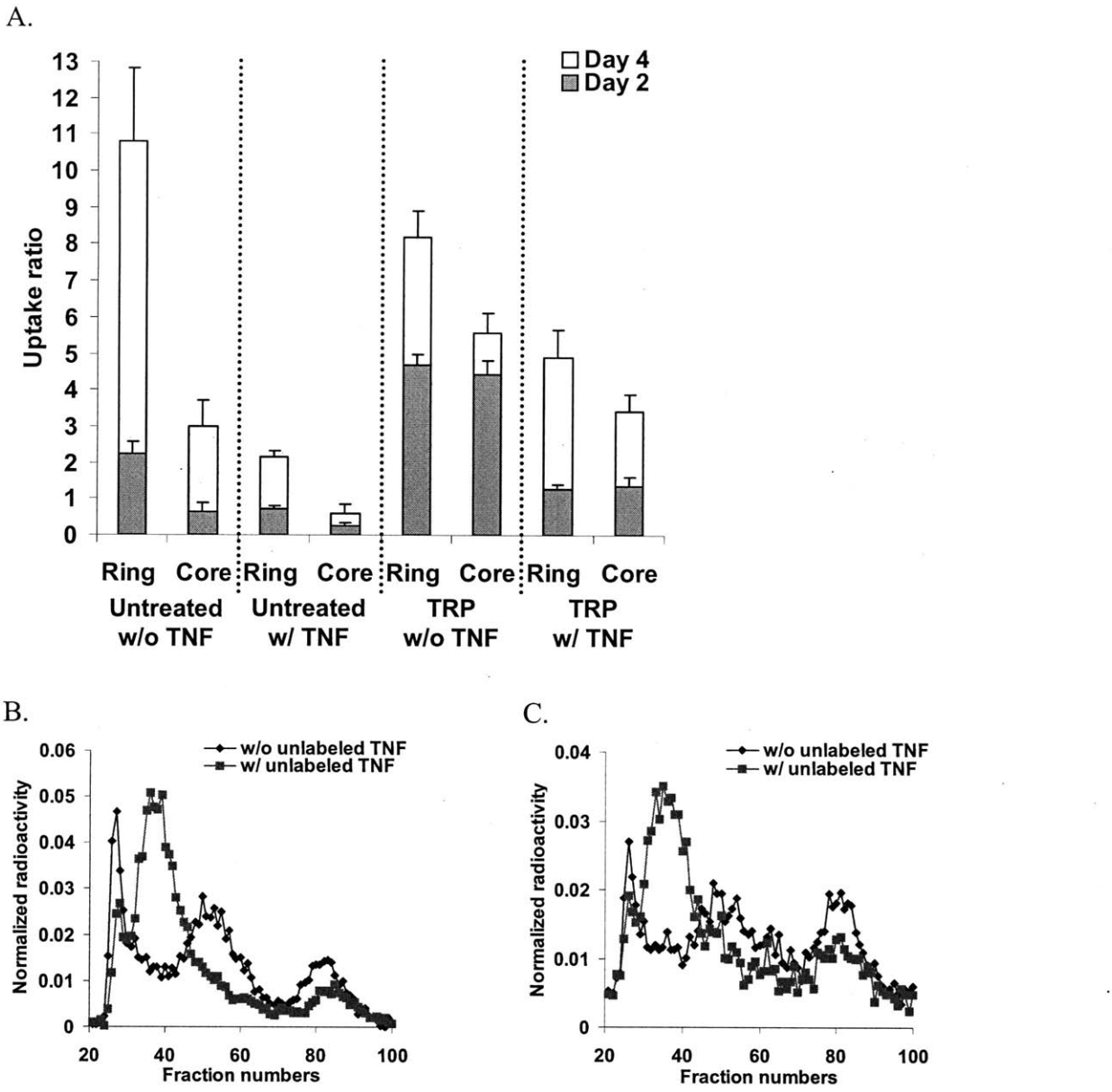

Figure 4.8 **A.** Uptake ratio of ^{125}I-TNFα in the ring and core of the bovine calf cartilage with the presence or absence of unlabeled TNFα (340 ng/ml = 20 nM). 1 mm-thick disks were maintained either free swelling (Untreated) or treated with 0.1 mg/ml trypsin for 48 hrs at 37°C (TRP) before being compressed to ~ 900 μm between impermeable platens. Disks were incubated with ^{125}I-TNFα (0.39 ng/ml = 0.023 nM) and unlabeled TNFα (0 or 20 nM) for up to 4 days in 1×PBS with 0.1% BSA, protease inhibitors, and 0.01% NaN_3 at 37°C (n = 4, mean ± SEM). **B.** Sephadex G75 chromatography analysis of equilibrating baths collected at day 2. **C.** Sephadex G75 chromatography analysis of equilibrating baths collected at day 4.

4.6 References

[1] Goldring MB. Osteoarthritis and cartilage: the role of cytokines. Curr Rheumatol Rep 2000;2:459-65.
[2] Arner EC, Hughes CE, Decicco CP, Caterson B, Tortorella MD. Cytokine-induced cartilage proteoglycan degradation is mediated by aggrecanase. Osteoarthr Cartilage 1998;6:214-28.
[3] Patwari P, Cook MN, DiMicco MA, Blake SM, James IE, Kumar S, Cole AA, Lark MW, Grodzinsky AJ. Proteoglycan degradation after injurious compression of bovine and human articular cartilage in vitro: interaction with exogenous cytokines. Arthritis Rheum 2003;48:1292-301.
[4] Sui Y, Lee JH, Dimicco MA, Vanderploeg EJ, Blake SM, Hung HH, Plaas AH, James IE, Song XY, Lark MW, Grodzinsky AJ. Mechanical injury potentiates proteoglycan catabolism induced by interleukin-6 with soluble interleukin-6 receptor and tumor necrosis factor alpha in immature bovine and adult human articular cartilage. Arthritis Rheum 2009;60:2985-96.
[5] Patwari P, Lin SN, Kurz B, Cole AA, Kumar S, Grodzinsky AJ. Potent inhibition of cartilage biosynthesis by coincubation with joint capsule through an IL-1-independent pathway. Scand J Med Sci Sports 2009;19:528-35.
[6] Stadler J, Stefanovic-Racic M, Billiar TR, Curran RD, McIntyre LA, Georgescu HI, Simmons RL, Evans CH. Articular chondrocytes synthesize nitric oxide in response to cytokines and lipopolysaccharide. J Immunol 1991;147:3915-20.
[7] Corti A, Fassina G, Marcucci F, Barbanti E, Cassani G. Oligomeric tumour necrosis factor alpha slowly converts into inactive forms at bioactive levels. Biochem J 1992;284 (Pt 3):905-10.
[8] Smith RA, Baglioni C. The active form of tumor necrosis factor is a trimer. J Biol Chem 1987;262:6951-4.
[9] Poiesi C, Albertini A, Ghielmi S, Cassani G, Corti A. Kinetic analysis of TNF-alpha oligomer-monomer transition by surface plasmon resonance and immunochemical methods. Cytokine 1993;5:539-45.
[10] Irie K, Uchiyama E, Iwaso H. Intraarticular inflammatory cytokines in acute anterior cruciate ligament injured knee. Knee 2003;10:93-6.
[11] Cameron M, Buchgraber A, Passler H, Vogt M, Thonar E, Fu F, Evans CH. The natural history of the anterior cruciate ligament-deficient knee. Changes in synovial fluid cytokine and keratan sulfate concentrations. Am J Sports Med 1997;25:751-4.
[12] Higuchi H, Shirakura K, Kimura M, Terauchi M, Shinozaki T, Watanabe H, Takagishi K. Changes in biochemical parameters after anterior cruciate ligament injury. Int Orthop 2006;30:43-7.
[13] Aggarwal BB, Kohr WJ, Hass PE, Moffat B, Spencer SA, Henzel WJ, Bringman TS, Nedwin GE, Goeddel DV, Harkins RN. Human tumor necrosis factor. Production, purification, and characterization. J Biol Chem 1985;260:2345-54.
[14] Maroudas A. Physicochemical properties of cartilage in light of ion exchange theory. Biophys J 1968;8:575-95.
[15] Maroudas A. Transport of solutes through cartilage: permeability to large molecules. J Anat 1976;122:335-47.

[16] Garcia AM, Szasz N, Trippel SB, Morales TI, Grodzinsky AJ, Frank EH. Transport and binding of insulin-like growth factor I through articular cartilage. Arch Biochem Biophys 2003;415:69-79.
[17] Bhakta NR, Garcia AM, Frank EH, Grodzinsky AJ, Morales TI. The insulin-like growth factors (IGFs) I and II bind to articular cartilage via the IGF-binding proteins. J Biol Chem 2000;275:5860-6.
[18] Lantz M, Thysell H, Nilsson E, Olsson I. On the binding of tumor necrosis factor (TNF) to heparin and the release in vivo of the TNF-binding protein I by heparin. J Clin Invest 1991;88:2026-31.
[19] Alon R, Cahalon L, Hershkoviz R, Elbaz D, Reizis B, Wallach D, Akiyama SK, Yamada KM, Lider O. TNF-alpha binds to the N-terminal domain of fibronectin and augments the beta 1-integrin-mediated adhesion of CD4+ T lymphocytes to the glycoprotein. J Immunol 1994;152:1304-13.
[20] Hershkoviz R, Goldkorn I, Lider O. Tumour necrosis factor-alpha interacts with laminin and functions as a pro-adhesive cytokine. Immunology 1995;85:125-30.
[21] Tufvesson E, Westergren-Thorsson G. Tumour necrosis factor-alpha interacts with biglycan and decorin. FEBS Lett 2002;530:124-8.
[22] Limb GA, Daniels JT, Pleass R, Charteris DG, Luthert PJ, Khaw PT. Differential expression of matrix metalloproteinases 2 and 9 by glial Muller cells: response to soluble and extracellular matrix-bound tumor necrosis factor-alpha. Am J Pathol 2002;160:1847-55.
[23] Kenig M, Gaberc-Porekar V, Fonda I, Menart V. Identification of the heparin-binding domain of TNF-alpha and its use for efficient TNF-alpha purification by heparin-Sepharose affinity chromatography. J Chromatogr B Analyt Technol Biomed Life Sci 2008;867:119-25.
[24] Vaday GG, Hershkoviz R, Rahat MA, Lahat N, Cahalon L, Lider O. Fibronectin-bound TNF-alpha stimulates monocyte matrix metalloproteinase-9 expression and regulates chemotaxis. J Leukoc Biol 2000;68:737-47.
[25] Kurz B, Jin M, Patwari P, Cheng DM, Lark MW, Grodzinsky AJ. Biosynthetic response and mechanical properties of articular cartilage after injurious compression. Journal of Orthopaedic Research 2001;19:1140-6.
[26] Sah RLY, Kim YJ, Doong JYH, Grodzinsky AJ, Plaas AHK, Sandy JD. Biosynthetic response of cartilage explants to dynamic compression. J Orthop Res 1989;7:619-36.
[27] Garcia AM, Lark MW, Trippel SB, Grodzinsky AJ. Transport of tissue inhibitor of metalloproteinases-1 through cartilage: contributions of fluid flow and electrical migration. J Orthop Res 1998;16:734-42.
[28] Jadin KD, Wong BL, Bae WC, Li KW, Williamson AK, Schumacher BL, Price JH, Sah RL. Depth-varying density and organization of chondrocytes in immature and mature bovine articular cartilage assessed by 3d imaging and analysis. J Histochem Cytochem 2005;53:1109-19.
[29] Webb GR, Westacott CI, Elson CJ. Chondrocyte tumor necrosis factor receptors and focal loss of cartilage in osteoarthritis. Osteoarthritis Cartilage 1997;5:427-37.
[30] Svenson M, Hansen MB, Bendtzen K. Binding of cytokines to pharmaceutically prepared human immunoglobulin. J Clin Invest 1993;92:2533-9.
[31] Venyaminov S, Metsis ML, Chernousov MA, Koteliansky VE. Distribution of secondary structure along the fibronectin molecule. Eur J Biochem 1983;135:485-9.

[32] O'Brien LE, Jou TS, Pollack AL, Zhang Q, Hansen SH, Yurchenco P, Mostov KE. Rac1 orientates epithelial apical polarity through effects on basolateral laminin assembly. Nat Cell Biol 2001;3:831-8.
[33] Aderka D, Engelmann H, Maor Y, Brakebusch C, Wallach D. Stabilization of the bioactivity of tumor necrosis factor by its soluble receptors. J Exp Med 1992;175:323-9.
[34] Aggarwal BB. Structure of tumor necrosis factor and its receptor. Biotherapy 1991;3:113-20.
[35] Macri L, Silverstein D, Clark RA. Growth factor binding to the pericellular matrix and its importance in tissue engineering. Adv Drug Deliv Rev 2007;59:1366-81.

4.7 Supplementary Data

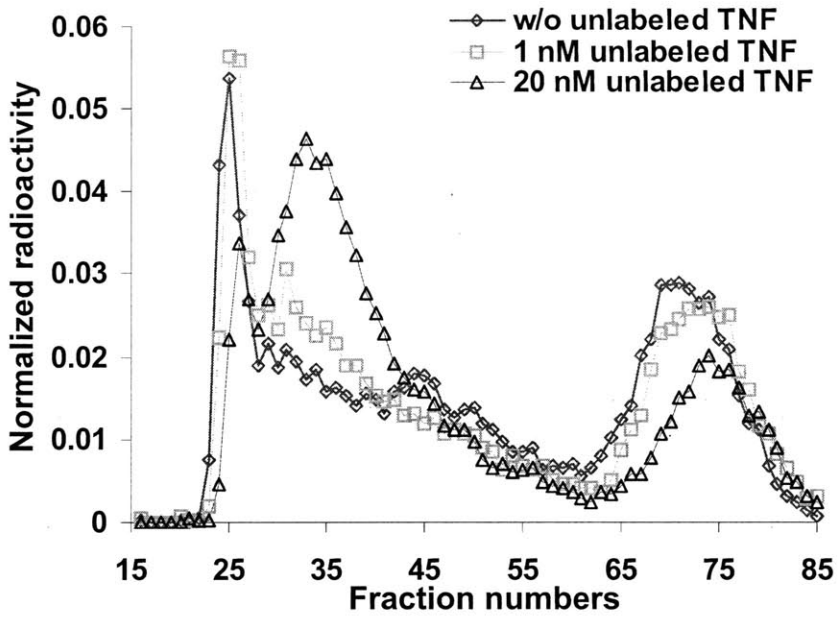

Figure 4S.1 Sephadex G75 chromatography analysis of samples from baths used in Figure 4.2B.

A.

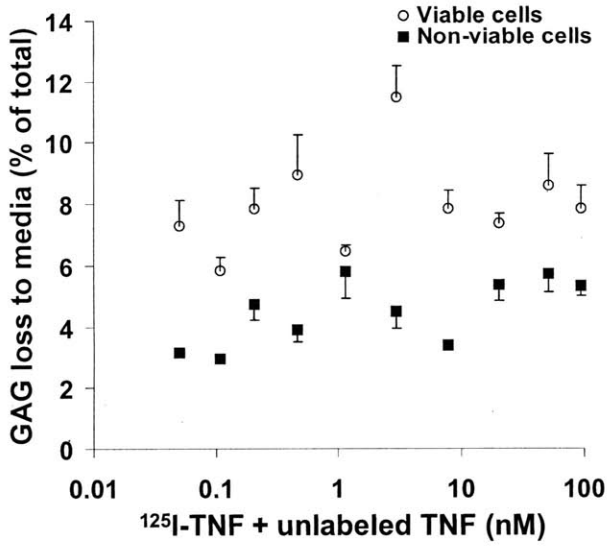

B.

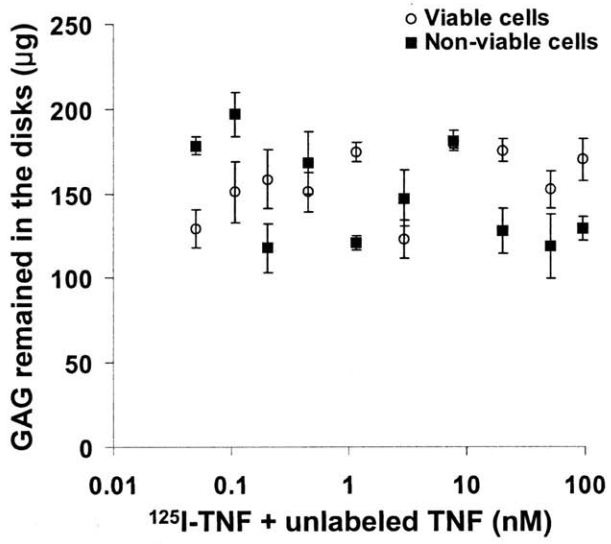

Figure 4S.2 GAG loss to media and GAG remained in the disks after 48 hrs incubation (from Fig. 4.2). Disks were incubated in DMEM with 1% ITS, and 0.1% BSA at 37°C for 48 hrs in the presence (closed square, non-viable cell) or absence (open circle, viable cell) of 0.01% sodium azide (NaN_3) + protease inhibitors. (n = 6, mean ± SEM). **A.** GAG loss to media. **B.** GAG remained in the disks.

A.

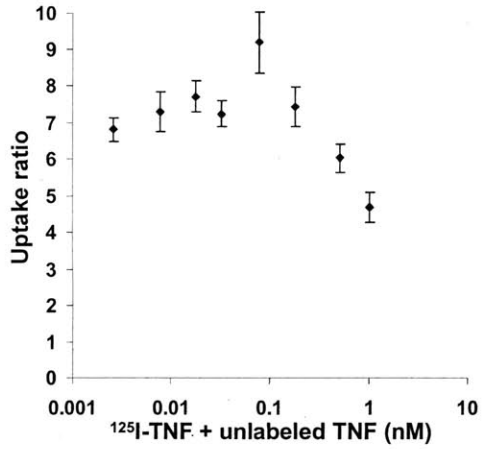

B.

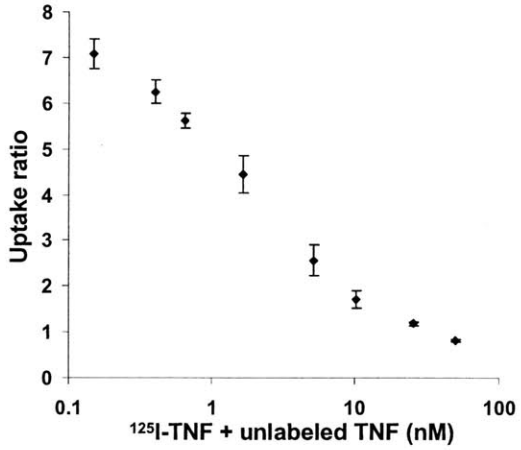

Figure 4S.3 Equilibrium uptake ratio of ^{125}I-TNFα in the bovine calf cartilage with two different ranges of the concentration of unlabeled TNFα. Disks were incubated in 1×PBS with 0.1% BSA, protease inhibitors, and 0.01% NaN_3 at 4°C for 48 hrs (n = 6, mean ± SEM). **A**. Uptake ratio measured with low concentration of unlabeled TNFα (^{125}I-TNFα = 0.044 ng/ml = 2.59 pM). **B.** Uptake ratio measured with high concentration of unlabeled TNFα (^{125}I-TNFα = 2.55 ng/ml = 0.15 nM).

A.

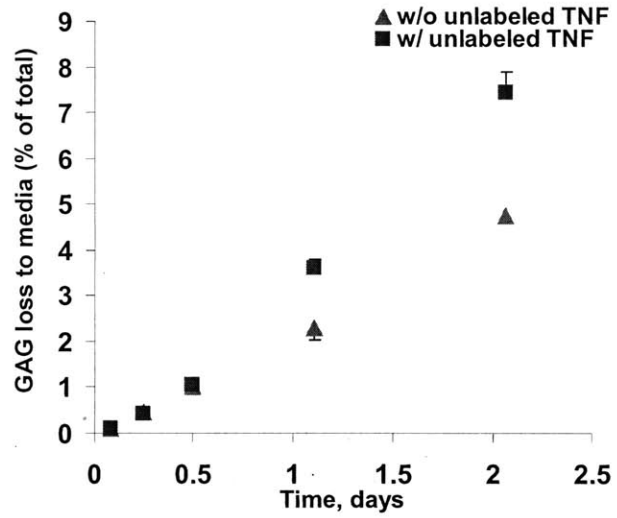

B.

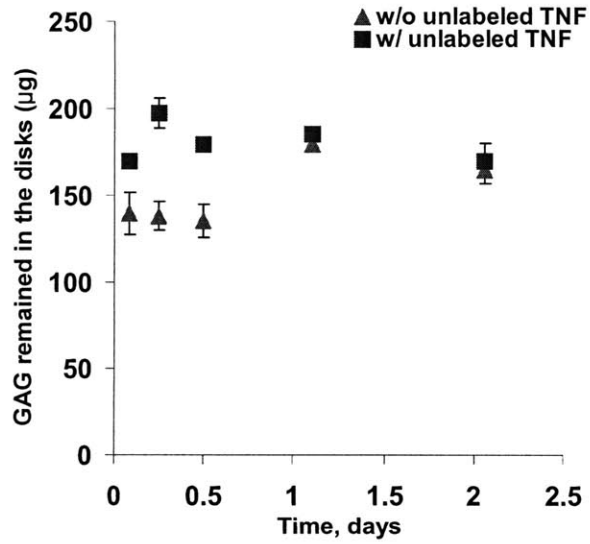

Figure 4S.4 GAG loss to media and GAG remained in the disks at each time point during 48 hrs incubation (from Fig. 4.3). Disks were incubated in DMEM with 1% ITS, and 0.1% BSA at 37°C up to 48 hrs with or without 340 ng/ml (20 nM) unlabeled TNFα. **A.** GAG loss to media. **B.** GAG remained in the disks (n = 6, mean ± SEM).

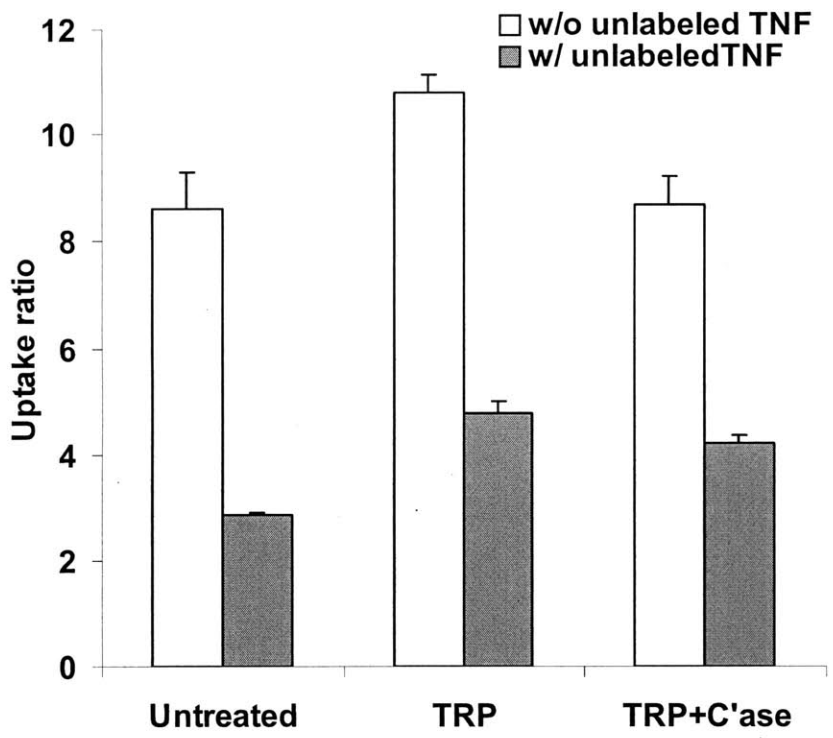

Figure 4S.5 Effects of trypsin and chondroitinase ABC treatment on the equilibrium uptake of ^{125}I-TNFα in the bovine calf cartilage with the presence or absence of unlabeled TNFα (340 ng/ml = 20 nM). Disks were either free swelled (Untreated), treated with 0.1 mg/ml trypsin for 48 hrs at 37°C (TRP), or trypsinized first then treated with 0.1 U/ml chondroitinase ABC for 4 days at 37°C (TRP+C'ase). Disks were incubated with ^{125}I-TNFα (2.39 ng/ml = 0.14 nM) and unlabeled TNFα (0 or 20 nM) for 48 hrs in 1×PBS with 0.1% BSA, protease inhibitors, and 0.01% NaN_3 at 37°C (n = 5, mean ± SEM).

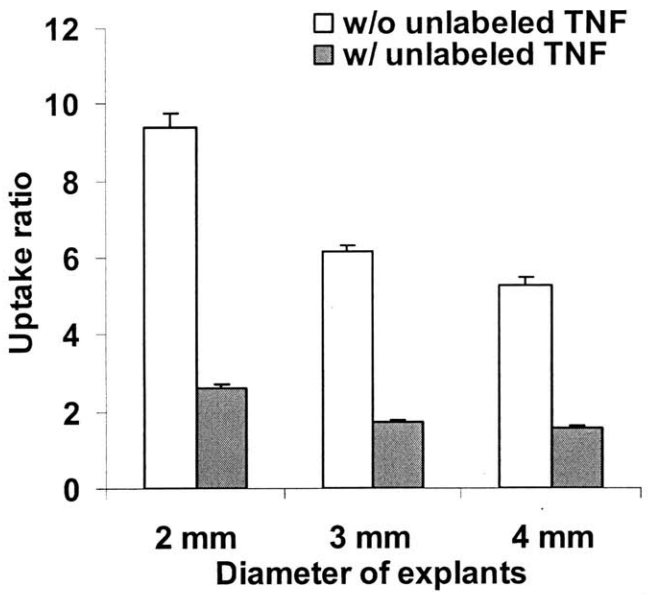

Figure 4S.6 Effect of the diameter of explants on the equilibrium uptake of ^{125}I-TNFα in the bovine calf cartilage with the presence or absence of unlabeled TNFα (340 ng/ml = 20 nM). 500 μm-think cartilage slices were punched to either 2 mm, 3mm, or 4 mm diameter disks. Disks were incubated with ^{125}I-TNFα (2.39 ng/ml = 0.14 nM) and unlabeled TNFα (0 or 20 nM) in DMEM with 0.1% BSA, 1% ITS at 37°C (n = 5, mean ± SEM).

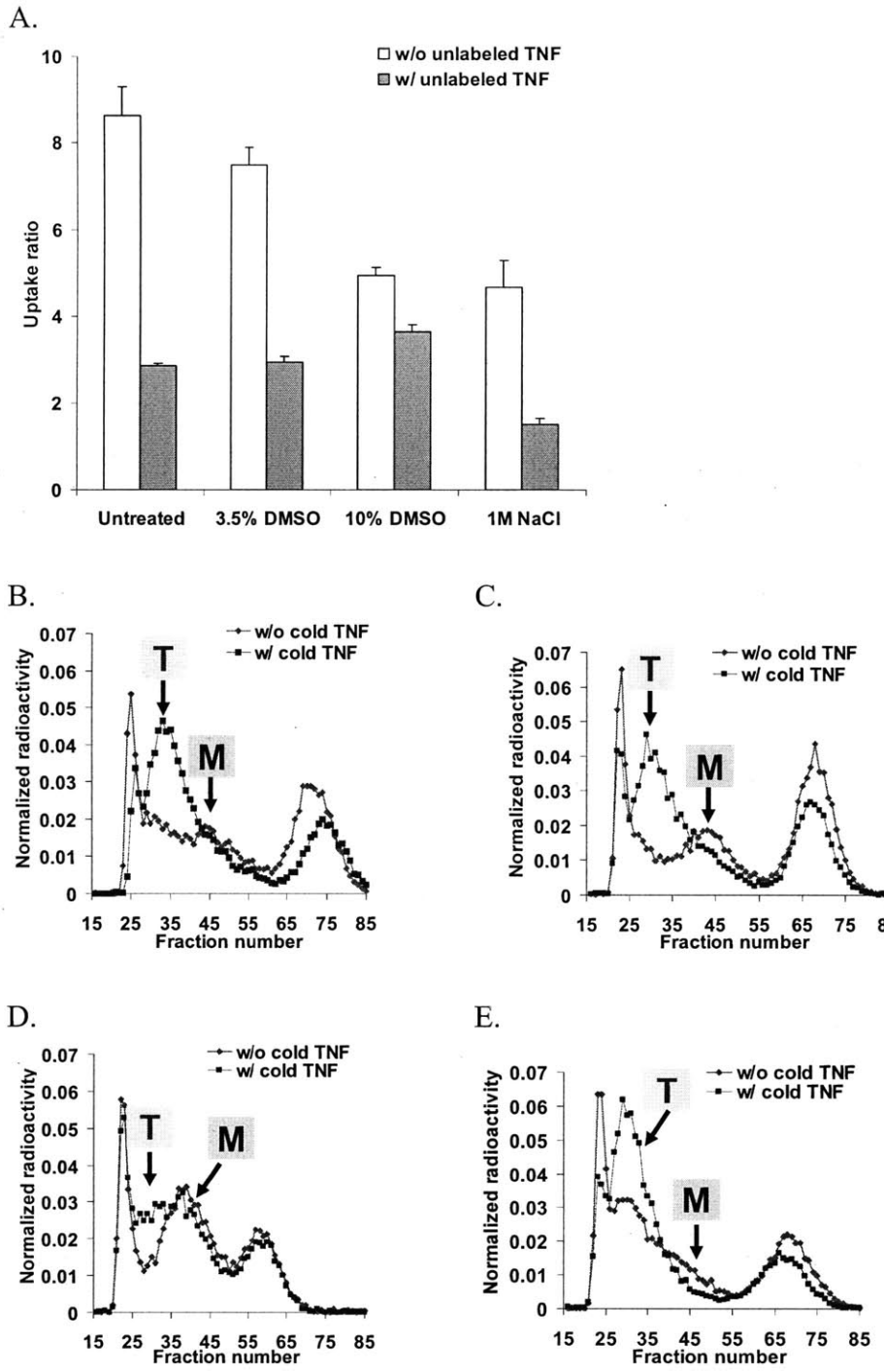

Figure 4S.7 Effects of DMSO and high ionic strength on the equilibrium uptake of ^{125}I-TNFα in the bovine calf cartilage with the presence or absence of unlabeled TNFα (340 ng/ml = 20 nM). Disks were incubated with ^{125}I-TNFα (2.39 ng/ml = 0.14 nM) and unlabeled TNFα (0 or 20 nM) for 48 hrs in the following equilibrating baths supplemented with 0.1% BSA, protease inhibitors, and 0.01% NaN_3 at 37°C (n = 5, mean ± SEM). "Untreated" = 1×PBS; "3.5% DMSO" = 1×PBS + 3.5% DMSO; "10% DMSO" = 1×PBS + 10% DMSO; "1M NaCl" = 1M NaCl. **A.** Uptake ratio of ^{125}I-TNFα in each bath condition. **B – E.** Sample from each

bath was analyzed by Sephadex G75 chromatography, which were pre-equilibrated with corresponding baths. **B.** Untreated. **C.** 3.5% DMSO. **D.** 10% DMSO. **E.** 1M NaCl.

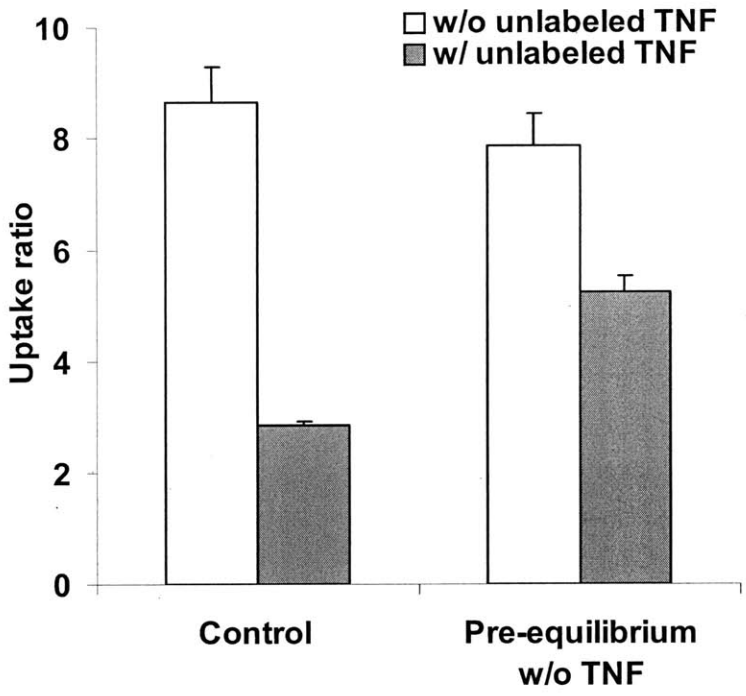

Figure 4S.8 Effect of reversible binding or trimerization on the uptake of ^{125}I-TNFα. "Control" = samples incubated for 48 hrs with or without 20 nM unlabeled TNFα; "Pre-equilibrium w/o TNF" = samples were pre-equilibrated for 48 hrs without unlabeled TNFα followed by another 48 hrs incubation with or without 20 nM unlabeled TNFα. Bovine calf cartilage disks were incubated with ^{125}I-TNFα (2.39 ng/ml = 0.14 nM) in 1×PBS with 0.1% BSA, protease inhibitors, and 0.01% NaN_3 at 37°C (n = 5, mean ± SEM).

A.

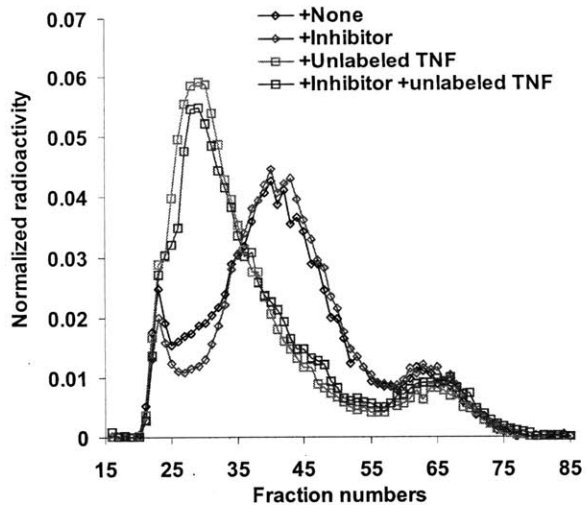

B.

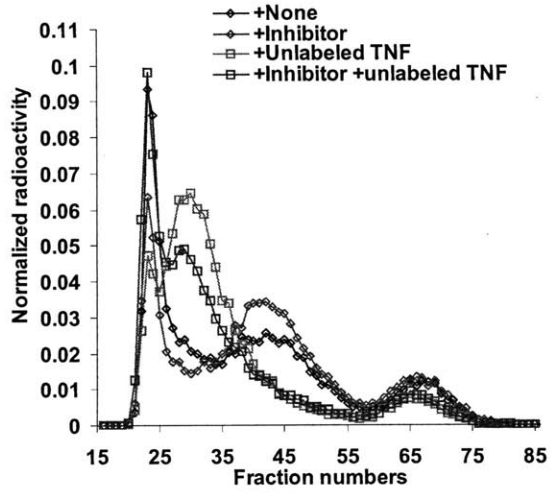

Figure 4S.9 Effect of small inhibitor of TNFα trimerization (Calbiochem, product number 654256). **A.** Sephadex G75 chromatography of ^{125}I-TNFα, incubated with ± 20 nM unlabeled TNFα ± 20 μM small inhibitor in 1×PBS with 0.5% DMSO, 0.1% BSA for 48 hrs at 37°C. **B.** G75 chromatography of ^{125}I-TNFα, incubated with ± 20 nM unlabeled TNFα ± 20 μM small inhibitor in 1×PBS with 1% DMSO, 0.1% BSA for 48 hrs at 4°C.

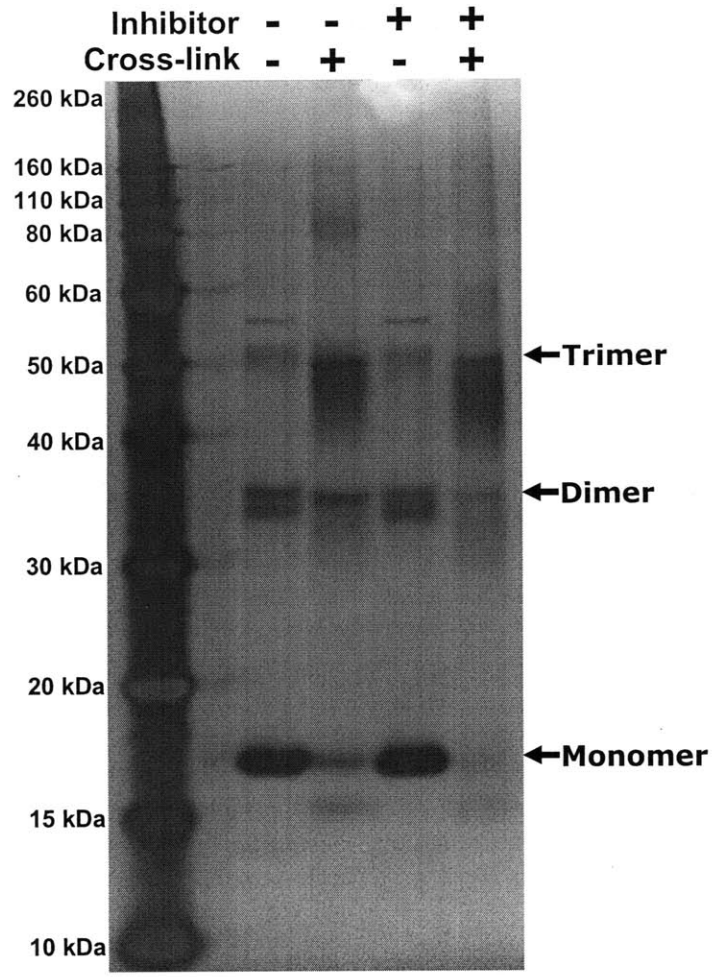

Figure 4S.10 SDS-PAGE analysis of native or cross-linked TNFα (0.78 μM), pre-incubated with or without small inhibitor (50 μM). TNFα was pre-incubated with or without small inhibitor for 30 min at room temperature. For cross-linking, BSOCOES was treated to TNFα for 30 min at room temperature. After quenching cross-linking, samples were kept at 4°C for overnight. Silver staining was used to detect TNFα.

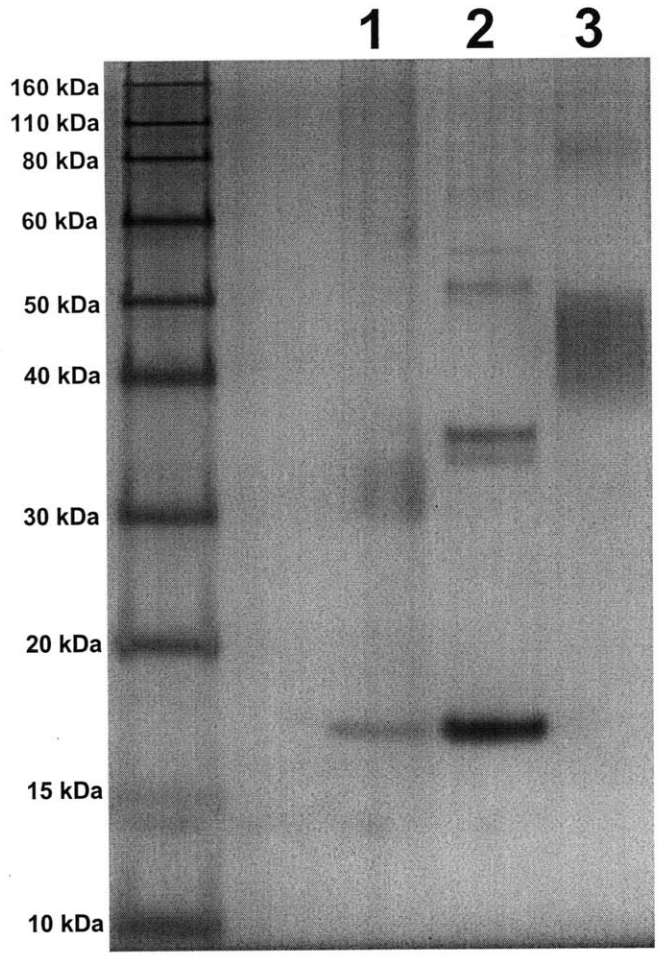

Figure 4S.11 SDS-PAGE analysis of native or cross-linked TNFα. **Lane 1**: Native TNFα filtered with 3 kDa Millipore. **Lane 2**: Native TNFα filtered with 30 kDa Millipore. **Lane 3**: Cross-linked TNFα was run through 30 kDa-cutoff centrifugal filter. For cross-linking (lane 2 and 3), BSOCOES was treated to TNFα for 30 min at room temperature.

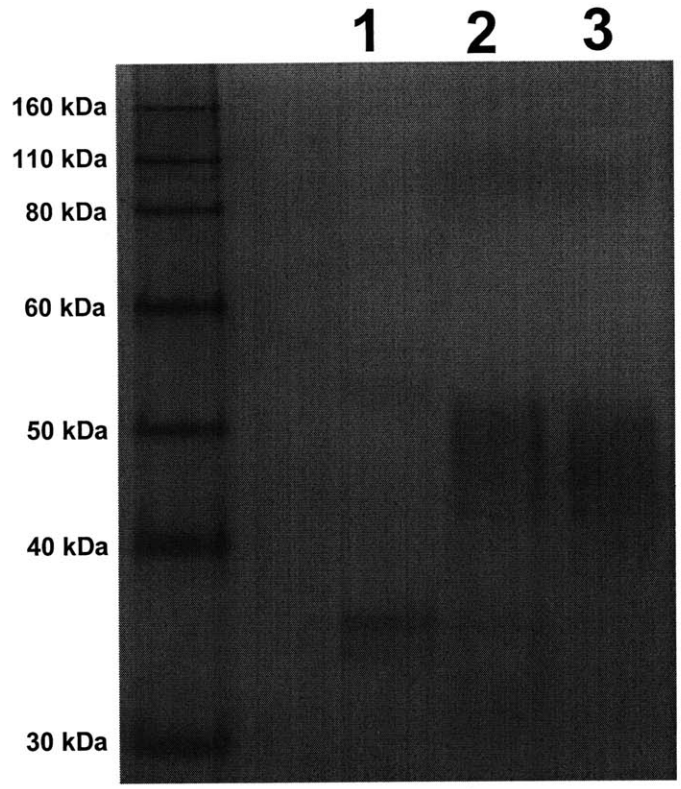

Figure 4S.12 SDS-PAGE analysis of native or cross-linked TNFα. **Lane A**: Native TNFα filtered with 30 kDa Millipore. **Lane B and C**: Cross-linked TNFα was run through 30 kDa-cutoff centrifugal filter. For cross-linking, BSOCOES was treated to TNFα for 10 min at 4°C (lane B) or at room temperature (lane C).

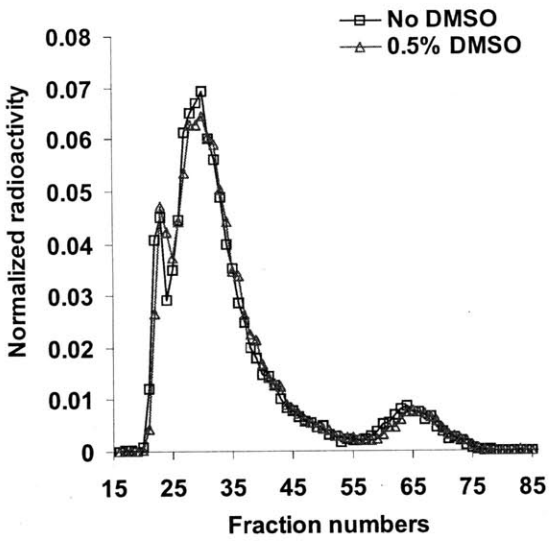

Figure 4S.13 Effect of 0.5% DMSO on dissociation of TNFα. ^{125}I-TNFα was incubated with 20 nM unlabeled TNFα in 1×PBS with 0.1% BSA and with or without 0.5% DMSO for 48 hrs at 37°C, followed by Sephadex G75 chromatography.

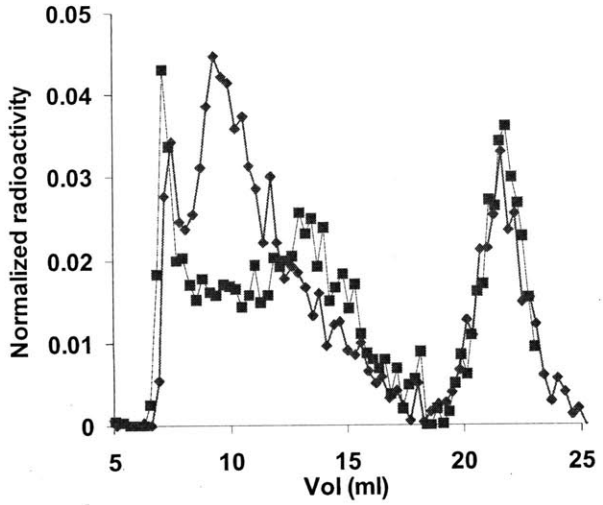

Figure 4S.14 Sephadex G75 chromatography of native ^{125}I-TNFα with or without native unlabeled TNFα from Fig. 4.6.

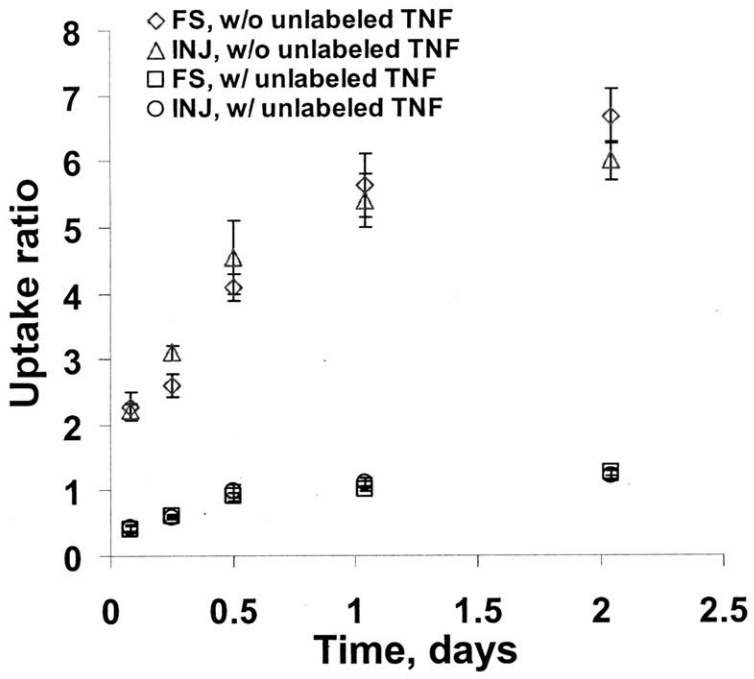

Figure 4S.15 Effect of mechanical injury on the transient uptake of ^{125}I-TNFα (2.55 ng/ml = 0.15 nM) in the presence or absence of unlabeled TNFα (250 ng/ml = 14.7 nM). Untreated or injured disks were incubated in 1×PBS with 0.1% BSA, protease inhibitors, and 0.01% NaN_3 at 4°C (n = 6, mean ± SEM).

4.8 Appendix

We modified the bimolecular binding reaction model to include the effect of monomer-trimer conversion on the diffusion and binding. First, the conversion among monomer, dimer, and trimer was modeled with a sequential process assuming a single dissociation constant, K_D (Alzani et al., Biochemistry, 1995).

$$\text{Monomer} + \text{Monomer} \leftrightarrow \text{Dimer} \tag{1}$$

$$\text{Monomer} + \text{Dimer} \leftrightarrow \text{Trimer} \tag{2}$$

Then, the concentrations of the monomer, dimer, and trimer can be related by

$$D = \frac{M^2}{K_D} \tag{3}$$

$$T = \frac{M^3}{K_D^2} \tag{4}$$

where, M, D, and T are the bath concentration of the monomer, dimer, and trimer, respectively. Once the total concentration of all species in the bath is given by

$$\text{Total concentration in the bath} = M + D + T \tag{5}$$

then we can form a cubic equation with respect to any concentration (M, D, or T) using Eqs. (3) and (4). The solution from this cubic equation gives the equilibrium concentrations of the monomer, dimer, and trimer in the bath.

Within the cartilage tissue, the same rule would govern the monomer-trimer conversion, as described above. Therefore, following the same method, we can find the equilibrium intra-tissue concentrations of the monomer, dimer, and trimer with the known total concentration of all three species within the cartilage, as given by

$$\overline{D} = \frac{\overline{M}^2}{K_D} \tag{6}$$

$$\overline{T} = \frac{\overline{M}^3}{K_D^2} \tag{7}$$

$$\text{Total concentration in the cartilage} = \overline{M} + \overline{D} + \overline{T} \tag{8}$$

where, $\overline{M}$, $\overline{D}$, and $\overline{T}$ are the intra-tissue concentrations of the monomer, dimer, and trimer, respectively.

In addition, the intra-tissue concentration of each species is affected by the partitioning from the bath, which is given by

$$\overline{M} = K_1 M \tag{9}$$

$$\overline{D} = K_2 D \tag{10}$$

$$\overline{T} = K_3 T \tag{11}$$

where, K_1, K_2, and K_3 are the partition coefficients of the monomer, dimer, and trimer, respectively. Combining Eqs. (3), (4), (6), (7), (9)-(11) gives strong restrictions on the partition coefficient, which is given by

$$K_2 = K_1^2 \tag{12}$$

$$K_3 = K_1^3 . \tag{13}$$

However, Eqs. (12) and (13) are based on a simple mathematical derivation without considering underlying physical principles to merge the equilibrium partitioning with monomer-trimer conversion. Therefore, Eqs. (12) and (13) may not be valid under certain circumstances, but for simplicity, in this section, we will assume that Eqs. (12) and (13) are valid.

Considering the presence of all three species, monomer, dimer, and trimer, the uptake raito is given by

$$R_U = \frac{\overline{M} + 2\overline{D} + 3\overline{T} + \overline{B}}{M + 2D + 3T} \tag{14}$$

$$\overline{B} = \overline{M}\frac{N_T}{K_{EQ} + \overline{M}} \tag{15}$$

where, $\overline{B}$ is the concentration of bound TNFα, N_T is the binding site density, and K_{EQ} is the dissociation constant of binding reaction between the monomer TNFα and binding sites. For simplicity, we assumed negligible binding of dimer and trimer to matrix sites. Using Eqs. (14) and (15), the new fit of the binding variable can be found from the same experimental results in Fig. 4.2a. Using revised model, the estimated binding parameters for the medium with sodium azide and protease inhibitors were N_T = 38.7 ± 7.47 nM and K_{EQ} = 3.29 ± 0.72 nM, assuming K_D = 5, K_1 = 0.5, K_2 = 0.25, and K_3 = 0.125 (arbitrarily chosen). The theoretical curve of the uptake ratio was constructed from these binding parameters as shown below.

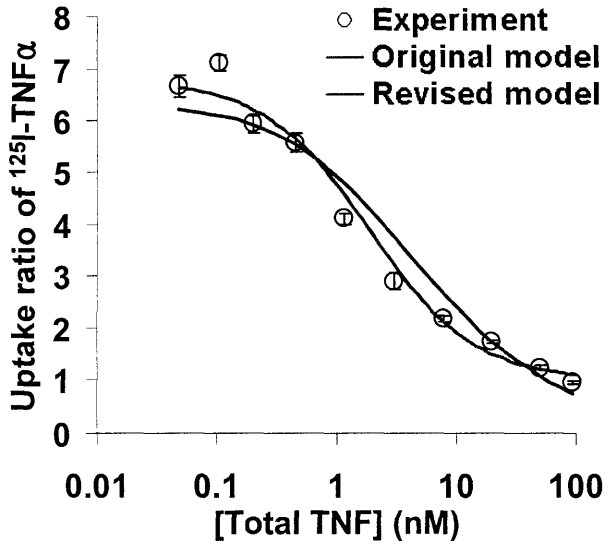

CHAPTER 5

Summary and Conclusions

The goal of this thesis was to characterize uptake and binding kinetics of proteins, biopharmaceuticals and small pharmaceutical compounds in articular cartilage and to evaluate the effect of joint injury and pro-inflammatory cytokines on transport properties.

The objective of Chapter 2 was to quantify and model the equilibrium uptake and transient transport kinetics in normal cartilage of specific pharmaceutical agents, Pf-pep, a 760 Da positively charged peptide inhibitor of the proprotein convertase PACE4. We found that there is little or no binding of Pf-pep to sites within the cartilage tissue. The uptake of Pf-pep was significantly higher in middle-deep zone compared to more superficial cartilage overall. Uptake of Pf-pep depended on glycosaminoglycan charge density, and was consistent with predictions of Donnan equilibrium given the known charge of Pf-pep. In separate transport experiments, the diffusivity of Pf-pep in cartilage was measured to be $\sim 1 \times 10^{-6}$ cm^2/s, close to other similarly-sized non-binding solutes.

The goal of Chapter 3 was to evaluate the effect of cartilage mechanical injury and inflammatory cytokines on the uptake of anti-catabolic therapeutics, and to relate the alteration in intratissue transport of these molecules with the extent of degradation of cartilage. Uptake of anti-IL-6 Fab fragment (48 kDa) in cartilage was significantly increased by mechanical injury, which also caused an increase in tissue hydration. Higher strain and strain rate during injurious

loading resulted in a further increase in uptake ratio. TNFα treatment combined with mechanical injury further increased the uptake, which was accompanied by GAG loss from the tissue. The spatial distribution of the Fab varied substantially with depth during the diffusion process before complete equilibration, with lower amounts of Fab detected in the deeper region of tissue. Competitive binding measurements with unlabeled Fab showed negligible change in uptake of ^{125}I-Fab up to 1 μM of unlabeled Fab. However, trypsin treatment of explants or long-term incubation revealed uptake ratios greater than 1, suggesting that there was either significant binding of Fab within the tissue, or that a significant amount of radiolabeled species had accumulated at tissue surfaces including the superficial zone.

In chapter 4, we characterized the uptake and binding of the major pro-inflammatory cytokine, TNFα, to discover the key factors determining transport process of TNFα into cartilage. We found that there is a significant binding of TNFα to matrix sites. Transient uptake of ^{125}I-TNFα depended on the bath concentration of TNFα, which affected the binding and also monomer-trimer conversion of TNFα. TNFα that was cross-linked to the trimeric form showed significantly less binding compared to native TNFα, suggesting that monomers bind more than trimers. Binding of TNFα was not disrupted by trypsin treatment, indicating that binding sites were not removed by trypsin. Measurement of uptake in separate ring-core regions using normal and trypsin treated cartilage showed that TNFα was able to penetrate into the center of both normal and trypsinized cartilage. In addition, depletion of matrix by trypsin resulted in faster penetration of TNFα. Further study is necessary to determine the identity of the binding sites in order to understand the role of these binding interactions between that matrix and TNFα.

In summary, injurious mechanical loading and inflammatory cytokines applied to cartilage changed the kinetics of uptake and retention of proteins and therapeutic agents within

the tissue via degradation and remodeling of the matrix. The extent of alteration in transport properties was correlated with the severity of the disruption of the matrix. This is important since transport of peptide or protein therapeutics into and within cartilage tissue is affected by the size and charge of the drugs as well as specific components of the cartilage matrix. The change in the accessibility of the inflammatory cytokines to the chondrocytes will further upregulate matrix degradation, forming a dynamic feedback between matrix integrity and transport of cytokine or other proteins.

APPENDIX A

Effects of pro-anabolic and anti-catabolic factors on cartilage matrix degradation and loss in an *in vitro* co-culture model

A.1 Objective

To determine the ability of pro-anabolic and anti-catabolic factors, i.e., dexamethasone, dynamic compression, an aggrecanase inhibitor, and an anti-IL-6 Fab antibody fragment, to ameliorate cartilage matrix degradation and loss using an *in vitro* model of cartilage degeneration in which mechanically injured cartilage is incubated with joint capsule tissue

A.2 Methods

Bovine cartilage explants were harvested from the femoropatellar grooves of a 1-2 weeks bovine calf (Research 87, Marlborough, MA) [1]. Briefly, 9-mm diameter cartilage-bone cylinders were cored and mounted on a microtome. Top superficial layer was removed to obtain 1 mm-thick middle zone slices. Four or five disks (3 mm-diameter, 1 mm-thick) were cored from each slice using a dermal punch. All bovine cartilage specimens were equilibrated

in serum-free medium (low-glucose DMEM, 1 g/L) supplemented with 1% insulin-transferrin-selenium (10 μg/mL insulin, 5.5 μg/mL transferrin, 5 ng/mL selenium, Sigma).

Human knee joints were obtained from the Gift of Hope Organ and Tissue Donor Network (Elmhurst, IL), approved by the Office of Research Affairs at Rush-Presbyterian-St. Luke's Medical Center and the Committee on Use of Humans as Experimental Subjects at MIT. Human cartilage explants were harvested from both femoropatellar groove and femoral chondyles [2]. Unlike bovine tissue, human explants included the intact superficial layer and the thickness was ~0.8 mm. All human cartilage specimens were equilibrated in serum-free medium (high-glucose DMEM, 4.5 g/L) supplemented with 1% insulin-transferrin-selenium (10 μg/mL insulin, 5.5 μg/mL transferrin, 5 ng/mL selenium, Sigma).

Cartilage disks to be injured were placed individually between impermeable platens of a polysulfone mechanical loading chamber (50 % strain, 100%/s strain rate), which is used to apply radially unconfined compression [3]. During the injury loading, the disks were compressed to 50% strain with a constant velocity of 1mm/second and immediately released at the same velocity (50 % strain, 100%/s strain rate).

Joint capsule explants were cut from the tissue immediately proximal to the articular cartilage. Joint capsule tissue was punched to individual pieces using 5-mm diameter dermal punch was and then equilibrated in the same medium used for cartilage explants. For co-culture, an individual joint capsule tissue was placed with a single cartilage explant in the same well of a 48-well dish during the incubation. For the condition co-culture with injury, a mechanically injured cartilage was incubated with a freshly cut joint capsule explant.

Aggrecanase inhibitor (Compound D) was kindly provided by Micky Tortorella and John Sandy. The compound is acyclic carboxylate, a small molecule inhibitor of aggrecanases

developed at Pfizer, having molecular weight 502 Da and IC_{50} values for inhibiting ADAMTS-4 and -5 of 0.39 and 2.2 nM, respectively. This compound is highly selective for ADAMTS-4 and -5 and is relatively inactive against MMPs and ADAMs (ADAM-8 and -17). The anti-IL-6 Fab fragment was kindly provided by Centocor. Its molecular weight is 48 kDa and EC_{50} against 500 pg/ml rhIL-6 is 8.5 pM.

The explants from the groups, untreated control, injury, co-culture, and co-culture with injury were left untreated or treated with pro-anabolic and anti-catabolic factors; dexamethasone (10, 50 or 100 ng/ml) was added to the medium; unconfined dynamic compression (10% offset ± 3%, 0.1 Hz) was applied to explants in polysulfone chambers; aggrecanase inhibitor (50 nM) was added to the medium; anti-IL-6 Fab fragment (35 μg/ml) was added to the medium.

The sulfated glycosaminoglycan (sGAG) content of the cartilage disks and medium were measured using the dimethylmethylene blue (DMMB) dye binding assay. To quantify biosynthesis rate, 5 μCi/ml $Na_2{}^{35}SO_4$ and 10 μCi/ml L-5-^{3}H-proline were added to bovine culture medium before termination of experiment (24 hrs or 48 hrs radio-labeling), as measures of proteoglycan and total protein synthesis rates, respectively. For human tissue, both concentrations of radiolabel were doubled to 10 μCi/ml and 20 μCi/ml, respectively. Radiolabel incorporation was measured using a liquid scintillation counter after digesting explants with proteinase K (Roche, Indianapolis, IN) [4].

A.3 Results and Discussion

Mechanical injury oc cartilage followed by co-culture with joint capsule significantly decreased cchondrocyte biosynthesis rates, consistent with previous observation [5]. Treating

with 100 nM dexamethasone increased biosynthesis rates of all groups (Fig. A.1). However, dexamethasone was not able to completely negate the effect to injury and co-culture, in which decreased biosynthesis persisted even in the presence of dexamethasone. Similar results were observed by adding 50 nM dexamethasone (Fig. A.2). However, 10 nM dexamethasone was not as potent as 50 or 100 nM dexamethasone in restoring biosynthesis rate (Fig. A.3).

Applying dynamic compression was not successful in rescuing sulfate incorporation rates in treated groups (Figs. A.4 and 5) and only the untreated control group showed slight increases in sulfate incorporation with dynamic compression. There was a significant effect of dynamic compression on proline incorporation in one animal but the rate was not completely restored to the control level. Applying the same level of dynamic compression, Kurz et al. observed that mechanically injured cartilage lost its anabolic response to dynamic compression [3]. Interestingly, cartilage tissue co-cultured with joint capsule was not able to respond to dynamic compression, suggesting co-culture blocked anabolic pathway, which was inducible by dynamic loading.

To test the effect of the aggrecanase inhibitor on blocking GAG degradation caused by injury and co-culture, the aggrecanase inhibitor was applied to the medium during the long-term incubation. Total GAG remained in the disks after 16-day incubation was decreased by injury and co-culture (Fig. 6c), consistent with the results reported by Lee et al [6]. However, our preliminary results using the aggrecanase inhibitor showed that it was not able to reduce GAG loss from the explants. In the presence of the aggrecanase inhibitor, the total GAG of the disks was decreased; measurement of the GAG lost to the medium will be needed to determine whether GAG loss as a percent of total was affected. Also, disks treated with aggrecanase inhibitor showed lower biosynthesis rates (Fig. A.7). It is interesting to note that, using the

same aggrecanase inhibitor, Lu showed that GAG loss induced by TNFα treatment was significantly blocked (Yihong C.S. Lu, MIT PhD thesis).

Initial results showed that the effect of the anti-IL-6 Fab on restoring biosynthesis rates in treated groups was not statistically significant in either human and bovine tissue (Fig. A.8). However, in human tissue, normal and injured cartilage co-cultured with joint capsule tissue showed an increase in sulfate incorporation upon addition of the anti-IL-6 Fab, suggesting that IL-6 from joint capsule may induce the decrease in biosynthesis rate. A positive control for testing the effect anti-IL-6 antibody showed that IL-6/sIL-6R did, indeed, decrease biosynthesis in human cartilage tissue, and this catabolic effect of IL-6/sIL-6R was blocked by adding the anti-IL-6 Fab. Interestingly, bovine cartilage did not respond to IL-6/sIL-6R and there was no effect of Fab on bovine tissue.

A.4 Figures

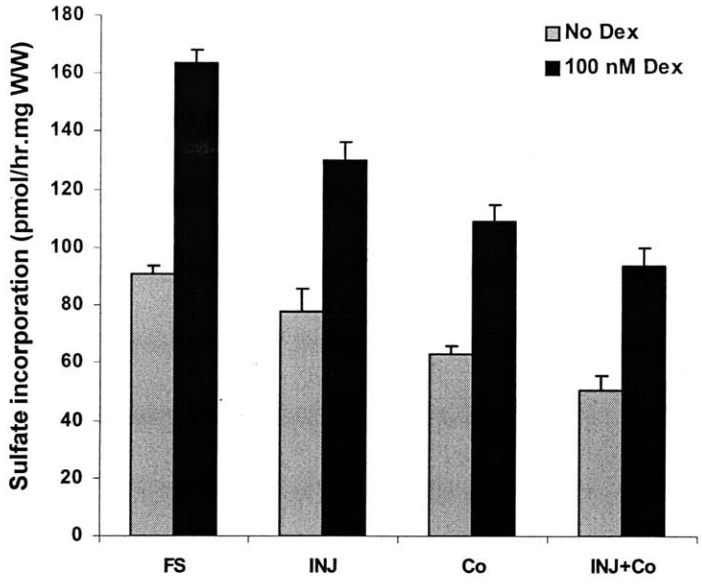

Figure A.1 The effect of 100 nM Dex on the sulfate incorporation rate of bovine calf cartilage explants subjected to mechanical injury, co-culture with joint capsule and both treatments. The explants were incubated for total 6 days and radio-labeled for last 48 hrs. 3-way ANOVA was used to evaluate the effects of injury, co-culture, and Dex, which revealed that significant effects of injury, co-culture, and Dex were present. In addition, there was significant interaction between co-culture and Dex. Mean ± SEM (n = 6 disks per condition).

A.

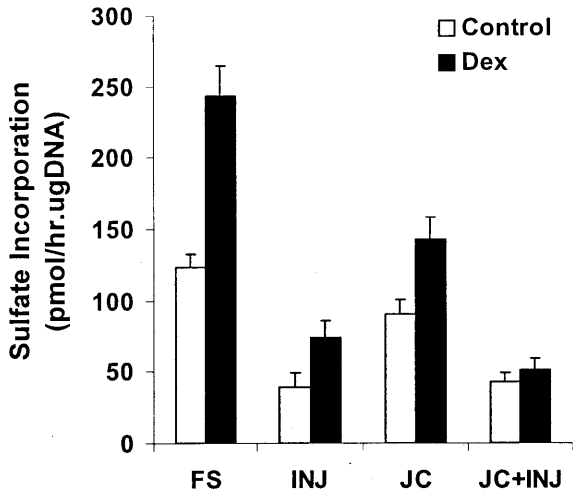

B.

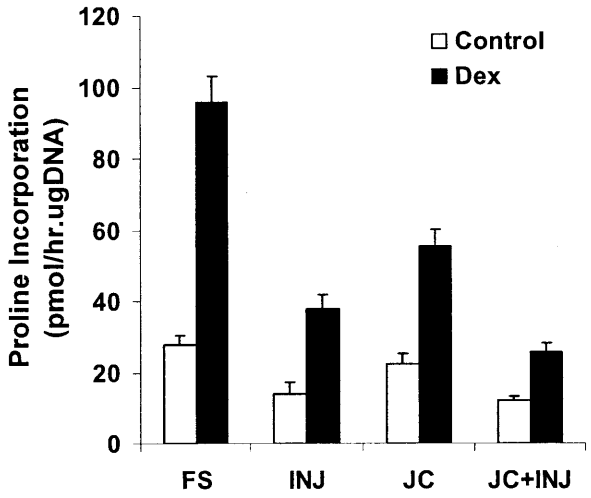

Figure A.2 The effect of 50 nM Dex on the biosynthesis rate of bovine calf cartilage explants subjected to mechanical injury, co-culture with joint capsule and both treatments. The explants were incubated for total 4 days and radio-labeled for last 24 hrs. 3-way ANOVA was used to evaluate the effects of injury, co-culture, and Dex. For both sulfate and proline incorporation rates, significant effects of injury, co-culture, and Dex were present. In addition, there were significant interactions between injury and co-culture, injury and Dex, and co-culture and Dex. No significant interaction among injury, co-culture, and Dex was observed. **A.** Sulfate incorporation rate. **B.** Proline incorporation rate. Mean ± SEM (n = 6 disks per condition).

A.

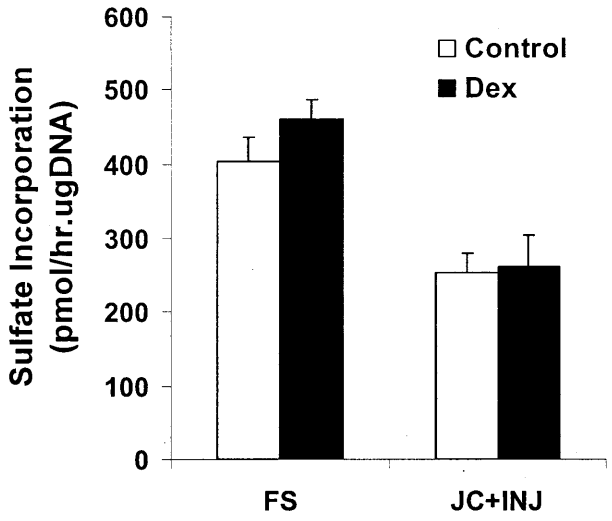

B.

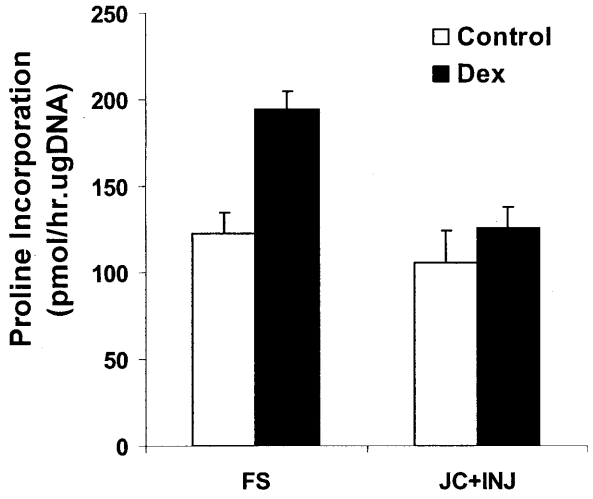

Figure A.3 The effect of 10 nM Dex on the biosynthesis rate of bovine calf cartilage explants subjected to the combined treatment of mechanical injury and co-culture with joint capsule. The explants were incubated for total 4 days and radio-labeled for last 24 hrs. 2-way ANOVA was used to evaluate the effects of the treatment (i.e. injury with co-culture), and Dex. For sulfate incorporation rate, significant effect of the treatment was present. For proline incorporation rate, significant effects of the treatment and Dex were present; in addition, there was significant interaction between the treatment and Dex. **A.** Sulfate incorporation rate. **B.** Proline incorporation rate. Mean ± SEM (n = 6 disks per condition).

A.

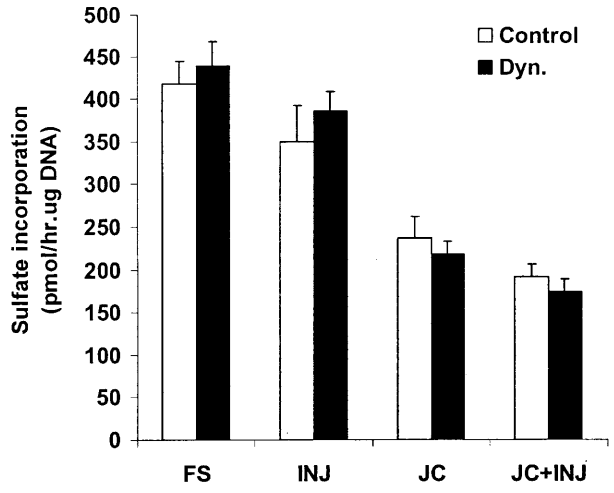

B.

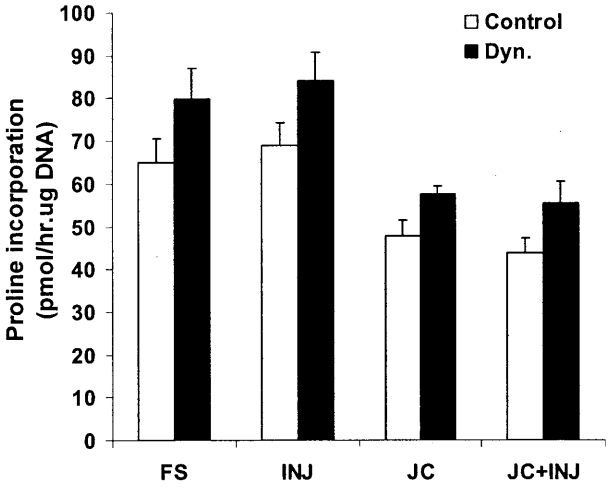

Figure A.4 The effect of 24-hr dynamic compression on the biosynthesis rate of bovine calf cartilage explants subjected to the combined treatment of mechanical injury and co-culture with joint capsule. The explants were incubated for total 4 days. During the last 24 hrs, explants were subjected to dynamic compression (10% offset ± 3%, 0.1 Hz) and radio-labeled simultaneously. 3-way ANOVA was used to evaluate the effects of injury, co-culture, and dynamic comprssion. For sulfate incorporation rate, there were significant effects of injury and co-culture. For proline incorporation rate, there were significant effects of co-culture and dynamic compressoin. **A.** Sulfate incorporation rate. **B.** Proline incorporation rate. Mean ± SEM (n = 6 disks per condition).

A.

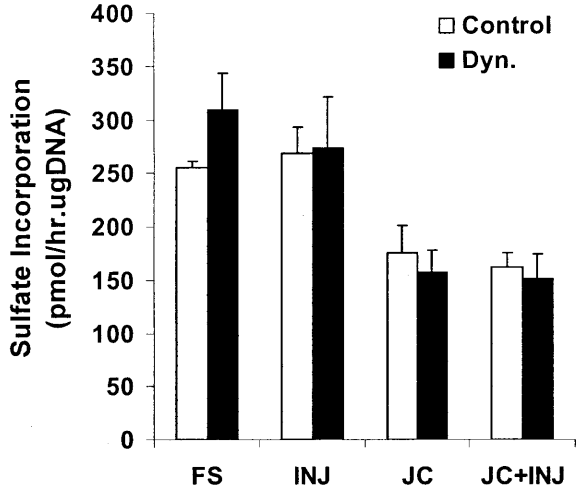

B.

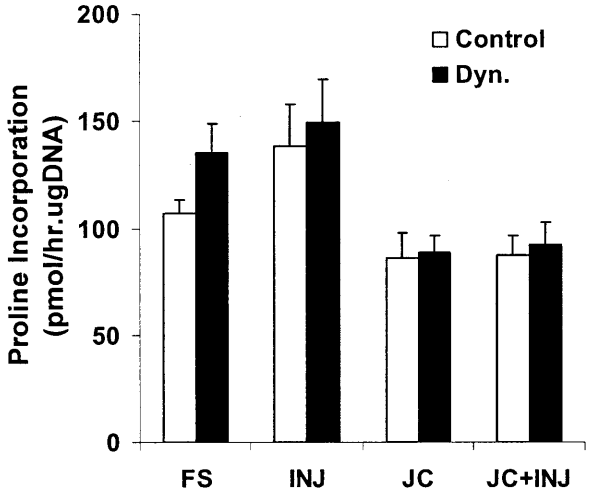

Figure A.5 The effect of 24-hr dynamic compression on the biosynthesis rate of bovine calf cartilage explants subjected to the combined treatment of mechanical injury and co-culture with joint capsule. The explants were incubated for total 4 days. During the last 24 hrs, explants were subjected to dynamic compression (10% offset ± 3%, 0.1 Hz) and radio-labeled simultaneously. 3-way ANOVA was used to evaluate the effects of injury, co-culture, and dynamic comprssion. For both sulfate and proline incorporation rates, there was significant effect co-culture, but no other effect was observed. **A.** Sulfate incorporation rate. **B.** Proline incorporation rate. Mean ± SEM (n = 6 disks per condition).

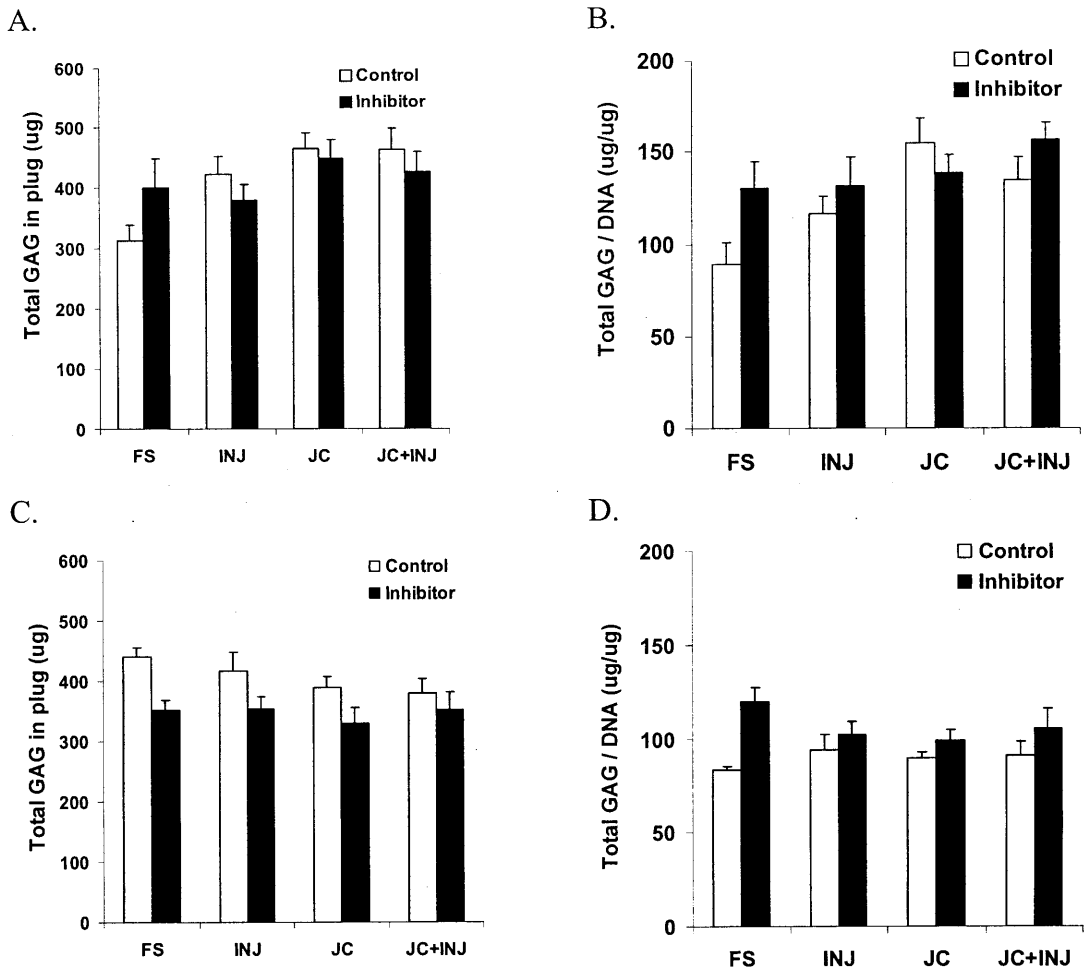

Figure A.6 The effect of aggrecanase inhibitor on the tissue GAG content. Bovine calf cartilage explants subjected to the injury, co-culture with joint capsule and both treatments. The explants were cultured up to 16 days and collected at day 8 and day 16 to measure remaining sGAG content and DNA content in the tissue. **A.** Total GAG content in the explants at day 8. **B.** GAG content normalized to DNA content in the explants at day 8. **C.** Total GAG content in the explants at day 16. **D.** GAG content normalized to DNA content in the explants at day 16. Mean ± SEM (n = 6 disks per condition).

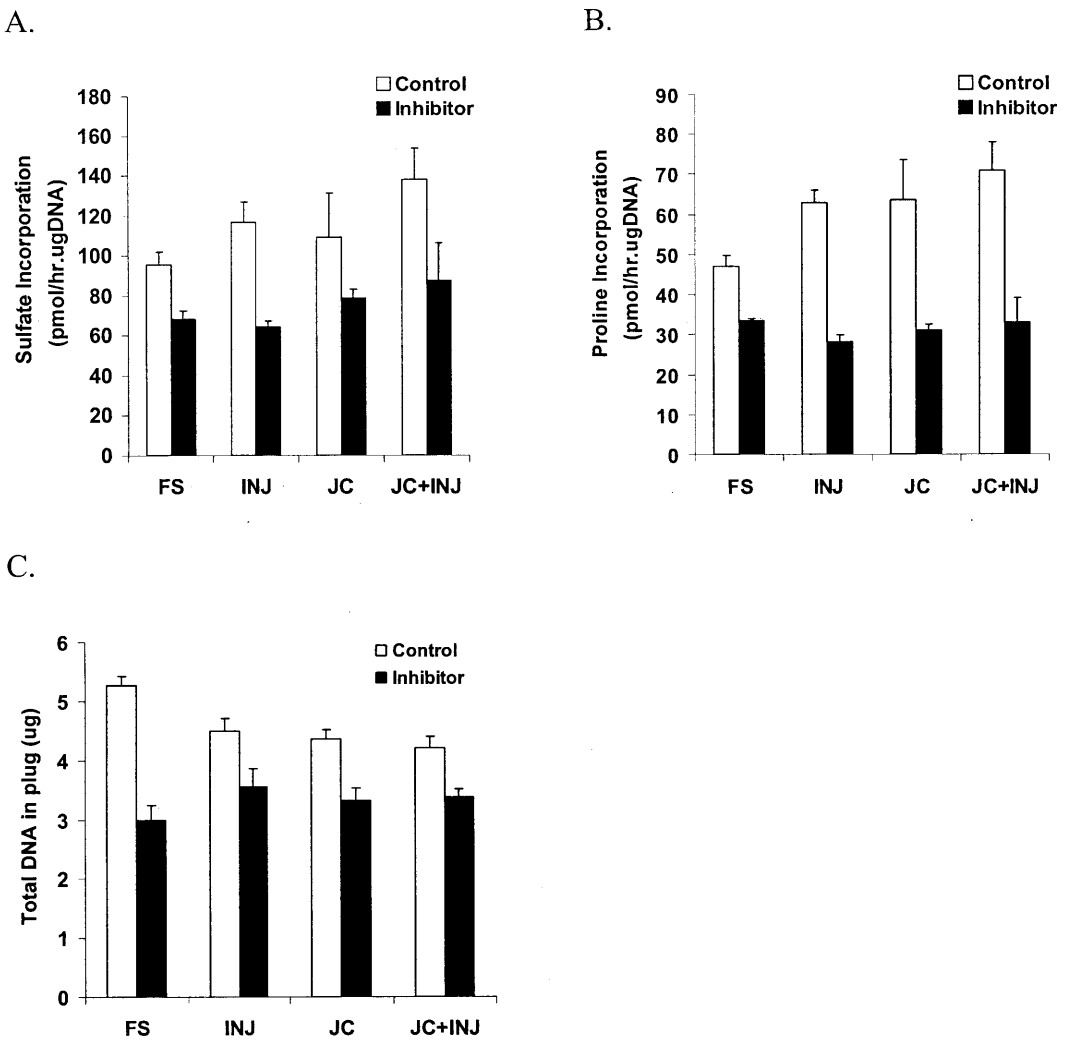

Figure A.7 The effect of aggrecanase inhibitor on the biosynthesis rate and DNA content. Bovine calf cartilage explants subjected to the injury, co-culture with joint capsule and both treatments. The explants were incubated for 16 days and radio-labeled for last 48 hrs. **A.** Sulfate incorporation rate. **B.** Proline incorporation rate. **C.** Total DNA content in the explants. Mean ± SEM (n = 6 disks per condition).

A.

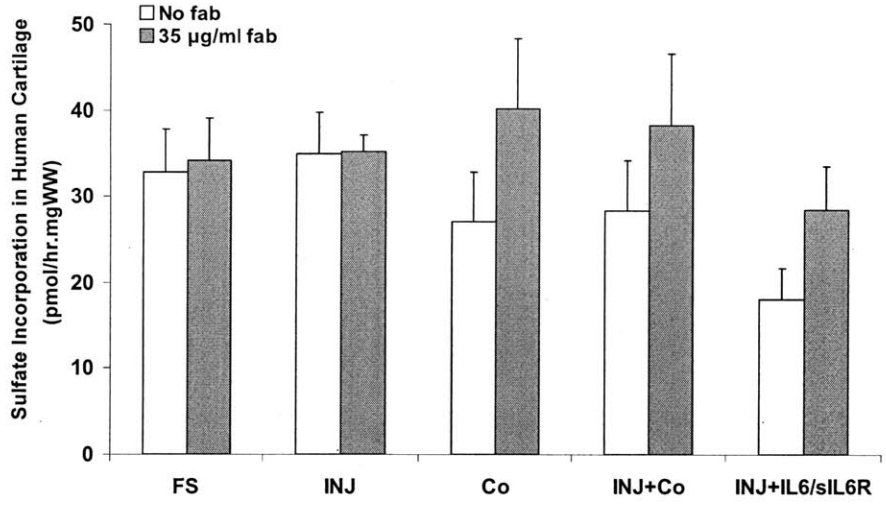

B.

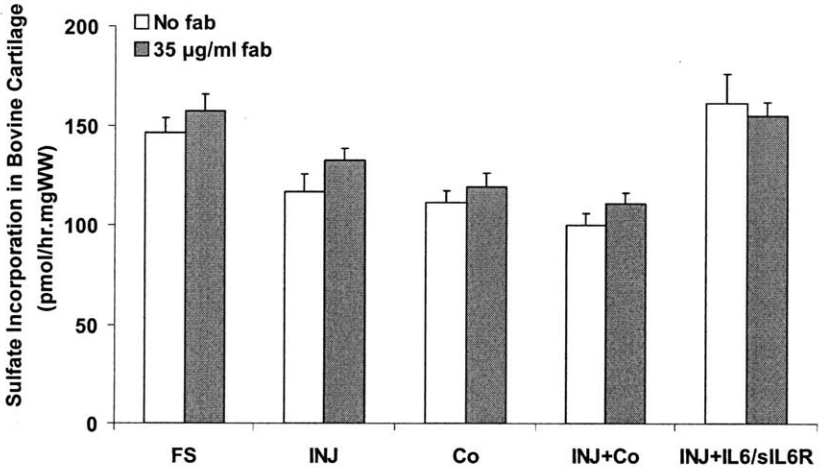

Figure A.8 The effect of anti-IL-6 Fab fragment on the sulfate incorporation rate. Adult human and bovine calf cartilage explants subjected to the injury, co-culture, co-culture with injury, and injury with IL-6 (50 ng/ml) /sIL-6R (250 ng/ml). The explants were incubated for 6 days and radio-labeled for last 48 hrs. 1-way ANOVA testing the effect of Fab did not find significant effect on sulfate incorporation for both human and bovine tissue. **A.** Sulfate incorporation rate in human tissue. **B.** Sulfate incorporation rate in bovine tissue. Mean ± SEM (n = 5 disks per condition).

A.5 References

[1] Garcia AM, Szasz N, Trippel SB, Morales TI, Grodzinsky AJ, Frank EH. Transport and binding of insulin-like growth factor I through articular cartilage. Arch Biochem Biophys 2003;415:69-79.
[2] Sui Y, Lee JH, Dimicco MA, Vanderploeg EJ, Blake SM, Hung HH, Plaas AH, James IE, Song XY, Lark MW, Grodzinsky AJ. Mechanical injury potentiates proteoglycan catabolism induced by interleukin-6 with soluble interleukin-6 receptor and tumor necrosis factor alpha in immature bovine and adult human articular cartilage. Arthritis Rheum 2009;60:2985-96.
[3] Kurz B, Jin M, Patwari P, Cheng DM, Lark MW, Grodzinsky AJ. Biosynthetic response and mechanical properties of articular cartilage after injurious compression. Journal of Orthopaedic Research 2001;19:1140-6.
[4] Sah RLY, Kim YJ, Doong JYH, Grodzinsky AJ, Plaas AHK, Sandy JD. Biosynthetic response of cartilage explants to dynamic compression. J Orthop Res 1989;7:619-36.
[5] Patwari P, Lin SN, Kurz B, Cole AA, Kumar S, Grodzinsky AJ. Potent inhibition of cartilage biosynthesis by coincubation with joint capsule through an IL-1-independent pathway. Scand J Med Sci Sports 2009;19:528-35.
[6] Lee JH, Fitzgerald JB, DiMicco MA, Cheng DM, Flannery CR, Sandy JD, Plaas AH, Grodzinsky AJ. Co-culture of mechanically injured cartilage with joint capsule tissue alters chondrocyte expression patterns and increases ADAMTS5 production. Arch Biochem Biophys 2009;489:118-26.